NBSIR 85-3027

DEVELOPMENT OF STANDARDS FOR SUPERCONDUCTORS

Interim Report
January 1982—December 1983

L.F. Goodrich, J.V. Minervini, A. F. Clark, F.R. Fickett, J.W. Ekin, E.S. Pittman
Electromagnetic Technology Division
Center for Electronics and Electrical Engineering
National Engineering Laboratory
National Bureau of Standards
Boulder, Colorado 80303

JANUARY 1985

Work performed under Department of Energy contract DE-AI01-76PR06010

NBSIR 85-3027

DEVELOPMENT OF STANDARDS FOR SUPERCONDUCTORS

Interim Report
January 1982—December 1983

L.F. Goodrich, J.V. Minervini, A.F. Clark, F.R. Fickett, J.W. Ekin, E.S. Pittman
Electromagnetic Technology Division
Center for Electronics and Electrical Engineering
National Engineering Laboratory
National Bureau of Standards
Boulder, Colorado 80303

JANUARY 1985

Work performed under Department of Energy contract DE-AI01-76PR06010

U.S. DEPARTMENT OF COMMERCE, Malcolm Baldrige, Secretary

NATIONAL BUREAU OF STANDARDS, Ernest Ambler, Director

CONTENTS

DEVELOPMENT OF STANDARDS FOR SUPERCONDUCTORS
Interim Report
January 1982--December 1983

L. F. Goodrich, J. V. Minervini, A. F. Clark, F. R. Fickett,
J. W. Ekin, E. S. Pittman

Electromagnetic Technology Division
National Bureau of Standards
Boulder, Colorado 80303

A cooperative program with the Department of Energy, the National Bureau of Standards, and private industry is in progress to develop standard measurement practices for use in large scale applications of superconductivity. The goal is the adoption of voluntary standards for the critical parameters and other characterizations of practical superconductors. Progress for the period January 1982 through December 1983 is reported. The major effort was the procurement, selection, and certification of the first superconducting wire for critical current measurements as a Standard Reference Material (SRM 1457). Other work reported here includes: effect of geometry on current transfer; lap-joint resistance; and ac losses.

Key words: critical current; critical parameters; losses; measurement methods; standards; superconductor.

1. INTRODUCTION

The development of standard measurement practices is essential to the success of any developing technology. In order to help ensure success in the field of large scale applications of superconductivity the Department of Energy and the National Bureau of Standards have undertaken a program to establish a uniform terminology and reliable measurement techniques for the many new aspects of superconductivity that are essential to good design. This report is the fourth in a series summarizing the progress in this program, which is jointly supported by the National Bureau of Standards and the Department of Energy through the Office of Fusion Energy and the Division of High Energy Physics.

The first three reports [1.0-1, 1.0-2, 1.0-3] summarized the progress in the first several years. The first report included: a large effort on the standardization of terminology, a preliminary assessment of measurement capabilities in the United States, the formation of an ASTM Subcommittee on Superconductors, some preliminary transient loss measurements, a comparison of

critical temperature measurements on practical superconducting materials, and extensive research on the many factors that affect critical current measurements. The second report concentrated on the development of a standard method for measuring critical current and included reports on contracts to the four U.S. wire manufacturers for research on various aspects of this measurement. The second report also included a survey of the state of the art of critical current measurement (including a round robin and an assessment of the criteria used), the final publication of the definition of terms, and the development of a draft standard for the determination of critical current for superconductors with a critical current less than 600 amperes. The major effort described in the third report was the development of a standard test method for critical current, the necessary back-up research, and the coordination of the adoption of the test method and standard terminology through the subcommittee level in ASTM. The two ASTM standards on superconductors [1.0-4, 1.0-5] were approved in December 1982.

This fourth report covers the period January 1982 through December 1983. It includes an evaluation of the present status (section 2), a summary of the preparation and dissemination of standards (section 3), three previously unpublished papers reporting work performed on the experimental program, and appendices including: papers published during this reporting period, a publication list, and copies of the announcement and certificate for SRM 1457.

1.1 References

[1.0-1] F. R. Fickett and A. F. Clark, "Development of Standards for Superconductors, Annual Report FY 79," NBSIR 80-1629, National Bureau of Standards, Boulder, Colorado (Dec. 1979).

[1.0-2] F. R. Fickett, L. F. Goodrich, and A. F. Clark, "Development of Standards for Superconductors: Annual Report FY 80," NBSIR 80-1642, National Bureau of Standards, Boulder, Colorado (Dec. 1980).

[1.0-3] A. F. Clark, L. F. Goodrich, F. R. Fickett, and J. V. Minervini, "Development of Standards for Superconductors, Interim Report, Oct. 1980 to Jan. 1982," NBSIR 82-1678, National Bureau of Standards, Boulder, Colorado (July 1982).

[1.0-4] Standard Definitions of Terms Relating to Superconductors, Annual Book of ASTM Standards, ASTM B713-82, Part 2.03, pp. 591-594, American Society for Testing and Materials, Philadelphia, Pennsylvania (1983).

[1.0-5] Standard Test Method for D-C Critical Current of Composite Superconductors, Annual Book of ASTM Standards, ASTM B714-82, Part 2.03, pp. 595-598, American Society for Testing and Materials, Philadelphia, Pennsylvania (1983).

2. EVALUATION OF PRESENT STATUS

It is important in an interactive research program such as this to continually assess the results with respect to the direction of future efforts. In this section we will summarize the major accomplishments and outline the possible future research topics. Due to the timing of this report, the accomplishments through 1984 are listed, and the list of possible future research topics is all encompassing to stimulate future efforts.

2.1 Summary of Major Accomplishments 1977-1984

I. Superconductivity

* Survey, workshops, and continuous interactions performed with manufacturers and users on measurement practices and problems for superconducting parameters. Determined the priorities and direction of the research and standards effort.

* Formed ASTM Subcommittee on Superconductors B01.08 as forum for impartial discussion of measurement problems. Involved many as 30 active participants representing all U.S. and one European wire manufacturer and all DoE and DoD laboratories.

* Standard definition of terms for superconductivity adopted by ASTM after extensive review, four open literature papers containing proposed definitions, and the ASTM voting procedure.

* Published more than 30 publications presenting research results in the open literature to the superconductivity community.

II. Critical Current

A. Small conductors (<600 A)

* Round robin test organized to assess the initial state-of-the-art measurement techniques. Critical evaluation done of test methods and needs.

* Extensive research assessment completed on 34 measurement parameters that affect the accurate determination of critical current. Results published in open literature.

* The first user, producers, and third party consensus ASTM standard test method for the measurement of critical current was adopted.

* First standard reference material (SRM) for the determination of critical current completely characterized and available for purchase.

* Current transfer identified as major parameter affecting critical current measurements and joint behavior. Experimental characterization and theoretical model completed.

B. Large conductors (>600 A)

* Parameters evaluated to identify those that affect large conductors. New or scaled up problems of major concern in research now.

* Survey and interactions performed with the National Laboratories on present methods and problem areas.

III. AC Losses

* Performed comparison of calorimetric, lock-in amplifier, and digital oscilloscope techniques. Literature reported factors of 10 difference reduced to 2 or 3.

* Developed digital multiplication technique for use with ac current and ac fields.

* Developed theoretical model for both ac current and ac field.

IV. Critical Field

* Assessment and critical evaluation done of test methods and needs.

V. Stability

* Assessment and critical evaluation done of test methods and needs.

* Parameters in I_c versus T studied on SRM.

2.2 Possible Future Research Topics

I. Critical Current

A. Large Conductor (600-6,000 A)

* Completion of parameter assessment on monolithic conductors.
* Large conductor SRM (ten times the small conductor critical current).
* Cable conductor measurement parameters.
* Set up of a critical current measurement service.
* Small lab test method.

B. Continuous Testing

* Moving current and voltage contacts and mechanical logistics.
* Standard test method.

C. Electromechanical Properties

* Bending and biaxial strain effects on critical current measurement.
* Standard test method for strain dependence of critical current.
* Strain effects on present SRM.

II. AC Losses

* Standard method development.
* Development of theoretical model of AC loss.
* ASTM coordination.
* Assessment of SRM needs.

III. Stability

* Standard method development.
* Disturbance spectra determination, sources and characteristics.
* Joint resistance measurements.
* ASTM coordination.

IV. Critical temperature, critical field

* Prove extrapolation techniques.
* Provide experimental guidelines.

V. Nonsuperconducting Magnet Materials

* Residual resistance ratio method in presence of superconductors.
* Very low level magnetic susceptibility.
* Internally supported conductors, effect on J_c measurements.

VI. Interactions

* Workshops with users and producers.
* Laboratory visits.
* ASTM coordination.

An essential component to the development of a research program such as this is input from producers, users, and researchers working with practical superconductors. Feedback about the relative importance of the topics listed above or other areas that need research is solicited and always welcome.

3. PREPARATION AND DISSEMINATION OF STANDARDS

The final goal of this program is the adoption of voluntary standards for practical superconductors. The first two standards, definition of terms and small conductor critical current, were adopted in December 1982. The next steps were to start research on a large conductor critical current test and to develop a Standard Reference Material (SRM) for the measurement of critical current. The SRM is now available through the NBS Office of Standard Reference Materials as "SRM-1457 Superconducting Critical Current - NbTi Wire" (See Appendices E and F). The minutes of two ASTM meetings held during this reporting period are given in section 3.1. The major problem areas where research is needed were identified at those meetings. Further discussions and observations were made at conferences and laboratory visits. A list of visits is given in section 3.2. A summary of the selection and certification of SRM 1457 is given in section 3.3. Also included as sections 3.4 and 3.5 are summaries of the evaluation of the measurement state of the art and an assessment of measurement needs of two possible research areas: stability and critical field.

3.1 ASTM B01.08 Subcommittee Minutes
by A. F. Clark

3.1 a. Minutes from Knoxville, Tennessee (November 1982)

ASTM B01.08 Subcommittee on Superconductors
November 29, 1982 7:30 pm
Andrew Jackson Room, Knoxville Hyatt Regency

A meeting of the ASTM B01.08 Subcommittee on Superconductors was held in conjunction with the 1982 Applied Superconductivity Conference on November 29, 1982 in Knoxville, Tennessee. The purpose of the meeting was primarily to assess the problem areas for a standard for critical current measurements on high-current (up to 20 kA) superconductors.

The chairman of the subcommittee, A. F. Clark, opened the meeting with a brief discussion of the progress in the DoE-NBS program for the development of standards for superconductors. Two draft standards, definitions of terms, and small conductor critical current, are presently out for ASTM society ballot. Research is underway on large conductor measurements and ac losses, and assessments are in progress on critical field and stability. Except for a short discussion on continuous testing, the meeting was devoted to presentations and discussions on the problems of large conductor critical current testing.

The discussion was initiated by informal presentations of methods of measurement now in use in their laboratories by John Miller of Oak Ridge National Laboratory, Al McInturff of Fermilab, and Bill Sampson of Brookhaven National Laboratory. Others contributing their experience were Karl Best of Vacuumschmelze, L. Intichar of Siemens, and Yuki Iwasa of Francis Bitter National Magnet Laboratory. John Miller listed several problem areas that proved to be common among the rest and included expense, sample mounting and orientation, current transfer resistance, criteria, self field, and cable vs. strand measurements. Al McInturff pointed out some of the problems that arise if production measurements are needed, and also the role of the power supply as a noise source in the voltage signals. Bill Sampson described an apparatus that used the distinct advantages of a dipole magnet and methods of data processing. A discussion ensued addressing such things as scaling experiments,

common test facilities, methods for small labs, the inclusion of Nb_3Sn conductors, and other methods. The question of whether a standard was even needed, and if so, what form it should take was raised by the chairman.

In summary, the subcommittee felt that a standard was definitely needed. The decision had the full support of the wire manufacturers and national labs that were represented. It was felt that it could start as a set of guidelines, but that would only be a step on the way to an ASTM standard. Major problem areas for research at NBS were identified as a) the expense of the test in money, time, and liquid helium, b) sample mounting techniques to contain the large stresses, c) power supply noise and alternate current sources, d) voltage signal processing including noise pickup, and e) current transfer. It was also felt that Nb_3Sn and all other developmental conductors should be included, and that one central test facility could probably not be responsive to all the needs.

In a final discussion, the need and desirability of a method for continuous testing of a length of wire or superconductor critical current was addressed. It was felt that this could be done, but that an assessment should first be made that would include a survey of potential users.

All in all, it was a fruitful exchange of information, a lively discussion, and generated some helpful guidance for future work.

3.1 b. Minutes from San Francisco, California (April 1984)

ASTM B01.08 Subcommittee on Superconductors
April 5, 1984 1:00 pm
Ramada Hotel, San Francisco, California

Chairman, A. F. Clark, called the meeting to order at 1:00 p.m. and presented the agenda, indicating that we would first evaluate the presently adopted standards, discuss the recent development of a standard reference material by NBS, hear an NBS research report on present progress and

measurement techniques, and finally, discuss future tasks. In attendance were seven members plus three guests.

The two present standards, B713-82 Definitions and B714-82 Critical Current, were brought up for discussion as to their applicability and usefulness. There were no comments on the Definitions. It was felt that people used them without question. On the standard measurement technique, several comments indicated a need for publicity and the need for soliciting feedback on its usefulness. Suggestions to accomplish this were: a short article in Cryogenics or a direct solicitation to wire manufacturers including both Europe and Japan. As far as the measurement technique, the value of including the bending strain was indicated, as well as a more varied range of electric field criteria. The question of the quench limit in NbTi and Nb_3Sn were compared as a justification for the need of a wider ranging electric field. Other than these criticisms it was felt that the standard measurement technique was useful, but needed to be applied more often. Also that a standard measurement needed to be extended to higher critical currents and we must, for that, add such things as aspect ratio, self field, and current transfer considerations.

Loren Goodrich presented the present status of the standard reference material being developed by NBS. It will be available in less than a month at a price of $219 for 2.2 meters of well-characterized, round, NbTi multifilamentary conductor. Questions were raised as to whether it was too short, the answer being no, and, are <u>all</u> the data available for the user. Loren indicated that a <u>complete</u> report is available and will probably be sent out with each SRM. The SRM will be publicized in the ASTM Standardization News and through a general mailing to the ICMC and Applied Superconductivity mailing lists. It was felt this should be adequate exposure.

Loren Goodrich and Alan Clark of NBS then gave a research report on the development of large conductor critical current tests and ac losses. Briefly, NBS is exploring aspect ratio, self field, and current transfer effects in conductor measurements up to 3,000 amperes, and using three or four ac loss measurement techniques to compare measurements on similar conductors. In the former a test technique should be available soon, and in the latter there are

extraordinary difficulties in getting measurements to agree. The committee felt that current transfer and large conductors is a major problem and that the extension to 6,000 amperes or more should come fairly quickly. The upper limit for large conductors should probably be on the order of 10-12,000 amperes. Whether an SRM should be created was discussed and before this were to take place, the committee felt that a survey of needs should be performed by NBS, which could also include a round robin testing of large conductors by those who can make such measurements. The only laboratories with this measurement capability are Oak Ridge, General Dynamics, Lawrence Livermore, and the M.I.T. Magnet Laboratory. The General Dynamics representative indicated they were setting up large conductor measurements because the wire manufacturers were showing differences of 40% on the same wire. The possibility of measuring forced flow conductors was raised, but the committee felt that because the currents were too high and the flow characteristics were too variable, the development of this kind of measurement was probably premature and that it is more important to go into complex geometries (i.e., cables, etc.), higher currents, and pursue the fundamental understanding of these measurements before the development of a test technique. As for ac losses, the committee felt that this measurement problem should be ranked second only behind large conductor critical current. The factors of 10 are still present in many measurements and form a big unknown for design parameters.

Finally, the areas of stability, critical field, and other measurements were raised. For stability the variability of magnet design is still wide ranging and still there, but the committee felt that it would be worth a try to develop a standard measure of this difficult parameter. This is principally because some magnet designs are getting used more and more and if some intrinsic properties could be identified for stability, this would be an immense help in magnet design. A principal point of research would be the influence of the disturbance spectrum on these measurements. As to critical field measurements, it was felt that H_{c2} was not a commercial parameter, but that the J_c-H curve is a very definite need. Thus, the cookbook extrapolation for H_{c2} may be adequate, but this would have to be proved by further research. Of much more importance is the absolute field measurement. Presently, Hall probes, search coils and NMR probes are used to try and develop the precision

to 8 T that is needed in magnet design (i.e., 1 part in 10^5). Most people use some sort of local in-house calibration and ancient techniques in these measurements. Another real need for the residual resistance ratio (RRR) was raised when these measurements are in the presence of a superconductor. The measurements of RRR are okay when they are done on the bulk copper, but there is a strong need to define a RRR in the presence of a superconductor and develop a technique for its measurement.

On Friday, April 6th, the subcommittee met with the full B1 Committee on Conductors, about 35 people, to give a report on the subcommittee meeting and on the progress of various tasks. In general, the main committee gave full support in the difficult task in the development of standards in a new field and offered their full support wherever possible, in particular, with properties of the copper stabilizer.

3.2 Summary of Laboratory Visits

Name	Date	Location	Subject
A. F. Clark and F. R. Fickett	3/1-3/82	Lawrence Livermore National Laboratory; Univ. of California at Berkeley; Stanford Linear Accelerator Center	Discuss contract and proposed research
A. F. Clark and L. F. Goodrich	4/4-8/82	Westinghouse (Pittsburgh); Oak Ridge National Laboratory	Discuss measurement programs and large conductor critical current measurements
		Richmond, Virginia	Attend ASTM B1 Committee meeting
A. F. Clark*	5/8-22/82	Kobe, Japan	Attend and chair a session at the joint ICEC9-ICMC
		Japanese National Railway Test Center; University of Kyushu; Tohoku University and Research Institute for Iron, Steel, and Other Metals; National Research Institute of Metals (NRIM); Electrotechnical Laboratory (ETL); High Energy Physics Laboratory (KEK); Furukawa Electric Company, Central Research Laboratory	Obtain the most recent developments of materials and measurements in Japan
F. R. Fickett*	9/27-10/4/82	National Magnet Laboratory, Boston, MA	Obtain critical field measurements
A. F. Clark*	9/29-10/3/82	Stanford University and Stanford Linear Accelerator Center	Discuss and observe superconductor measurements
A. F. Clark*	11/29-12/3/82	Knoxville, Tennessee	Attend Applied Superconductivity Conference; chair ASTM meeting; attend Cryogenics Editorial Board meeting

* Travel funded by NBS

Name	Date	Location	Subject
L. F. Goodrich	11/29-12/3/82	Knoxville, Tennessee	Attend and present a paper at the Applied Superconductivity Conference and attend ASTM meeting
A. F. Clark*	5/15-19/83	Massachusetts Institute of Technology; Magnetic Corporation of America (Boston, Massachusetts)	Discuss superconductor measurements
L. F. Goodrich	8/15-19/83	Colorado Springs, Colorado	Attend and present paper at ICMC
A. F. Clark*	8/21-23/83	Copper Mountain, Colorado	Cochair workshop on Problems in Superconductivity
A. F. Clark*	8/28-9/16/83	Paris, France; Grenoble, France;	Attend IIR and MT8 conferences and present paper
		Karlsruhe, FRG; Oxford, England Southampton, England	Perform superconductor measurements and research

* Travel funded by NBS

3.3 Summary of Standard Reference Material Development

by L. F. Goodrich

This is a summary of the work and the report [3.3-1] that led to the first superconducting wire for a critical current measurement Standard Reference Material (SRM 1457). The report reviews the selection and certification of the SRM. The SRM is intended to provide a means for checking the performance of measurement systems used in the commerce and technology of superconductors. SRM 1457 should prove valuable in determining the overall accuracy of a critical current measurement system that is dependent on numerous variables and effects that can make this seemingly easy measurement very difficult. SRM 1457 may be purchased for $219 from the Office of Standard Reference Materials, Room B311, Chemistry Building, National Bureau of Standards, Washington, DC 20234.

An effort was made to keep the use of this SRM as unrestricted as possible. The precautions listed on the certificate, together with the American Society for Testing and Materials (ASTM) Standard Test Method (B714-82), are sufficient for any valid user measurement technique. Some deviations in testing technique from the method on which the certification was based were accommodated by in creasing the total uncertainty in the certified critical current. The deviations that are allowed, and the ones that are not allowed, are identified in the precautions sections of the certificate.

The critical current was measured using a 2 cm voltage tap separation on a coil specimen holder with a 3.18 cm diameter (specimen bend diameter of about 3.23 cm) and a two turn per centimeter pitch length. The general technique used to measure the critical current was the ASTM standard test method B714-82 [3.3-2]; however the variables were held to much tighter limits in order to get a lower total uncertainty including the sample inhomogeneity. The acquisition and analysis of the raw data were carefully developed to measure the criti cal current with accuracy and precision. The limits to systematic and random errors of the principal variables that effect the critical current (current, electric field, magnetic field, temperature and strain) were estimated. Other concomitant variables and effects considered in the development and certification of this SRM were: voltage filtering and response time; current ramp

rate; liquid helium hydrostatic head and stratification; inductive and thermoelectric voltage; magnetic field of the specimen coil; and winding tension.

Preliminary screening measurements were performed on each of five candidate SRM samples. Two of these conductors displayed short- or long-range inhomogeneity that made them seem unfit for use as an SRM. One of the remaining conductors was eliminated becaused the length delivered was considered too short. One of the two candidates left had the lowest copper-to-superconductor ratio, so it was eliminated in favor of the other. Further measurements and tests were made on the conductor chosen to be the SRM.

The conductor designated as SRM 1457 was wound onto 500 distribution spools, each with approximately 2.2 m of wire. Nine of these spools were selected at nearly equal distances along the whole length of wire, including the spools at each end. Critical current measurements on the sample spools were obtained for 36 combinations of three factors affecting critical current: magnetic field, temperature, and electric field.

Although there were no obvious trends along the length of wire, substantial variation in critical current was evident, especially at lower magnetic fields. These variations were associated with material variability, or inhomogeneity, of the wire, and were incorporated into a statistical model that was derived from an empirical equation for the dependence of critical current on temperature and electric field at any given magnetic field.

SRM 1457 has been certified at magnetic fields of 2, 4, 6, and 8 T for temperatures from 3.90 to 4.24 K and electric field criteria from 0.05 to 0.2 μV/cm. Because material variability could not be ignored, the uncertainty in the certified values of critical current (excluding systematic errors) is a statistical tolerance interval. The resulting tolerance limits allow for inhomogeneity by estimating limits for the critical current of individual spools, rather than limits on the average critical current of all spools.

The statistical tolerance limits and estimated systematic error have been combined to give a total uncertainty on the certified values. The final estimated uncertainties are no greater than 2.57% of the reported critical current at any of the four magnetic fields.

3.4 Summary of Study to Assess Development of Stability Standards

by J. W. Ekin

A study of the various types of superconductor stability has been made along with a survey of experimental methods currently used to measure stability. The potential for developing stability measurement standards was assessed. This is a summary of the main conclusions of that study. A more detailed report is under preparation.

STABILITY TYPES

A major conclusion of the study is that there are only two fundamentally different types of stability: flux-jump stabilization and cryogenic stabilization. There are many names for cryogenic stabilization corresponding to different assumptions used in solving the power-balance equation that is the heart of this type of analysis. They are all solutions to the same general equation under different simplifying conditions. This is shown in detail for the so-called Stekly criteria, the Cold-End Recovery criterion, the Cold-End Minimum-Propagation-Zone criterion, the Critical-Current Margin criterion, and the Spherical and Elliptical Minimum-Propagating-Zone criteria.

STABILITY STANDARDS

From the standpoint of standards, two questions need to be answered affirmatively before a stability standard can be considered: 1) Is there a meaningful measure of stability; and 2) Is a stability measurement likely to be repeated often in the utilization of superconductors (i.e., does anyone care?).

For flux-jump stabilization, the answer to the first question is yes but the answer to the second question in most cases is no. There usually is not much need to test for flux jumps -- they are taken care of through proper sizing of superconductor filaments.

For cryostabilization, on the other hand, both questions can be answered affirmatively, as discussed in the following two sections.

A PROPOSED PRACTICAL MEASURE OF CRYOSTABILITY

For each of the cryostability criteria the study shows that the expression for obtaining cryostability contains the relative current density, $j(\equiv J/J_c)$, as a parameter. Cryostability can always be obtained by operating at a low enough j. This current stability limit can be measured for any system. Thus, although there is no consensus on how stability should be measured, at least one meaningful measure of cryostability exists: the current stability limit. Also, it is an engineering parameter which is needed in most large magnet designs. For many large magnet designs it is as important as, if not more important, than the superconductor critical current. Because its measurement is not easy to do correctly, there probably is an eventual need for a standard procedure to measure it.

MEASUREMENT OF CURRENT STABILITY LIMIT

Two basic experimental methods are possible for determining such a current stability limit prior to the construction of the final winding. Basically they go hand in hand. The first method is to determine the parameters needed if cryostability has been achieved, particularly the cooling rate which is quite variable. It depends strongly on the surface condition, cooling channel geometry, and orientation of each conductor relative to vertical. The second method is to construct a section of winding which simulates as closely as possible the projected cooling conditions of the final winding structure. The current stability limit is then measured as the steady-state conductor current when thermal runaway is initiated by a heater embedded in the winding. The heater drives a portion of the experimental winding into the normal state.

The measurement is critically dependent on simulating the cooling conditions to be actually encountered in the final magnet, and therefore any standard measurement procedure would have to be adaptable to individual magnet cooling conditions. As such it is a measurement standard that probably would have to be specified or performed by the magnet manufacturer, as opposed to the conductor manufacturer.

One exception to this would be superconductors with complicated surface geometries, such as cable conductors, internally cooled conductors, or conductors with augmented surfaces (such as cut surfaces or sintered coatings). For such superconductors it would be useful to have a measurement procedure for

determining the surface cooling rate for an individual conductor. Such a measurement could be performed by the conductor manufacturer and might well be useful in a calculation of the current stability limit, or at least as a figure of merit in conductor selection.

SUMMARY

To summarize, stability measurements are still in the evolutionary stage, but at least there appear to be methods for measurement of the current stability limit. The current stability limit is, furthermore, a critical parameter that is variable enough that there is a need for its measurement as a common engineering parameter, at least in cryostable magnet design. It is a measurement performed at present primarily by magnet designers, but surface cooling rate data (under pool-boiling conditions) for certain conductors could become a common critical parameter supplied by the conductor manufacturers.

A key question for advanced stability considerations is the quantification of the internal disturbance spectrum. As long as this question is not solved, potentially powerful measurements for achieving limited cryostability remain unfortunately of only limited significance. In addition to studying trends, such as scaling of disturbance magnitude with magnet size and field level, future work should possibly be concentrated more strongly on disturbance spectra, particularly information on detailed stress distributions and microscopic energy release events in common magnet structures.

CONCLUSIONS OF THE STUDY

1) There is no need for a flux-jump stability standard.
   - reliability has been achieved by making the filament and strand size small
   - not of engineering concern
2) There is a strong engineering need for a cryostability standard.
   - first need to answer some basic questions about measurement specification (heater geometry, cooling geometry, heat pulse duration, etc.)
   - magnet designs also need some settling time
3) It is suggested that a first practical engineering parameter for determining cryostability is the current stability limit. Proposed symbol "I_s."

4) I_s is already measured in some form or another for most cryostable magnet designs because of its dependence on:
   - conductor surface condition
   - internal conductor configuration (thermal conductivity, heat capacity)
   - cooling channel geometry
   - conductor orientation
   - disturbance spectrum
5) Measurement of I_s is performed at present primarily by magnet designers, not conductor manufacturers.
6) There are two methods for determining I_s a priori:
   a) Calculate from measured quantities, such as surface cooling rate, using formulas given in papers.
   b) Measure directly using a small coil with heaters.
7) Surface cooling rate data could become a common parameter supplied by conductor manufacturers for certain superconductors.
   - conductors with augmented surfaces (fins, sintered coatings)
   - cabled conductors
   - internally cooled conductors (cooling defined by conductor design, not magnet design)
   - augmented internal heat capacity
8) Key question for improved performance -- WHAT IS THE DISTURBANCE SPECTRUM?

3.5 Summary of Critical Field Assessment

by F. R. Fickett

This is a summary of a paper entitled "Standards for Measurement of the Critical Fields of Superconductors," which has been prepared by F. R. Fickett and is to be published in the March-April 1985 issue of the NBS Journal of Research.

In the paper, the origins, definitions, and measurement of the various critical magnetic fields associated with superconductors are reviewed. The potential need for a consensus standard for the measurement of these fields is evaluated. Measurement techniques, as practiced both in industry and in the national laboratories, and extrapolation techniques commonly used to determine the upper critical fields of the newer materials are presented. Sources of error in the experimental determination of critical fields are assessed for the various common techniques. A comprehensive bibliography of the modern literature on critical field measurement and interpretation is included in the publication. Here we briefly summarize the conclusions reached in that paper.

The purpose of the investigation was to evaluate the desirability and feasibility of creating a standard for measurement of the critical field of practical superconducting materials. The type of standard under consideration is that typically produced by organizations such as ASTM to assist in commerce. Two standards already exist in the field of superconductivity, one for general definitions and the other for the measurement of critical currents below 600 A. Such standards are created by consensus among all interested parties and must be able to be used by industrial laboratories in their day-to-day operation. A further consideration is that there should be a demonstrated need for the standard, at least in the foreseeable future.

A standard of this type can take several forms. It may be any of the following: a list of definitions; a manual outlining accepted measuring and reporting methods; a detailed method of measurement in which apparatus, technique, and report format are specified; or an artifact or standard reference material (SRM). Whatever the form, it is essential that the standard be backed up with adequate research to document the need for each requirement of the standard. This is not a trivial problem, and it is often neglected in the rush to create a standard to solve a particular problem. Our feelings regarding the need for and structure of a H_{c2} standard are given below. In summary,

it seems that the time is not yet ripe for a full-fledged standard, but there is some justification for creating a list of standard definitions and, perhaps, an "operation manual" or similar document for the determination of upper critical field. A standard reference material approach might also prove useful but would be quite expensive.

Standards of the sort discussed here are usually created in response to a need expressed by the community. In the case of critical field, there has been a limited expression of need. The commercial materials now in use are, in general, adequately characterized by their critical current versus field characteristic. Critical field information is of most use to that group of researchers who are trying to construct better practical materials for high field applications by modification of the crystallographic or electronic structure of various existing materials. This group should agree among themselves on the requirements for an acceptable measurement of the critical field, but that is not adequate reason for creating a standard. It is entirely conceivable that very high field materials may become feasible in the future, and the need could become great for a critical field standard for commercial versions of those superconductors. We do feel that a few definitions related to the critical field measurement should be added to the general definitions standard, mostly the various modifications of H_{c2} now in common use. Furthermore, it is possible that certain groups, such as DoE, might want to specify a critical field measurement method and data analysis technique for a particular material. This could be done, but it would require that some of the research mentioned below be performed first if the document were to have very wide application.

Our investigation indicates that the creation of a detailed single measurement standard for critical field is probably impossible given the current state of knowledge regarding the factors that influence H_{c2} and the inhomogeneous nature of the superconducting portion of the practical conductor composite. However, if an attempt were to be made, there are a few items that should be considered. The only measurement technique that is likely to be widely used in industry is the resistive method applied at 4.2 K. A clever application of an inductive technique might also be possible, but none has appeared to date. Similarly, the possibility of routine direct measurement is remote because of the expense of high field magnets. Thus, extrapolation techniques would have to be used and most likely those would be critical

current versus field extrapolations with the measurements made at 4.2 K. Extensive research on the pinning force phenomenon would be necessary. Significant advances in understanding the effect of crystallographic and metallurgical variations on the critical field would be required. All these requirements could be mitigated somewhat by the use of a standard reference material, but research on measurement methods and their related errors would still be needed. A standard method should use a relatively high current density, probably in excess of 100 A/mm^2, so as to avoid some potential problems.

The SRM approach to the standardization of critical field measurements is probably the most appealing for the present circumstances. Unfortunately, it is also a very expensive solution. The idea is to make a series of very well characterized materials that could then be distributed for the calibration of apparatus. Such materials could also be used to evaluate the various extrapolation techniques. The characterization would require very careful work, expertise in several measurement and analysis techniques, access to high field magnets, and a consensus as to the proper choices for the important parameters. However, considerable progress is now being made in understanding the interactions between the metallurgy and the superconducting properties of these materials which may well result in an advanced (practical) superconductor with well-documented homogeneity and internal structure in the near future. This conductor, if it can be made in significant quantities, would be an ideal candidate for a critical field SRM.

3.6 References

[3.3-1] L. F. Goodrich, D. F. Vecchia, E. S. Pittman, J. W. Ekin, and A. F. Clark, "Critical Current Measurements on an NbTi Superconducting Wire Standard Reference Material," NBS Special Publication 260-91, National Bureau of Standards, Boulder, Colorado (1984).

[3.3-2] Standard Test Method for D-C Critical Current of Composite Superconductors, Annual Book of ASTM Standards, ASTM B714-82, Part 2.03, pp. 595-598, American Society for Testing and Materials, Philadelphia, Pennsylvania (1983).

4. EXPERIMENTAL PROGRAM

This section contains three unpublished papers on work performed in the experimental program. The first, section 4.1, describes how the critical current measurement geometry will affect the observed current transfer characteristic. Current transfer voltages are ever present, although at different magnitudes. These voltages can interfere with the determination of critical current even for small NbTi conductors and it will be more of a problem for large conductors. In the second paper, section 4.2, the measurement and modelling of lap-joint resistance between multifilamentary superconductors is presented. The results can be used to estimate the lap-joint resistance. An unexpected result was the dominance of the joint interface resistance. The third paper, section 4.3, is on the principles of ac loss theory and the methods by which the losses can be experimentally measured. The general focus is to develop an understanding of the loss mechanisms within an individual superconducting filament.

4.1 Effect of Geometry on Current Transfer in Critical Current Measurements

by L. F. Goodrich

The experimental results and discussion of a program to evaluate current transfer in multifilamentary superconductors are presented with comparisons to existing theories. Specific areas of current transfer covered are: magnitude and current dependence of the current-transfer electric field as a function of distance away from the current contact in both parallel and perpendicular magnetic fields; dependence on current contact length; variation in a region of changing magnetic field angle or magnitude; symmetry of current transfer; response to multiple parallel and perpendicular magnetic field regions.

INTRODUCTION

The voltage that results from current transfer in multifilamentary superconductors can interfere with the determination of critical current. The experimental results, comparisons to existing theories, and discussion presented here summarize the information gathered on the source, magnitude, and shape of the transfer characteristic for various sample measurement configurations.

Current transfer results from a number of sources, namely; joints, inhomogeneities (change in local superconducting properties), strain, self field, and changes in the magnitude and angle of the magnetic field. For each of these, the current distribution among the superconducting filaments is locally disturbed from equilibrium. This non-equilibrium distribution of current causes spatial, flux-flow voltage gradients among the filaments and resistive voltages from the normal metal. These spatial voltage gradients drive some of the current through the interfilament material (normal metal) in the process of attaining a new equilibrium distribution. The result is a redistribution of the current among the superconducting filaments over a length of wire that causes a voltage drop along the wire. This voltage drop is referred to as the current-transfer voltage, V_t, and the corresponding electric field, E_t. The current-transfer voltage will be a function of both current and position along the wire due to each source. The physical extent of current transfer depends on the magnitude of the redistribution (largest near a joint), the resistivity of the interfilament material (the resistivity

of bronze is much greater than that of copper), the diameter of the wire, and the sharpness of the superconductor's flux-flow resistivity transition.

Current transfer exists in commercial multifilamentary superconductors. The most direct evidence of this phenomenon is the electric field, E, as a function of current, I, and distance from the current contact, x. A plot of this is given in figure 4.1-1. The lower current portion of the curves change significantly with distance from the current contact. This indicates that the lower current portion is not intrinsic to the sample and the position dependence indicates that its source is the current contact (joint). The joint is the predominant source of current transfer exhibited here because of the magnitude of the current redistribution and the measurement conditions, which minimized the effect of the other sources. Some of the other sources of current transfer are discussed below.

The theory of current transfer in multifilamentary superconductors has been the subject of several papers [4.1-1-3]. These theories deal only with transfer adjacent to a current contact, which is where the effect is largest. Each of these theories assumes that the intrinsic resistivity of the superconducting filaments, ρ_s, is given by

$$\rho_s = \rho_c \left(\frac{J}{J_c}\right)^n \qquad (4.1\text{-}1)$$

where J_c is the critical current density, ρ_c is the corresponding resistivity criterion (in general these would be reference values, but for convenience let them be the critical values), J is the current density and n is a constant for the superconductor (Ref. [4.1-3] uses m-1 instead of n). The value of n is determined from the shape of the flux-flow resistivity transition near the critical current, and this equation is a reasonable representation of the shape [4.1-4]. Typical values of n range from 10 to 60. Notice that this assumption implies that the superconductor has a finite resistivity at any non-zero J, thus current transfer will take place among the superconducting filaments at every current. One result of these theories is an approximate expression (for large n and within geometric factors) for the current transfer resistivity, ρ_t. The expression in Ref. [4.1-2] is

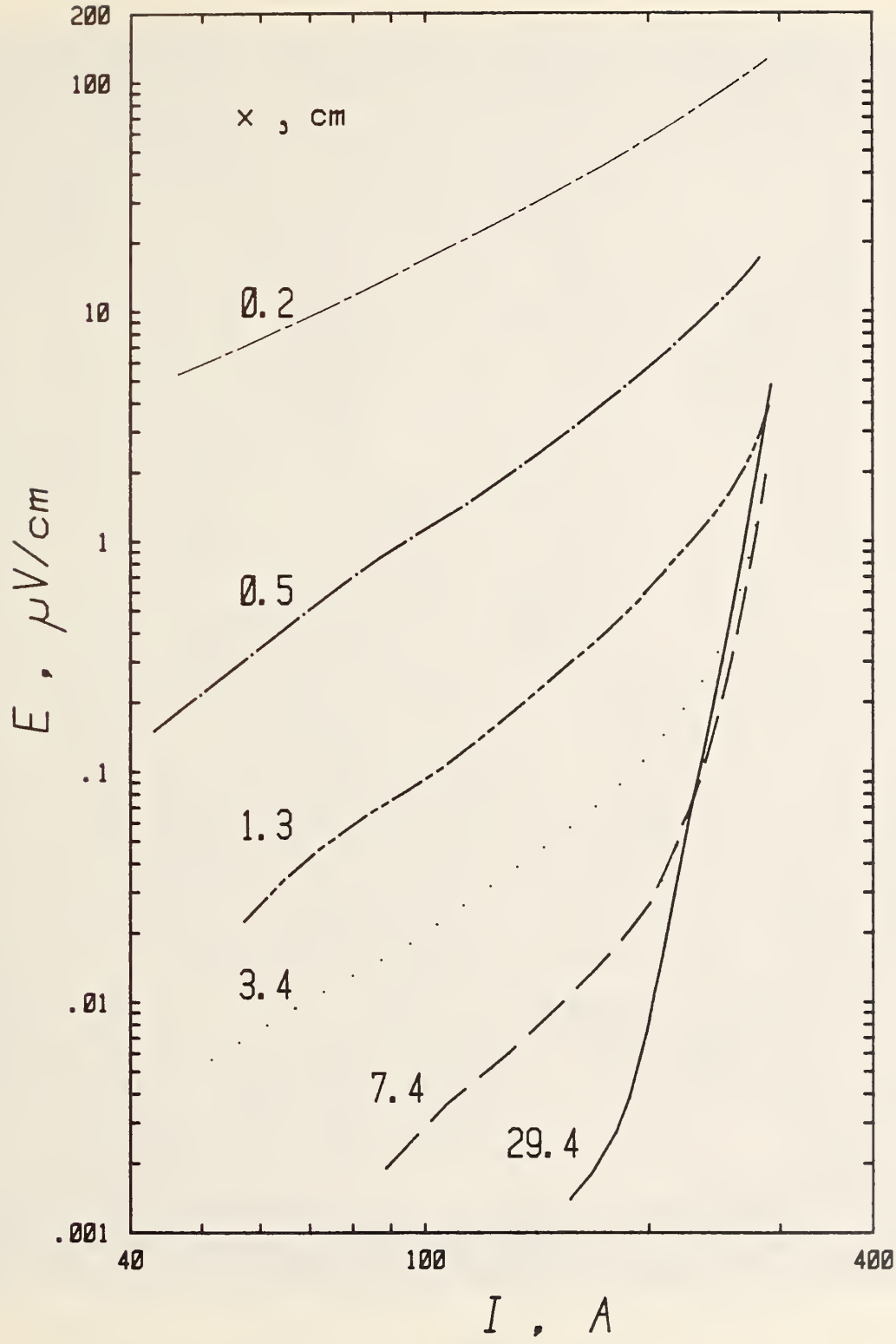

Figure 4.1-1. The electric field as a function of current for various distances from the current contact, x, at 4 T.

$$\rho_t \cong (0.1/n)\rho_m (d/x)^2, \qquad (4.1\text{-}2)$$

and Ref. [4.1-3]'s expression is

$$\rho_t \cong (0.25/(n+2))\rho_m (d/x)^2, \qquad (4.1\text{-}3)$$

where n is defined by eq (4.1-1), ρ_m is the transverse resistivity of the wire's filament region, d is the diameter of the wire's filament region, and x is the distance from the current contact. If the only variable in these expressions is x, then the current transfer portion (low current) of the voltage-current (V-I) curve should be linear. Another result is the introduction of a current transfer length, x_t, in Ref. [4.1-2] which is a specific value of x in eqs (4.1-2) and (4.1-3) where ρ_t is equal to a chosen value of resistivity, ρ^*. Usually ρ^* is of the order of the critical current criterion. Thus, x_t is a measure of the distance from the current contact at which $\rho_t \leq \rho^*$. For example, with $\rho^* = 10^{-12}$ Ω•cm, x_t would be approximately 100 d for a Nb_3Sn superconductor and 8 d for a NbTi superconductor.

All of the current transfer data presented here were taken on a commercial multifilamentary superconductor based on niobium-tin (Nb_3Sn). A photograph of the cross section is given in figure 4.1-2. The wire has a diameter of 0.70 mm. It has an outer copper jacket separated by a tantalum diffusion barrier from the core of bronze, Nb, and Nb_3Sn. The diameter, d, of the filament region enclosed by the barrier, is 0.40 mm. The wire was originally not twisted and unreacted, thus it could be either twisted or left untwisted and formed to shape prior to its reaction. Critical current data on this wire are given in table 4.1-1 for various critical current criteria.

Table 4.1-1. Sample critical current data.

		I_c, A for various criteria		
$\mu_o H$, T	n	E_c = 1 μV/cm	E_c = 1 nV/cm	$\rho_c = 10^{-12}$ Ω•cm
4	15.5 ± 1	275	181	232
8	12.4 ± 2	124	74	97

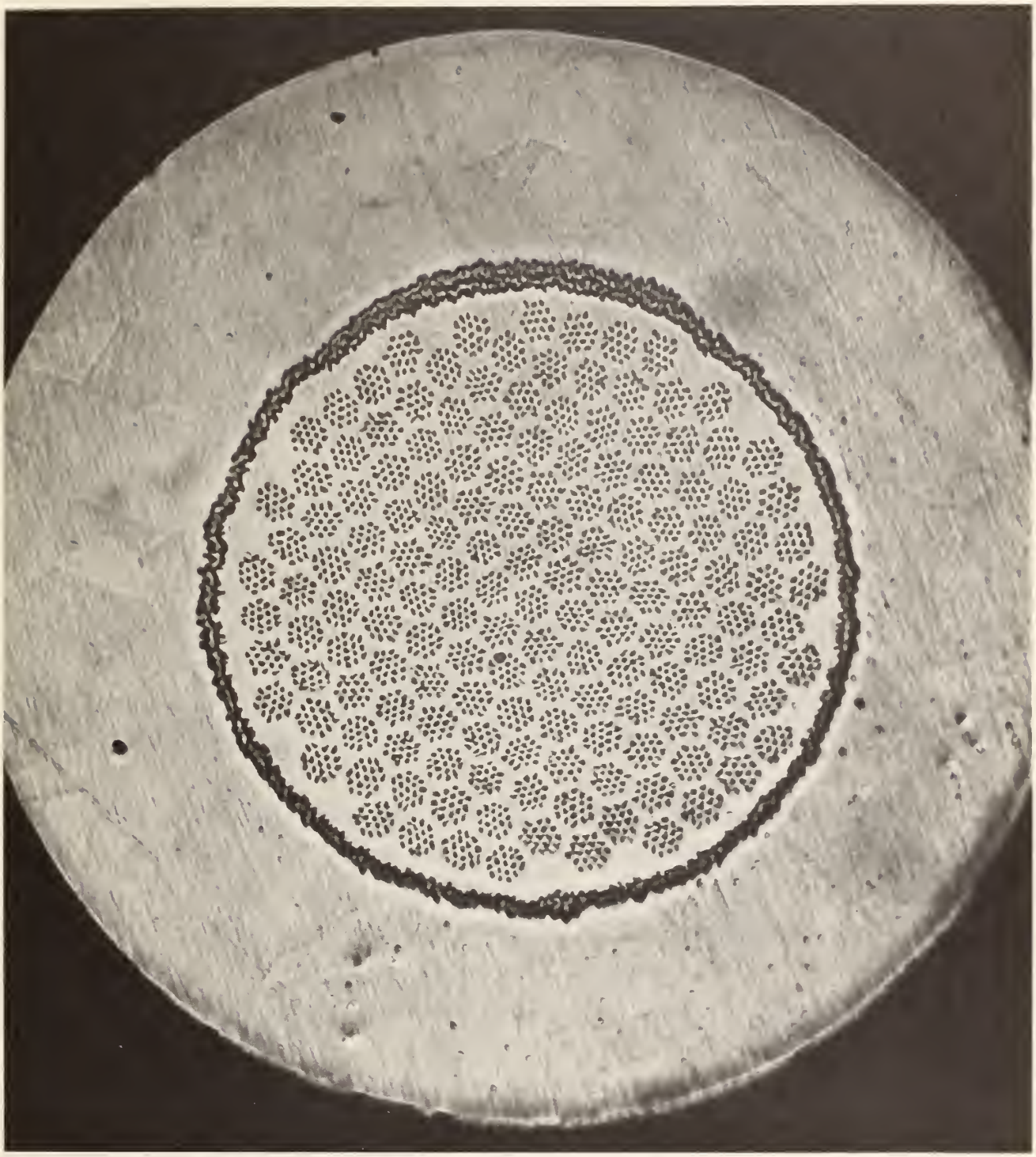

Figure 4.1-2. A cross-sectional photograph of the Nb_3Sn multifilamentary superconductor sample.

The rest of the paper is divided into five major sections presenting the results from particular measurement configurations representing the sample shape: coil, long straight, hairpin, short straight, and "nested" geometries. Each of these sections details different aspects of current transfer as exhibited by the geometry. The first four geometries are commonly used in critical current measurements and are illustrated on figure 4.1-3. The "nested" geometry is a unique one used to study current transfer symmetry and current transfer response to multiple parallel and perpendicular field regions.

COIL GEOMETRY

The coil geometry is the best geometry for studying current transfer in a relatively uniform applied magnetic field with long current contacts and a long active sample length (length between the current contacts). In this geometry the magnitude and current dependence of E_t were measured as a function of current contact length, ℓ_{cc}, and of distance, x, from the current contact with the magnetic field essentially perpendicular to the wire axis. Both twisted and untwisted multifilamentary Nb_3Sn samples were measured to determine if twisting had any effect on current transfer. A comparison of E_t (I, x, ℓ_{cc}) is made below between data from this geometry and the theories.

The effect of current contact length on current transfer was determined by making a set of measurements of the voltage between adjacent taps on the coil sample and then cutting the sample in the current contact region and repeating the measurements. This allowed a systematic study of the effect of the length of the current contact. The value used for x (the distance from the current contact) of a pair of voltage taps was obtained by an iterative process that takes into account the electric field as a function of x. The taps were relatively close together so x was not a strong function of the iterative process, especially at large x.

The current dependence of E_t is more complicated than was implicit in the theories. Figure 4.1-1 shows that this dependence is not linear as predicted, but can be approximated by a power law,

$$E_t \propto I^{p(x)} , \qquad (4.1\text{-}4)$$

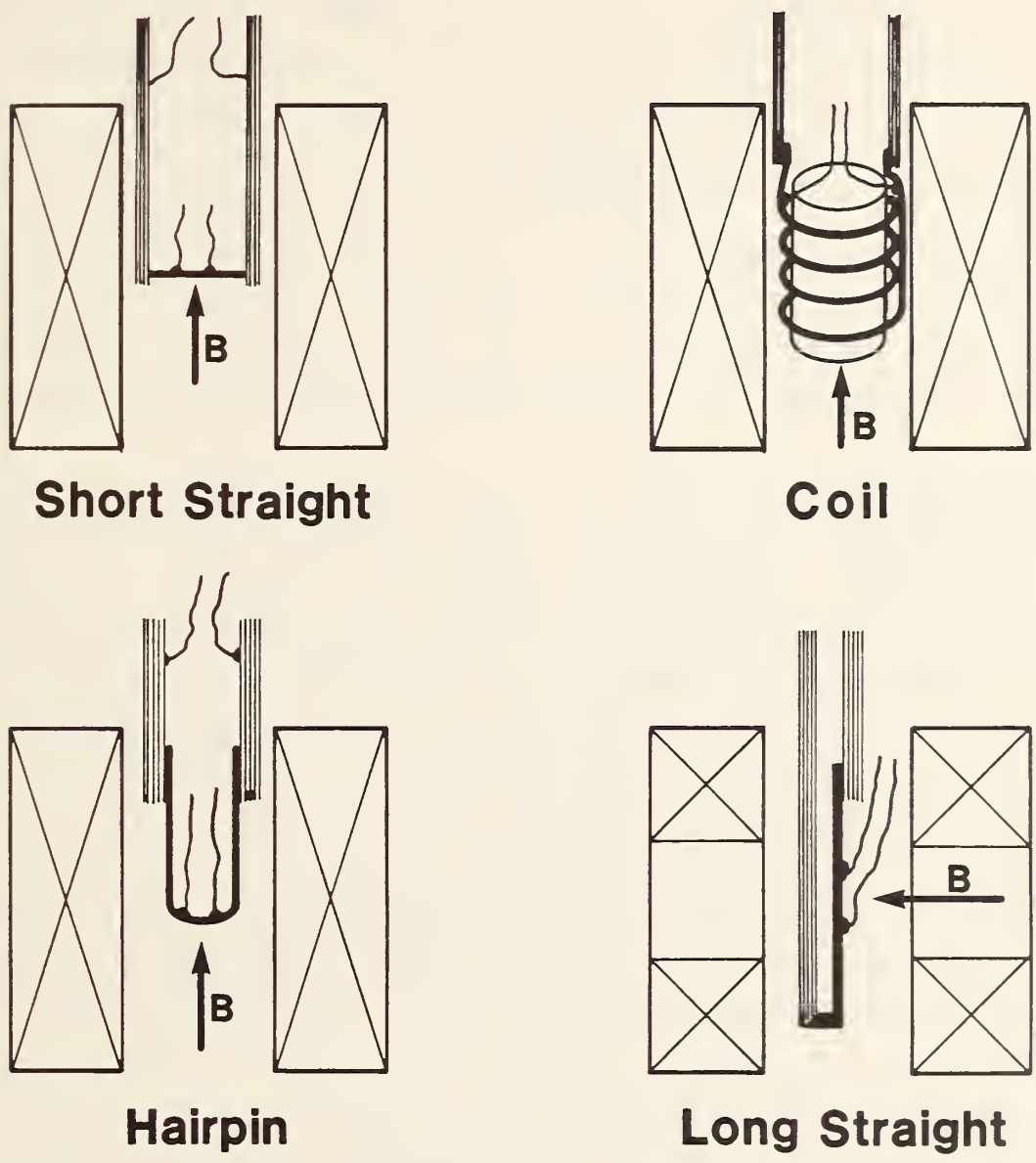

Figure 4.1-3. The four common critical current measurement configurations.

where p is nearly independent of distance from the current contact (except very near the current contact) and may be a function of sample as well. This empirical approximation works well for all of the data, but the power does tend to increase slightly with current. The value of p was determined from data (30 to 60% of I_c at 10^{-12} Ω·cm) on a twisted sample with three different values of ℓ_{cc} (0.29, 1.27, and 5.15 cm) in a magnetic field of 4 T. The values of p as a function of x are plotted on figure 4.1-4. For the lowest x (x = 0.18 cm, x/d $\cong$ 4.2) p is approximately 1.6 and it increases with distance very quickly to an asymptote of 2.5 ± 1 for x greater than 1 cm. For the larger values of x/d there was more uncertainty in p because of the low E_t, thus the larger range. The value of p had little dependence on either ℓ_{cc} or the magnetic field, and data on an untwisted sample gave similar results.

Extending the theory of Ref. [4.1-2] can give insight into the empirical power law dependence of E_t on current and on position [4.1-5]. The theory in Ref. [4.1-2] starts by modeling the conductor as two regions, a cylindrical rod and a concentric cylindrical shell. What results from considering current transfer between these two regions is eq (4.1-2), which has an implicit linear current dependence of E_t. Extending this to a continuum of concentric cylindrical shells, however, does not give the same linear result. If the transfer between two shells is linear, then the transfer among three shells will be linear for the lower currents, until J in the second shell approaches J_c for that shell, then there will start to be superposed another linear dependence. Thus, together there will be two linear segments with different slopes. Extending to a continuum of concentric cylindrical shells should give a smooth curve with p > 1. The transfer voltage at small x may be dominated by the current flowing in the outer copper jacket (essentially two conducting shells) rather than the current transfer taking place through the interfilament copper matrix (approaching a continuum of conducting shells). This could be why the transfer characteristic has a slope close to one for small x and an almost constant (asymptotic) slope for large x.

There are cases where a linear transfer characteristic (p = 1) would be expected. These cases have a single or dominant transfer barrier between parallel conductive paths. An example of a single transfer barrier would be a monofilament or a single layer superconductor in a normal metal matrix. An

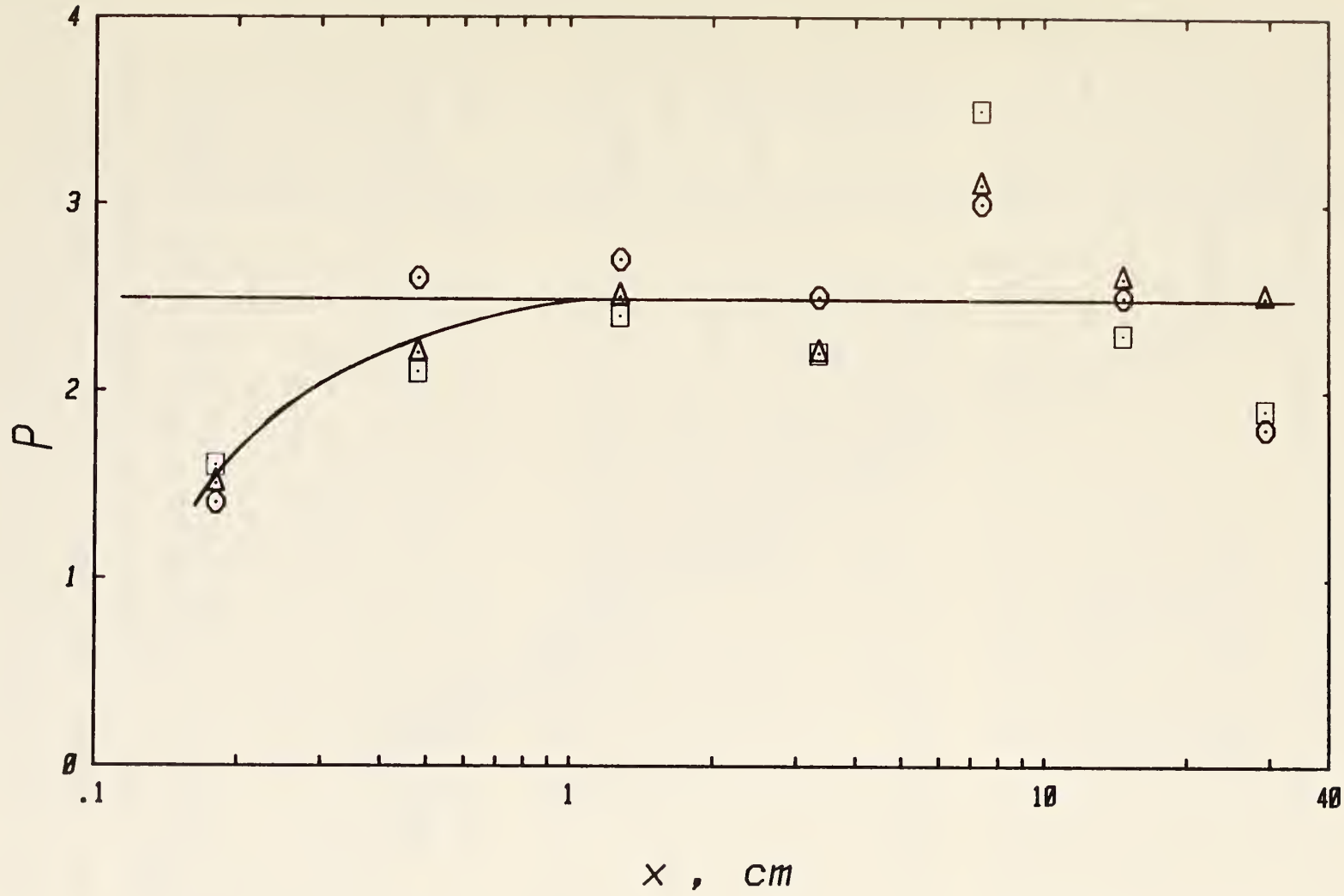

Figure 4.1-4. The value of p determined on a twisted sample with three different values of ℓ_{cc} (0.29 cm: square, 1.27 cm: triangle, 5.15 cm: circle) in a magnetic field of 4 T.

example of a dominant transfer barrier would be a monolithic, multifilamentary Cu-NbTi composite soldered over its entire length to a copper shunt. In this case the solder interface could dominate the transfer due to the relative resistance of the interface compared to the copper. If the superconductor is long enough, all of the current will transfer into the superconductor; however, the voltage drop across the solder may dominate the nonlinear transfer voltage of the copper matrix. Multiple linear segments in the transfer characteristic may be caused by a filament distribution that has rings or regions of filament that are separated by a relatively thick ring of normal metal, a high resistivity diffusion barrier, or the intrastrand material of a cabled conductor.

Data taken on the magnitude of E_t as a function of x and ℓ_{cc} is shown in figure 4.1-5 for a 338 cm long coil sample of twisted Nb_3Sn. Plotted are values of E_t at 140 A (60% of I_c at 10^{-12} $\Omega \cdot cm$) in a magnetic field of 4 T, as a function of x for various ℓ_{cc}. Similar data were obtained at 8 T. The points on the plot at the largest x were taken on voltage taps positioned around the center of the coil sample. E_t was also measured on the other side of the sample center at two values of x, 3.2 and 14.6 cm. These data indicate that the current transfer is symmetric; the transfer in has the same profile as the transfer out. This symmetry will be described further in the discussion of the other sample geometries.

$E_t(x)$ has a strong dependence on ℓ_{cc} at low x (see fig. 4.1-5). This is most likely due to variations in the local critical current. The percent difference between the measured values of $I_c(x)$ of the twisted coil and I_c at the center of the coil (264 A) is also given on figure 4.1-5. The largest change in I_c occurs in the region that is not monotonic. The variations in I_c were caused in part by the defects (inhomogeneities, filament breakage, and nonuniformity) introduced by the twisting and also by the slight change in magnetic field along the coil. The latter effect could account for a 2.5% change in I_c. The defects introduced by the twisting are thought to account for the rest of the variations in I_c, and these give the irregular $E_t(x)$. The dominant source of current transfer is still the joint, except at the very low E_t or large x, where the variations in I_c start to dominate.

The other two sources of current transfer, bending strain and self field, are probably not significant, although if either of these two sources were

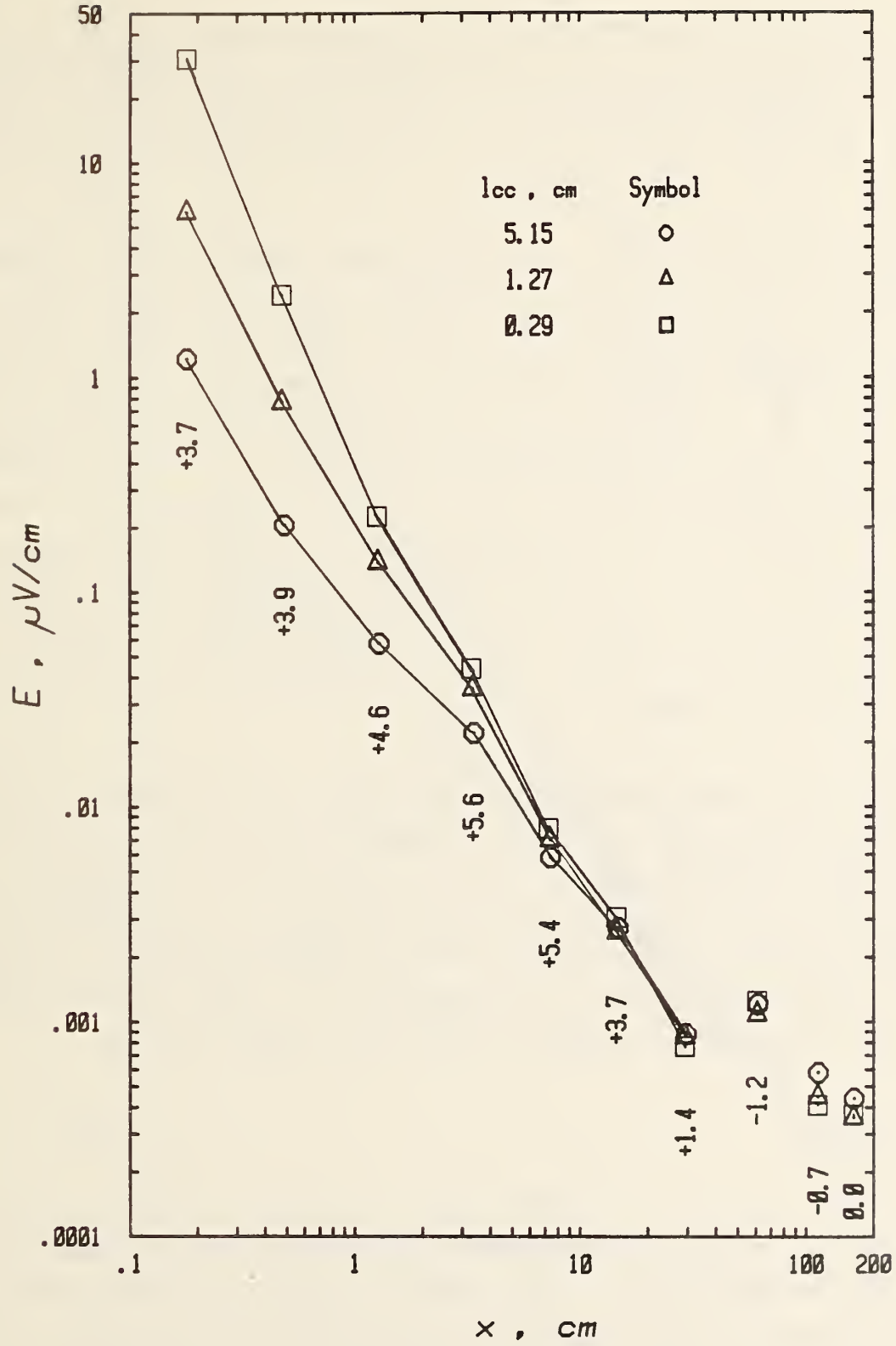

Figure 4.1-5. E_t as a function of x and ℓ_{cc} at 140 A (60% of I_c at 10^{-12} Ω·cm) and 4 T. The percentage difference of the critical currents are indicated under each position.

present, they would cause E_t to be less dependent on x. The bending strain effect should be negligible, because the sample was reacted in shape. The self field source, just like bending strain, only occurs near I_c, so it should be negligible at this current.

A comparison of data taken on a twisted sample (same as fig. 4.1-5) and on an untwisted sample (85 cm long coil sample) is shown on figure 4.1-6. As mentioned above, the dependences of E_t on I and ℓ_{cc} are very similar for the twisted and untwisted samples. Furthermore, as can be seen on figure 4.1-6, the magnitude of E_t as a function of x is only slightly different for the two samples at low x. This difference is probably due to a systematic difference in the current contacts or of the position x = 0, for the two runs. The points at the largest x, for the untwisted sample, are those from voltage taps across the center of the coil; this is why they are slightly higher than the twisted data. Thus, the effect of twisting is insignificant, except as mentioned above for the very low E_t where the inhomogeneities introduced by twisting cause E_t to be higher.

A comparison of the experimental $\rho_t(x/d)$ with that predicted for this sample by the current transfer theories is shown on figure 4.1-7. Plotted are the experimental values of ρ_t extrapolated to I_c (using eq (4.1-4)) in a magnetic field of 4 T, as a function of x/d for various ℓ_{cc}. The theories are in reasonable agreement with each other (within geometric factors), and they are close to the experimental ρ_t at the shortest ℓ_{cc}. This indicates that their initial conditions are closest to this current contact length.

HAIRPIN GEOMETRY

The hairpin geometry is an example where the sample axis changes along its length from parallel, to perpendicular, to parallel with the relatively uniform applied magnetic field. This creates a change in the local critical current of the sample along its length that results in current transfer. In general the transition from parallel to perpendicular can be gradual in the case of the round bottom hairpin (constant radius semicircular) or more abrupt as in the flat bottom hairpin (two small radius of curvature sections and a flat section) . Measurements made on samples in both these geometries are described below.

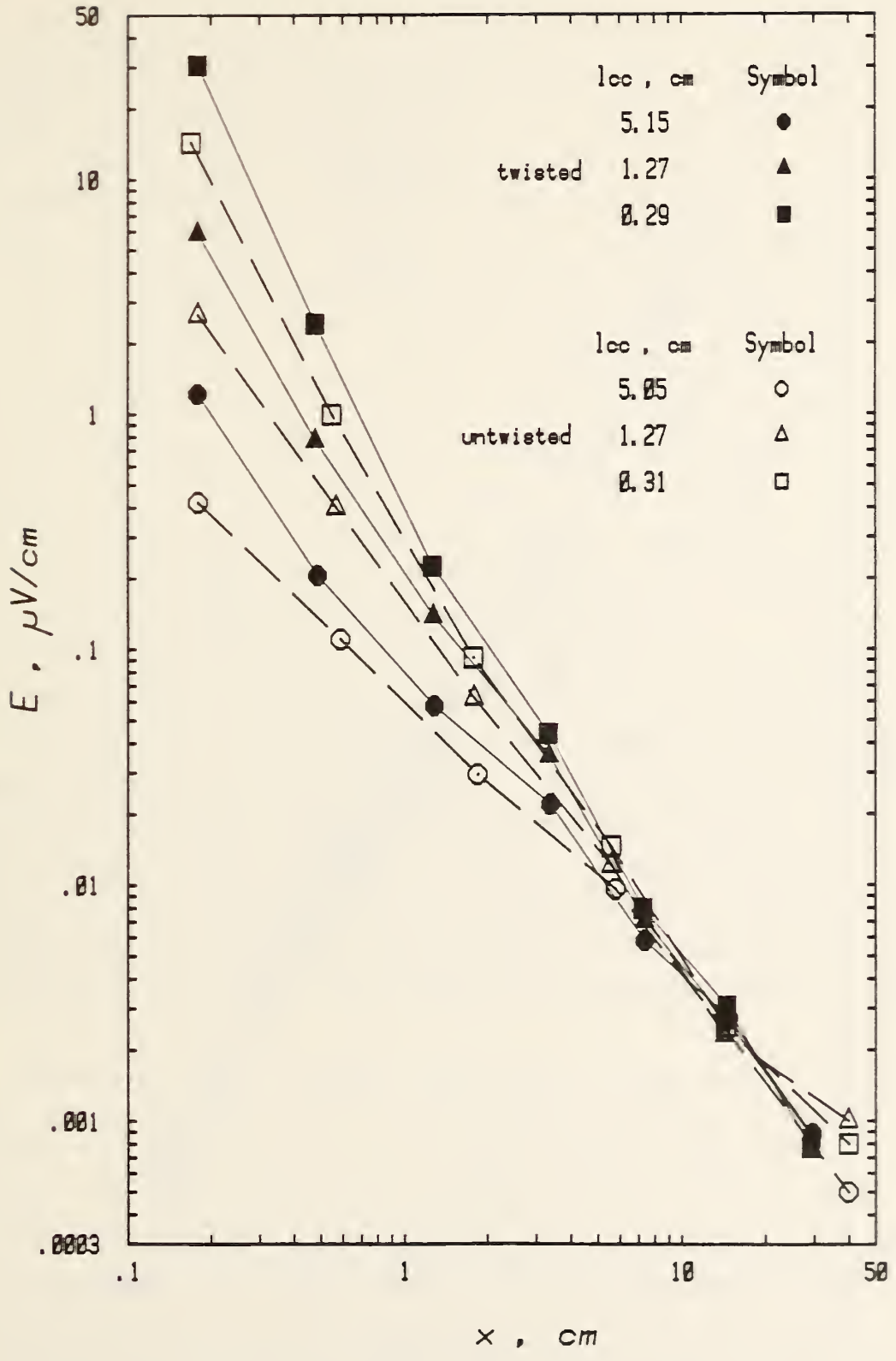

Figure 4.1-6. E as a function of x and ℓ_{cc} at 140 A and 4 T for twisted and untwisted samples.

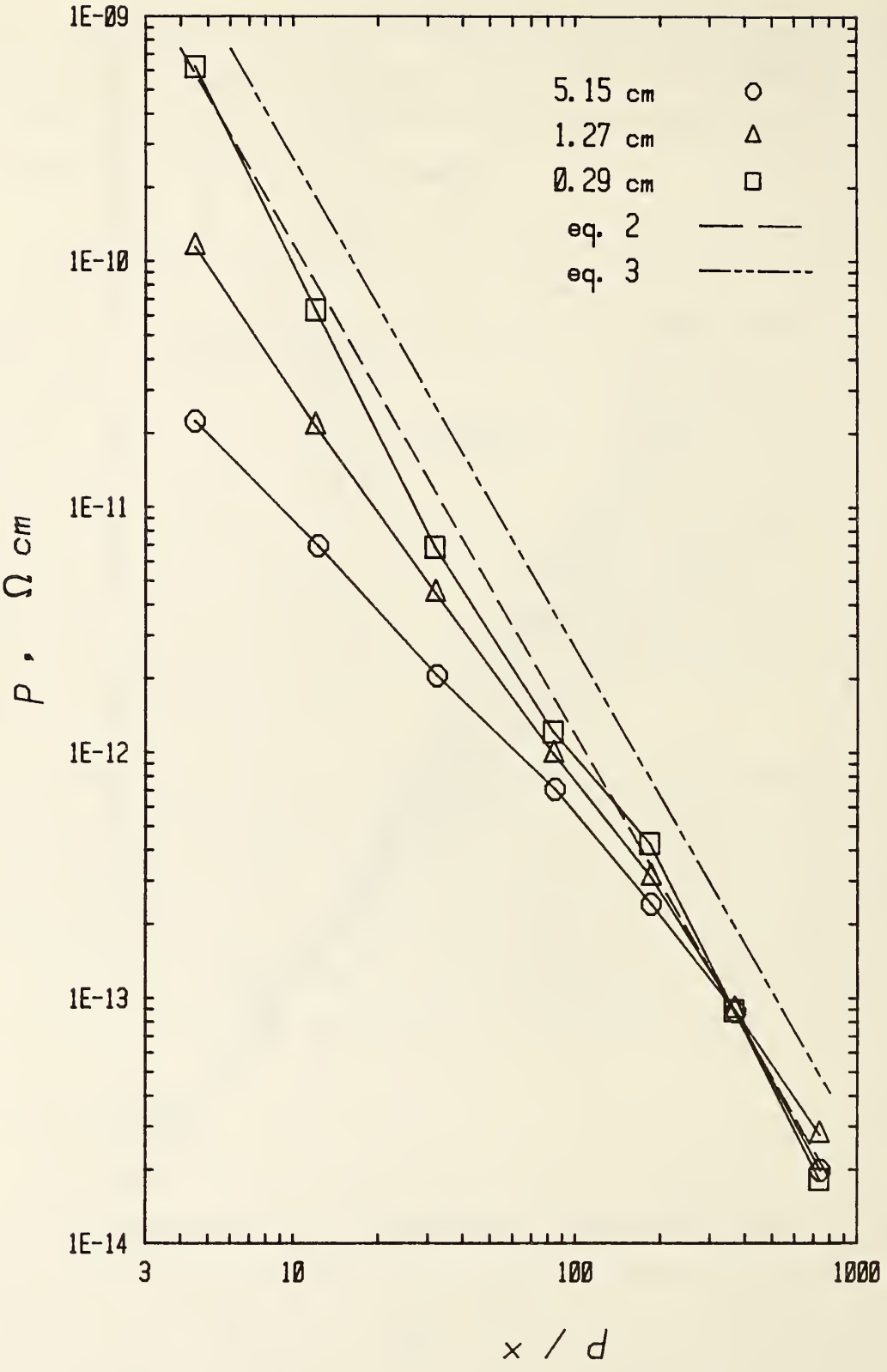

Figure 4.1-7. ρ as a function of x/d extrapolated to I_c at 4 T for three different values of ℓ_{cc} compared with eqs (4.1-2) and (4.1-3).

The current transfer profile, $E_t(x)$, was measured on the parallel field sections of a hairpin sample and compared with that in a perpendicular (coil geometry) field of the same magnitude. The profiles are shown on figure 4.1-8 for a current of 140 A, 4 T field, and the same ℓ_{cc}, 1.3 cm. The data for the perpendicular field were adjusted from data with ℓ_{cc} = 1.27 cm to ℓ_{cc} = 1.3 cm (the same as the hairpin), but this adjustment was only 3% at the lowest x and even less for larger x. Values of E_t for the two geometries at the lowest x are very close and E_t in the parallel field drops much faster with x, especially for the larger x. Also, when E = 1 nV/cm, x is $\sim$4 cm in the parallel field and about ten times this value, 40 cm, in perpendicular field. The difference between current transfer in these two orientations is due to the dependence of ρ_s on the critical current. It is not clear if these data indicate whether or not the assumption in eq (4.1-1) is valid; however, these data do indicate that, if at all, it would take a very long length in parallel field before the current distribution would be uniform. In any case, however, it is advantageous to keep the joint and associated current transfer away from the critical current measurement region. The electric field profiles of each end of the sample in the parallel field were symmetric, implying that the transfer into the conductor occurs in the same way as the transfer out. A similar parallel-field current transfer profile was measured on the parallel-field sections of the "nested coil" geometry described below. Also, the results of the measurements on current transfer in the low-field region of the long geometry were consistent with these data, which suggest an equivalence of the current transfer in low field with that in parallel field.

Additional current transfer takes place on the bottom of the hairpin, since the distribution has to be more uniform than in the parallel field section. As the angle between the applied magnetic field and the sample axis changes, I_c changes; thus, ρ_s changes and the rest of the transfer occurs. The distributed nature of this cause for current transfer makes the current transfer profile more complex. The current transfer profile, $E_t(x)$, for the round bottom hairpin geometry is given at 140 A and 4 T in figure 4.1-9. The horizontal line sections of the histogram-like curve are the measured average electric field between the voltage taps. The dashed line is an estimate of the shape of the actual curve. The current transfer electric field increases from the parallel-field value of less than 1 nV/cm to a peak of several

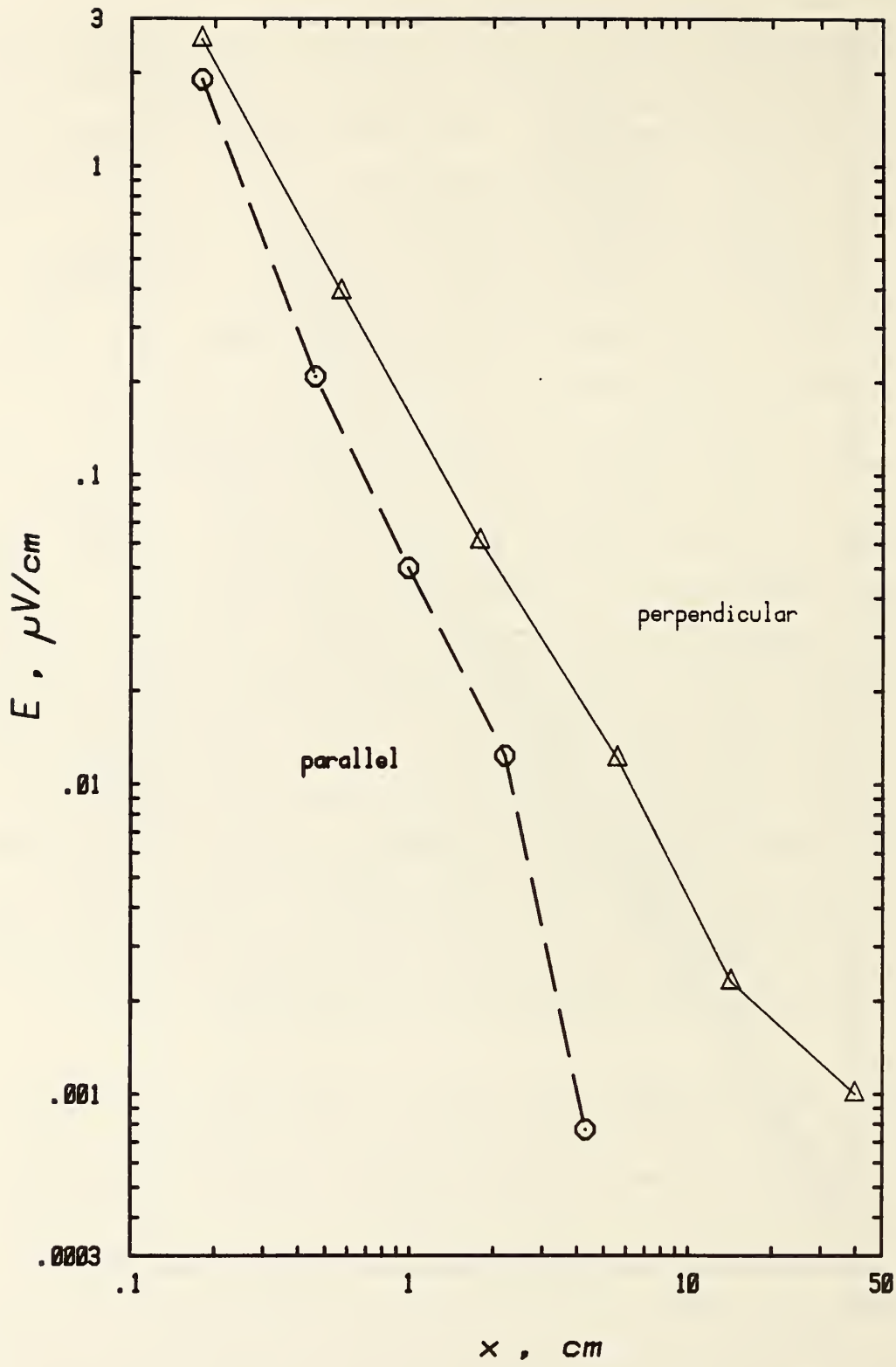

Figure 4.1-8. E as a function of x at 140 A, 4 T, and ℓ_{cc} = 1.3 cm for perpendicular and parallel magnetic fields.

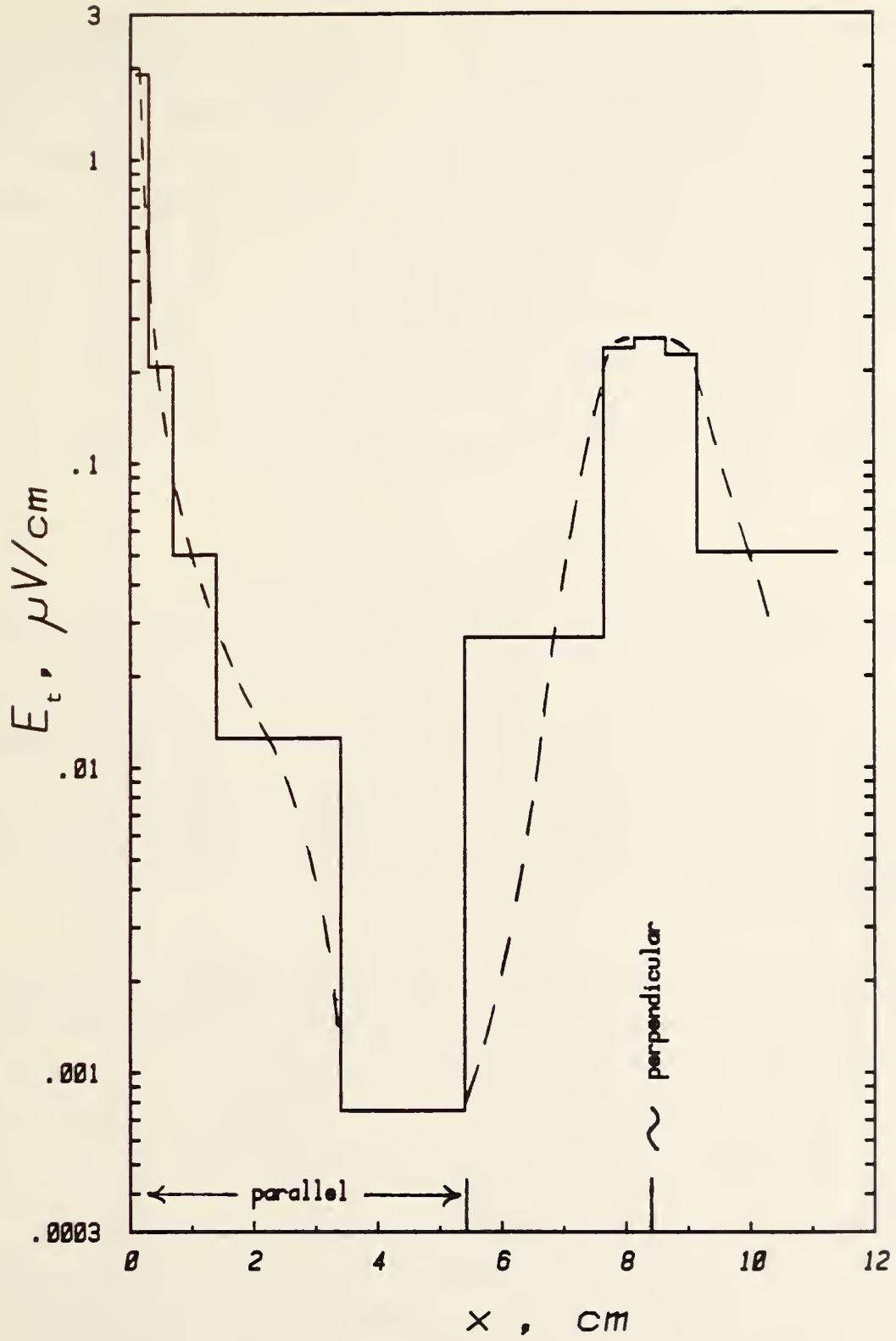

Figure 4.1-9. E_t as a function of x at 140 A and 4 T for the hairpin geometry (parallel and perpendicular magnetic field regions).

hundred nV/cm at the center of the round bottom, the essentially perpendicular-field region. For the flat bottom hairpin geometries the current transfer electric field increases more rapidly from the parallel-field value to peak value of several hundred nV/cm just around the corner in the perpendicular field. It decreased slightly at the center of the flat bottom. In both hairpin geometries the current transfer electric fields were symmetric about the center of the perpendicular-field region just as in the parallel-field region. This implies that the current starts to transfer to the outer filaments on the other side of center, symmetric with the inward transfer. The results of measurements on current transfer in the field-gradient region of the long geometry showed a similar symmetry about the center of the field.

LONG GEOMETRY

In the long geometry, figure 4.1-3, the sample traverses several magnetic field regions; from low, to gradient, to relatively uniform perpendicular, to gradient, and then to low again. This creates a change in the local critical current of the sample along its length similar to that in the hairpin geometry and thus a current transfer phenomenon that is similar to that of the hairpin geometry. The measurements made on the sample in the low-field regions of the long geometry were consistent with that observed in the parallel field regions of the hairpin geometry.

Additional current transfer takes place in the gradient and uniform magnetic field regions, since the distribution has to be more uniform than in the low field regions. The current transfer profile, $E_t(x)$, for the long geometry is given in figure 4.1-10 at 140 A and 4 T. The horizontal line sections of the histogram-like curve are the measured average electric field between the voltage taps and the vertical line sections just connect the adjacent horizontal lines. Some percentages of the central magnetic field are given on the linear x axis which correspond to the vertical lines of the histogram curve. The dashed curve is an estimate of the shape of the actual curve. E_t rises sharply between 50% and 75% of the central magnetic field, it peaks between 95% and 99%, and decreases slightly in the central region. Measurements were made with the current in the other direction, and the values of the voltage at the same current magnitude were the same to within 1% ±5 nV.

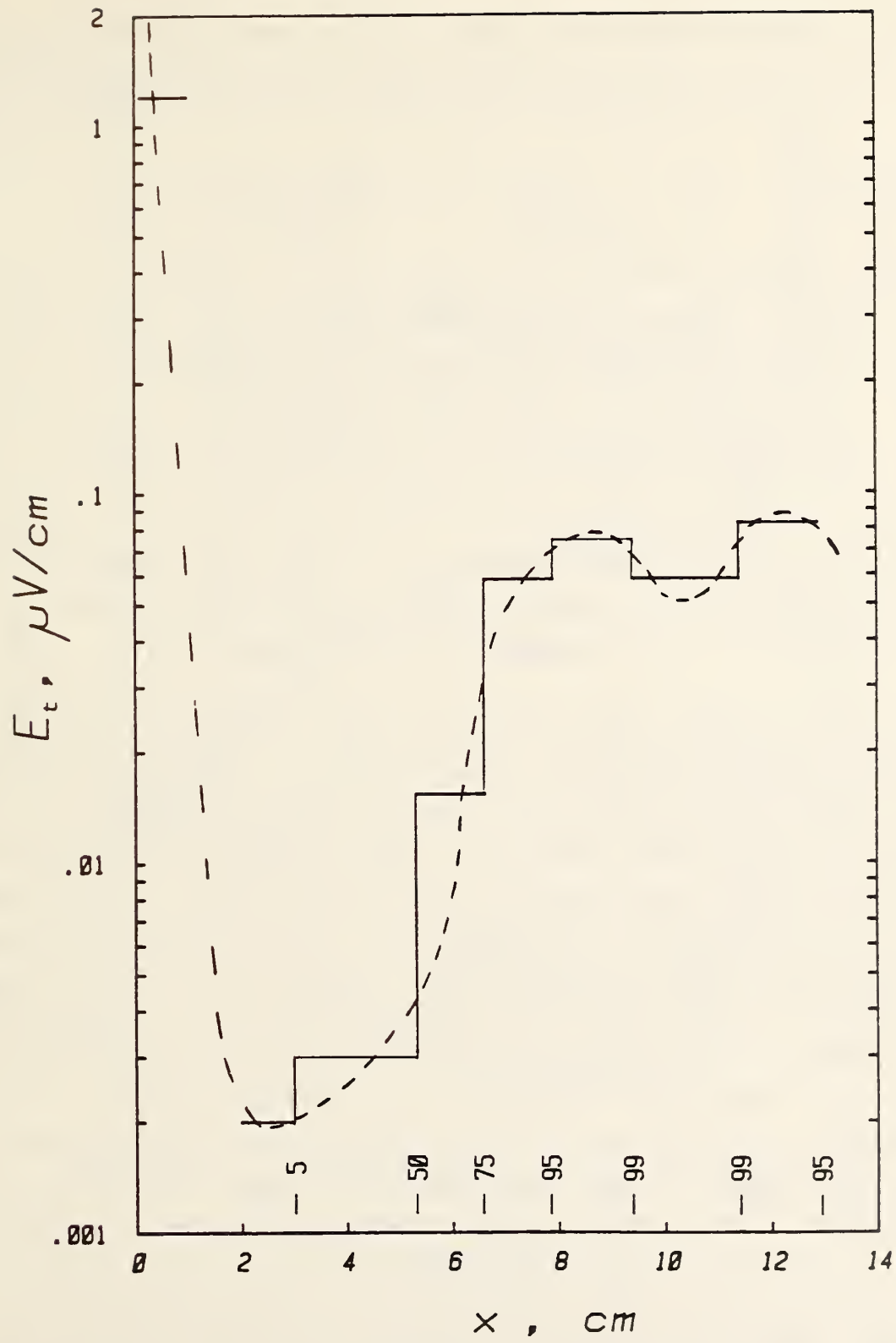

Figure 4.1-10. E_t as a function of x at 140 A and 4 T for the long geometry, with the percentage of the central magnetic field also indicated along the x-axis.

These data, as with the hairpin data, imply that the current starts to transfer to the outer filaments on the other side of center, symmetric with the transfer in.

SHORT GEOMETRY

The short geometry, figure 4.1-3, can be the worst case as far as current transfer is concerned since the overall sample length, current contact length, and separation of current contact and voltage taps are limited by the bore of the magnet. It is, however, the easiest geometry and thus it is often used. Generally in this simple geometry eq (4.1-2) or (4.1-3) can be used to estimate the current transfer resistivity. However, in cases where the current injection into the sample is not symmetric, the current transfer voltage can be larger than calculated by these equations. It can be negative and can even be significant for NbTi superconductors [4.1-6]. This was the subject of extensive study in Ref. [4.1-6], which will only be summarized here.

Data taken on short samples of commercial multifilamentary superconductors have uncovered anomalous V-I characteristics. A voltage was detected at currents well below the sharp upturn in the V-I characteristic near I_c. It was apparently due to current transfer but larger in magnitude than would be expected from previous current-transfer analysis [4.1-2, 4.1-3]. Further data indicated that the voltage was strongly dependent on the voltage tap location. In fact, the voltage measured below I_c in the current direction between some taps was negative. In all cases, as I_c was approached, the V-I characteristic returned to "normal." Experimental data on a Cu-NbTi superconductor is given in figure 4.1-11. This effect can be much larger in Nb_3Sn samples. It was demonstrated that this effect was due to a combination of current injection, current transfer, and superconducting filament twist pitch. This study also demonstrated that if the current injection were made more symmetric, either by making the current contact longer than a twist length or having a symmetric current contact, then the current transfer could be estimated by eq (4.1-2) or (4.1-3). Due to the large difference in the resistivity of the copper jacket and the bronze core, the current injection into most Nb_3Sn samples is symmetric. However, most Cu-NbTi superconductors do not have this large difference, so current contacts as long as a twist length may be required.

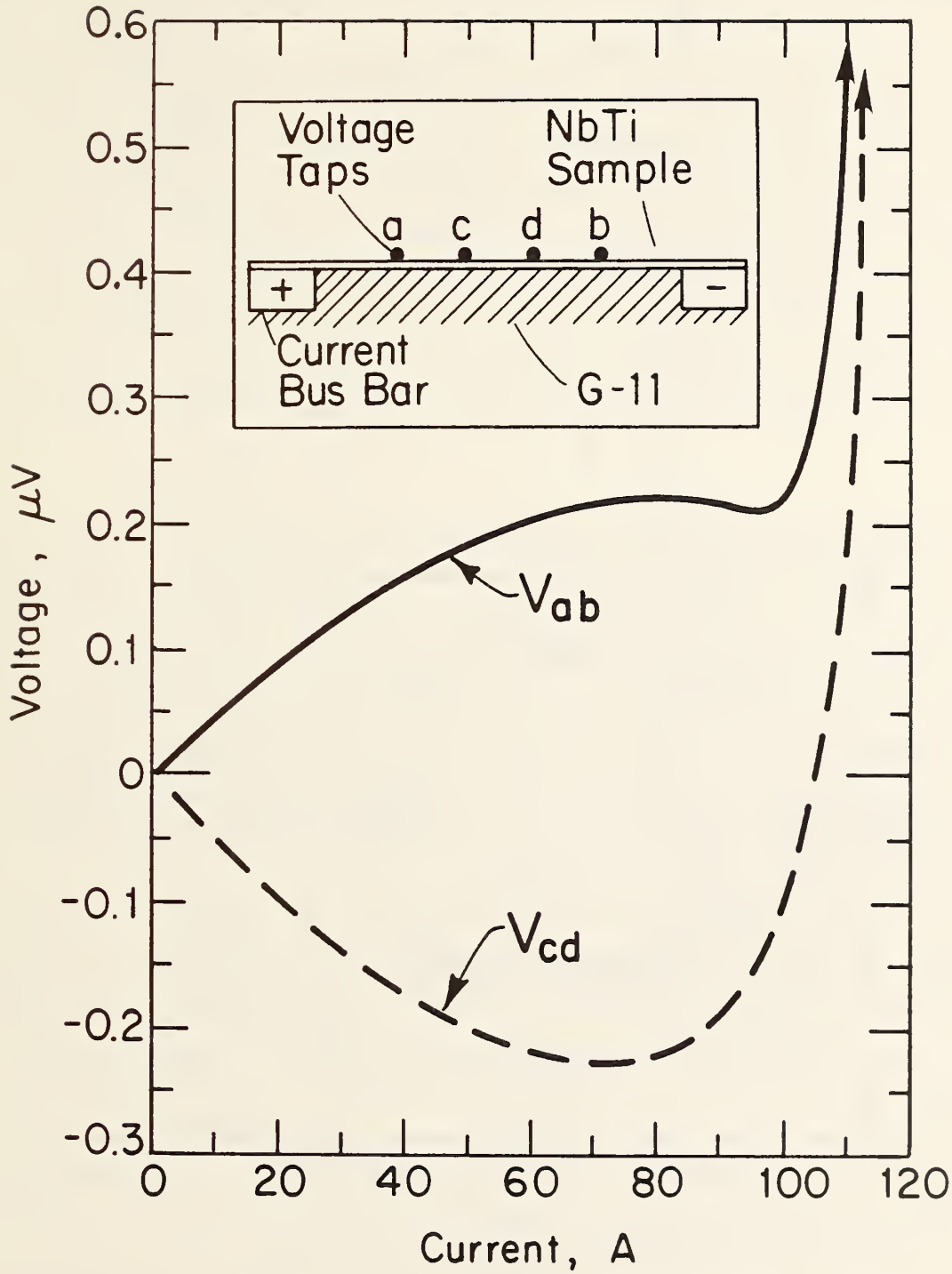

Figure 4.1-11. Experimental voltage versus current on a Cu-NbTi superconductor with nonsymmetric current injection.

NESTED GEOMETRY

A logical extension of the hairpin and long-geometry results is to ask what would happen if there were multiple parallel and perpendicular field sections? Would the current transfer in and out among the filaments on every perpendicular field section? If it did, this would have a serious implication for superconducting magnet design in cases where the windings are such that the magnitude or angle of the magnetic field cycles many times. It would affect the persistence, refrigeration load, and the stability of the system. The nested geometry was designed to answer these questions. It was the subject of a recent paper [4.1-7] and the main point will only be summarized here.

The specially shaped sample for this study was formed, prior to its reaction, in a rectangular pancake coil, nested geometry, as illustrated in figure 4.1-12. Measurements were made with the magnetic field in the plane of the coil, pointed down in the figure. This configuration has a number of sections that are essentially parallel or perpendicular to the magnetic field. The ends of the sample are in parallel field. These sections are sequentially numbered for reference on figure 4.1-12 so that all of the odd-numbered sections are in parallel field and the even-numbered in perpendicular field.

Evidence of the response of the current to multiple parallel and perpendicular field sections is also given on figure 4.1-12. The measured voltage and tap separation of each adjacent pair of taps is indicated for a current of 75 A in a field of 8 T (same sample as in table 4.1-1). These voltages changed sign and had about the same magnitude when the current direction was reversed. This indicated a symmetry of current transfer with the direction of electron flow. Furthermore, there is a symmetry of current transfer voltage about the center of the configuration, section 6.

The symmetry of current-transfer voltage can be explained with equipotential lines as indicated by the data. When the current reaches the first perpendicular-field section, 2, it then has to transfer into the inner filaments, since the reduced critical current forces the distribution of current among the filaments in this region to be more uniform than that in the parallel

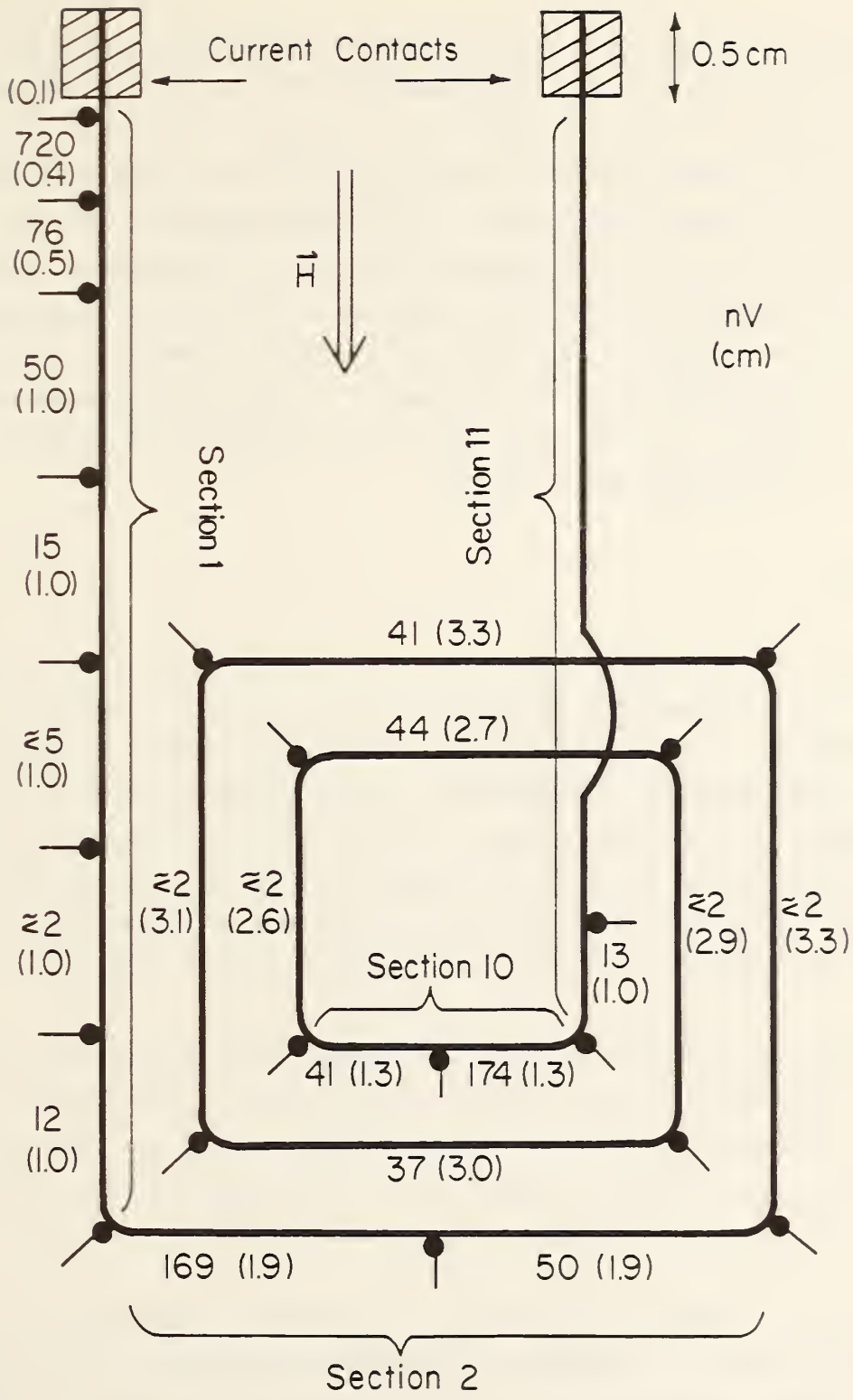

Figure 4.1-12. Nested sample geometry with voltage in nV (tap separation in cm) for each adjacent pair of taps at a current of 75 A, with a magnetic field of 8 T in the plane of the coil.

field region, 1. Now consider the symmetric section, 10, here the voltage profile indicates that the current, in this the last perpendicular field section, starts to transfer to the outer filaments in the same way that it transferred to the inner ones in section 2. This may seem surprising at first, but can be explained using a time-reversal argument. If the presence of the current contact creates equipotential lines in the superconductor for current entering, it will have the same equipotential lines for current leaving the superconductor. Thus, these data indicate that once the current distribution is uniform among the filaments, it will not change much (except due to inhomogeneities in the superconducting properties) until the last part of the last perpendicular-field region.

CONCLUSIONS

Transfer characteristic measurements on samples with short current contacts (10 wire diameters) had good agreement with the existing current transfer theories. The transfer voltage for samples with long current contacts (100 wire diameters) was smaller by as much as a factor of 10 in the region adjacent to the current contact (within 10 wire diameters). This would reduce the heating and increase the stability of the critical current sample. The transfer voltage far away from the current contact (more than 100 wire diameters) was relatively independent of current contact length.

The largest discrepancy between the measurements reported here and the theories is the shape of the transfer characteristic. The transfer voltage can depend on current to a power as high as 2.5. There are cases where the relationship can be linear (a small effect can always be approximated as linear), but the continuum filament distribution should give a curve.

Another conclusion of this study is that the full-magnitude, perpendicular magnetic field is necessary to complete the transfer. The length in lower or parallel magnetic field will not complete the transfer no matter how long it is. Associated with this, the current transfer into a conductor is symmetric with the transfer out of a conductor. The current will transfer to the outer filaments of a conductor in the last full-magnitude, perpendicular magnetic field before a lower or parallel field region is reached. A possible

application of this effect would be to put the two ends of the wire through a seperate high field coil to force the current into a more uniform distribution.

Current transfer that results from nonsymmetric current injection can cause very strange voltage-current curves, often with peaks or negative voltages that are larger than theory would predict. This is very common in low voltage measurements on copper stabilized, multifilamentary NbTi superconductors. It has been explained by a combination of current transfer and filament twist. The magnitude of this effect can be reduced by making the current injection more symmetric.

4.2 Lap-Joint Resistance of Multifilamentary Superconductors

by L. F. Goodrich and E. S. Pittman

INTRODUCTION

Lap joints between superconductors are important for most magnet designs, and studying them will also help understand the role of the current contact in critical current measurements. Lap joints were made by overlapping two lengths of a superconducting wire and joining them with Pb-Sn solder. Lap joints of various lengths were measured on commercial multifilamentary niobium-titanium (NbTi) and niobium-tin (Nb_3Sn) samples. The voltage-current characteristics of the joint were measured at 4 K as a function of joint length, L_j, magnetic field, H, and orientation of the magnetic field with respect to the joint.

This work is an extension to the study reported in Ref [4.2-1]. Here, measurements were made on Nb_3Sn samples and on longer NbTi joints. The components of the lap-joint resistance (solder and boundary; surface copper; and transfer) were identified and separated. The emphasis here is on the shape and magnitude of the current transfer component. A model for the lap-joint resistance is compared to the experimental data.

EXPERIMENT

The lap-joint resistance data presented here were taken on two commercial multifilamentary superconductors. These two were superconductors based on NbTi and Nb_3Sn. The NbTi sample had cross-sectional dimensions of 0.53 x 0.68 mm, with 180 filaments and a copper to non copper ratio of 1.8. The NbTi filaments had a twist length of 1.25 cm per twist and the wire had a critical current of about 103 A at 8 T, 4 K and 0.1 μV/cm. The Nb_3Sn sample was 0.70 mm in diameter, with 2869 filaments and a copper to non copper ratio of 1.7. The Nb_3Sn sample was originally not twisted and unreacted, thus it could be twisted and formed to shape prior to its reaction. The samples measured here were twisted with a twist length of about 1.3 cm per twist and reacted on a coil mandrel. The Nb_3Sn wire had a critical current of about 93 A at 8 T, 4 K and 0.1 μV/cm.

Digital measurements were made of the voltage, V, across the lap joint as a function of current, I. The lap-joint resistance, R, as a function of current was defined as V/I (not as the local slope of the V-I curve). At each magnetic field, several current sweeps were made to reduce the time between the zero-current readings (thermoelectric voltage check points) and thus reduce the change in thermoelectric voltage. Repeat measurements were made at the lower currents because of the increased error in those measurements due to the lower voltage levels. The estimated limits to accuracy were the larger of 50 nV or 1% for the voltage and 50 mA or 0.25% for the current. The estimated limits to precision were the larger of 10 nV or 0.2% for the voltage and 10 mA or 0.05% for the current.

The magnetic field and current dependence of the lap-joint resistance was used to separate the three components of this resistance. Figure 4.2-1 shows an illustration of the lap joint with the components indicated. The value of the resistance extrapolated to zero current was defined as R0. R0 has two separable components, a part that does not have magnetoresistance and a part that is separated by assuming a certain magnetoresistance. The first part of R0 is the combination of solder and boundary (solder/copper) resistance which will be defined as R1. The second part of R0 is the resistance of the surface layer of copper, defined as R2, that was separated from R0 using the estimated magnetoresistance. The third component, defined as R3, of the lap-joint resistance is the current dependent part or transfer resistance above R0. This component may also have a contribution from the boundary resistance between the copper and the NbTi filaments. The current dependence of the transfer resistance scales with magnetic field when the current is normalized by dividing by the critical current, I_c. Data from a wide range of magnetic fields were used to test this normalization.

Magnetoresistance measurements were not made on the copper or the solder used in this study. The copper values were estimated using the transverse resistivity Kohler plot [4.2-2] and the measured resistivity ratio (70.5). Longitudinal magnetoresistance does not follow a universal Kohler-like plot. It saturates with magnetic field, and the difference between transverse and longitudinal magnetoresistance is less for lower resistivity ratio copper [4.2-3]. A further discussion of this is given in the NbTi result section.

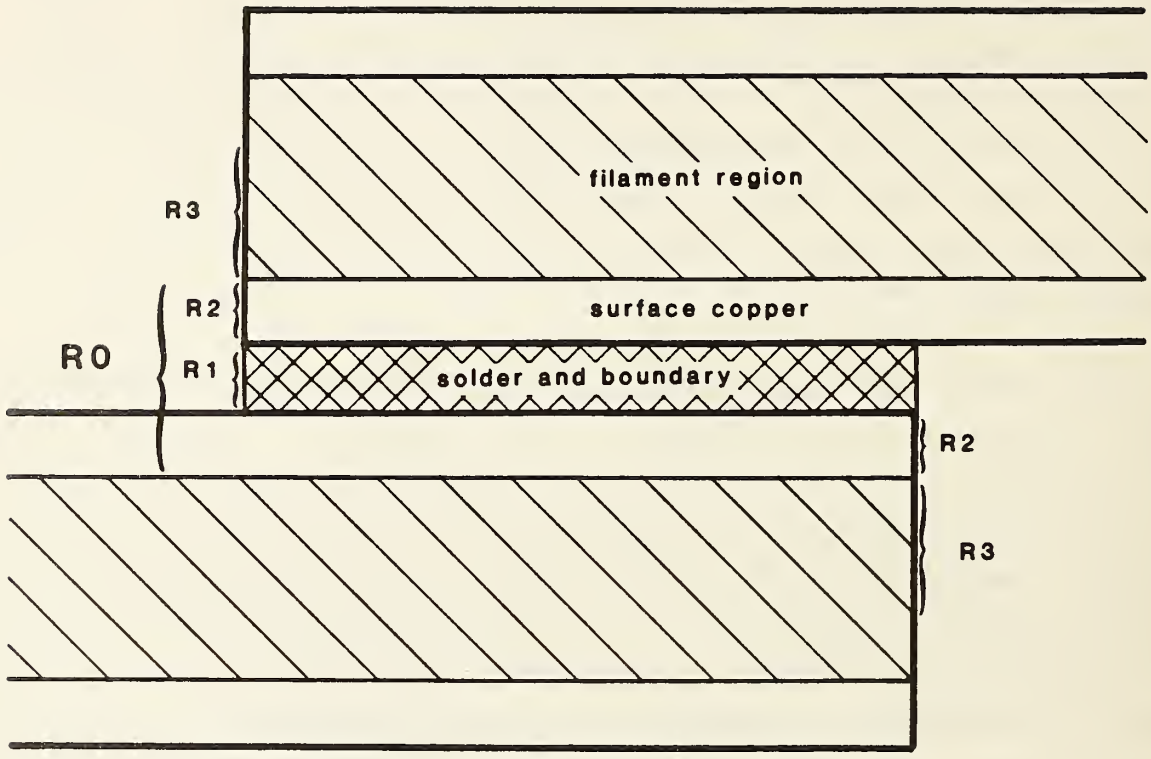

Figure 4.2-1. Illustration of the lap joint with the components of resistance indicated.

The magnetoresistance of the solder was obtained from Ref. [4.2-4]. The magnetoresistance of the solder was ignored because the resistivity of the solder was expected to change by about 7% at 9 T, compared to an expected 157% change for the copper. Furthermore, it was not known a priori how much of R1 is solder resistance and how much is boundary resistance.

Resistivity measurements were made on both wire samples and a number of solders. The low temperature measurements were made just above the transition temperature. The copper resistivity was determined from measurements on the composite superconductor and on the superconductor after the copper was chemically removed. The low temperature resistivity of two Sn-50Pb solders were measured, one with a resin flux core (0.36 μΩ·cm) and the other solid (0.58 μΩ·cm). The cross-sectional area of the cored solder was determined by density measurements. The resistivity ratio, room temperature to low temperature, was 35.9 for the cored and 26.2 for the solid, which indicates that impurity variation is the cause of this difference. The resistivity from Ref. [4.2-4] for Sn-50Pb was 0.59 μΩ cm. A sample of the solder used to make the lap joints was not available, so the more conservative value of resistivity was used, 0.58 μΩ cm. The measured low temperature resistivity of Sn-37Pb solder was 0.64 μΩ cm.

RESULTS FOR NbTi JOINTS

The NbTi joints were made by lapping the wider sides of two pretinned wires and soldering with Pb-Sn solder. An effort was made to keep the joint aligned and as thin as possible, using a minimum amount of solder. Measurements were made with a coil sample geometry in a simple solenoidal magnet and with a straight sample geometry in a radial access magnet.

Six lap joints were measured on the coil geometry. The joints were clamped and soldered in a pair of concentric semicylinders of fiberglass-epoxy. All of the coil geometry joints were soldered with Sn-50 Pb alloy. Two samples were made; each with three joints. Adjacent joints were separated by about 10 cm (190 times the wire thickness). Each voltage tap was more than 3.8 cm (70 times the wire thickness) from the edge of the lap joint.

The joint was oriented so that the magnetic field was essentially perpendicular to the wire axis (coil pitch approximately 5 degrees) and parallel to the wider face of the wire (in the curved plane of the joint interface). A fiberglass-epoxy shim was used to support one wire on each joint as it made the transition to the coil form. A small amount of varnish was used to hold the wire and shim in place. The range of overlap lengths was from 2.4 to 29.6 mm (4.5 to 56 times the wire thickness). Joint areas were from 1.6 to 20 mm^2.

Two lap joints were measured on the straight geometry in a radial access magnet, where the effect of joint interface orientation was studied (keeping the magnetic field perpendicular to the wire axis). The fiberglassepoxy sample holder had a step machined in the bottom of a groove to support the wire in the joint region. The sample was also varnished in the groove to reduce motion as the Lorentz force was rotated from into the bottom of the groove to one side of the groove. One of the joints was soldered with Sn-50 Pb alloy (3.8 mm lap) and the other with Sn-37 Pb eutectic alloy (4.6 mm lap). Each voltage tap was more than 1.2 cm (20 times the wire thickness) from the edge of the lap joint.

Typical lap-joint resistance data as a function of normalized current is shown in figure 4.2-2. The normalizing I_c was about 690 A at 1 T and 63 A at 9 T. This normalization produces a relatively uniform family of curves over this wide range of magnetic fields and critical currents. The increase in R0 (the resistance extrapolated to zero current) with magnetic field is attributed to the magnetoresistance of the surface copper layer (R2). The difference between the joint resistance extrapolated to I_c and R0 (the transfer resistance, R3) also has a magnetoresistance due to the interfilament copper. There is a slight heating effect evident in these data at the highest current for the lowest magnetic field, where the resistance is higher than expected. This effect was more pronounced in the shorter joints, but it should only affect the determination of R3. Figure 4.2-3 is a plot of the current dependent joint resistance, normalized by R3, versus normalized current at 7 T for all eight NbTi joints. The shape is very similar for all of the joints tested.

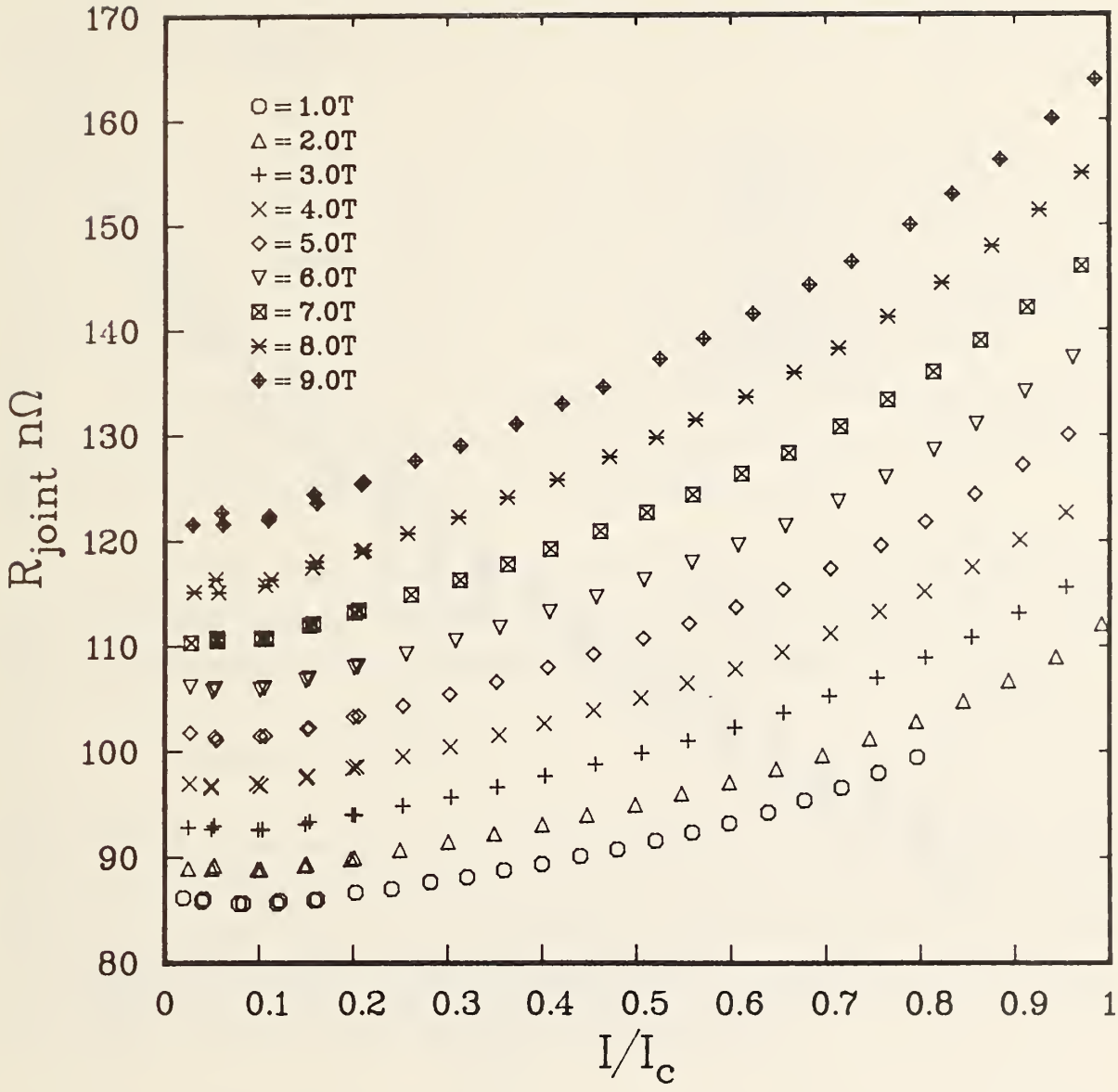

Figure 4.2-2. Typical NbTi lap-joint resistance as a function of normalized current for various magnetic fields.

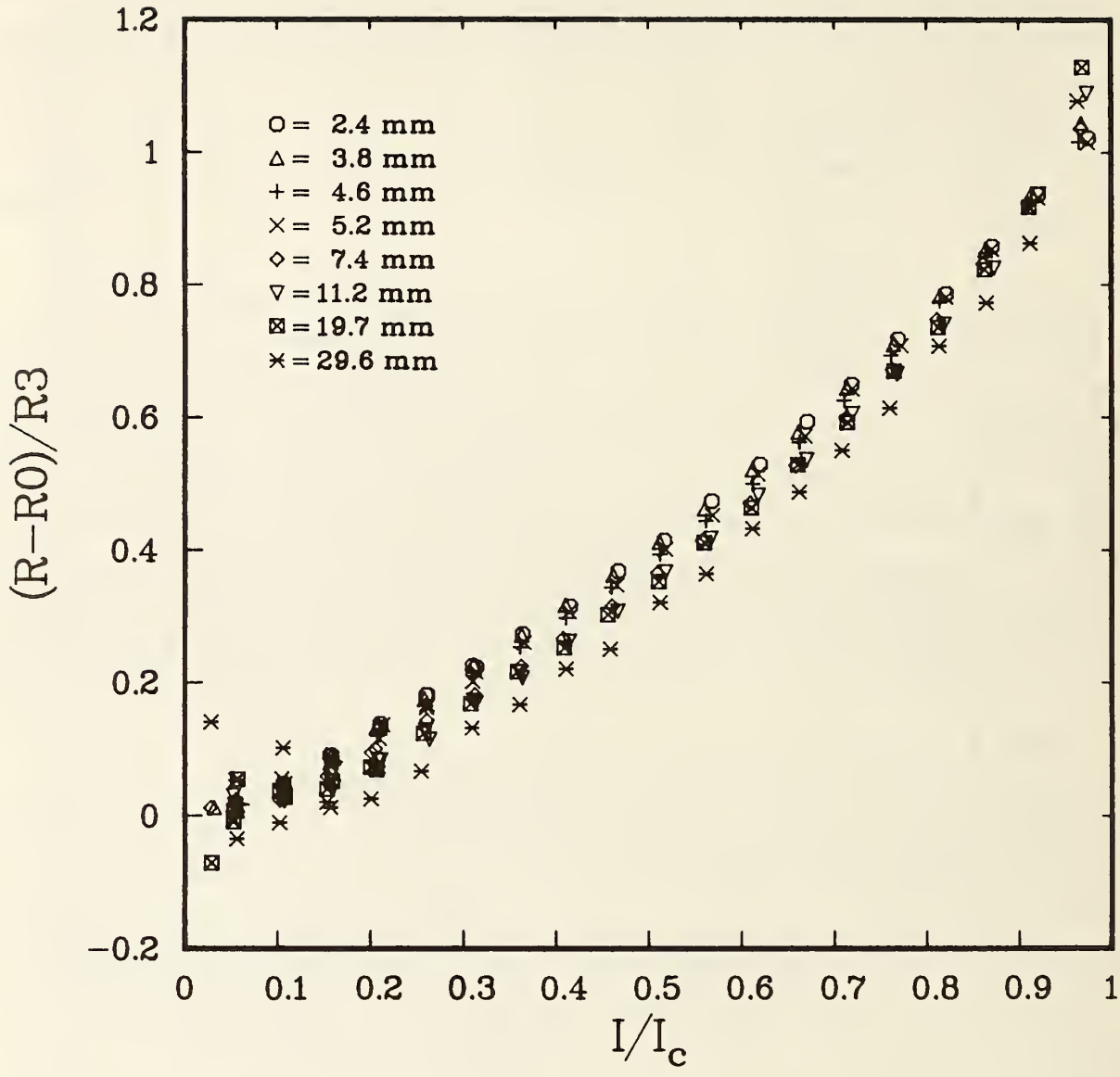

Figure 4.2-3. Current dependent joint resistance, normalized by the resistance at I_c, versus normalized current at 7 T for all eight NbTi joints.

A simplified model of the current dependent resistance of a rectangular wire lap joint is given in Appendix 4.2-A. The result is

$$R = \frac{\rho t}{wL} \frac{I}{I_c} \quad , \tag{4.2-1}$$

where ρ is the resistivity of the filament region, t is the thickness and w is the width of the filament region of each wire. This gives a resistance that increases linearly with I (and a voltage that goes as I^2). The measured R increases with current faster than linear (see fig. 4.2-2), approximately as the current raised to the power of 1.52 ± 20% for magnetic field of 4 T and above, for all eight joints. The nonlinear resistivity of the superconducting filaments and their distribution in the cross section are the most likely cause of this current dependence of the joint resistance.

The R0 values were determined for each magnetic field, for each lap joint. The lower current resistance data (up to 33% of I_c) were fitted with a least-squares routine to the empirical current dependence

$$R(I) = R0 + cI^{1.5}. \tag{4.2-2}$$

The determined R0 values were not a strong function of the value of the power, as long as the fit was restricted to the lower currents. This restriction was somewhat arbitrary, but it was a compromise between forcing the fit or having a small number of points. These R0 values for each joint were then fit with a least-squares routine to the magnetic field dependence

$$R0(H) = R1 + R2\ F(H) \quad , \tag{4.2-3}$$

where

$$F(H) = \frac{r(H)}{r(H=0)}, \tag{4.2-4}$$

a unitless parameter that has the magnetoresistance dependence expected for the surface copper $(1+\Delta r/r)$. Notice that F=1 at H=0.

An intrinsic parameter, $\rho\ell$, for the solder and boundary resistance can be obtained for each lap joint by taking the product of R1 and the lap-joint area. This quantity, $\rho\ell$, is the product of the resistivity and length in the direction of current transfer from one wire to the other. Table 4.2-1 gives the R1 and $\rho\ell$ values for each lap joint, and figure 4.2-4 is a plot of $\rho\ell$ versus L_j. The average value of $\rho\ell$ is 3.5 $n\Omega\cdot cm^2$ (±40%). The variation in this parameter with lap-joint length seemed to be random and is probably due to variation in the thickness of the solder layer and boundary resistance. The 3.8 and 4.6 mm lap joints were measured in the straight geometry. The 4.6 mm lap joint was the only one soldered with eutectic SnPb solder (the others were soldered with Sn-50Pb), but its $\rho\ell$ wasn't significantly different from that of the others.

The thickness of the solder layer was measured for the five longest joints in order to estimate the solder contribution to R1. Each joint was ground and polished perpendicular to the curved plane of the joint interface. Photographs were taken along the length of the joint at two levels, approximately 1/3 and 2/3 of the way into the joint width. The average solder thickness was estimated from measurements taken on these photographs. The average solder thickness for each of the three longest joints was about 3 μm,

Table 4.2-1. R1 and R2 components of NbTi lap-joint resistance.

L_j (mm)	R1 (nΩ)	$\rho\ell$ (nΩ·cm)	R2 (nΩ)	ρ (nΩ·cm)
2.4	251.5	4.2	55.2	44
3.8	113.8	3.0	39.1	49
4.6	119.1	3.8	31.8	49
5.2	119.3	4.3	33.5	58
7.4	59.5	3.1	23.8	59
11.2	63.2	4.9	14.2	53
19.7	18.5	2.5	8.9	58
29.6	10.5	2.2	5.3	52

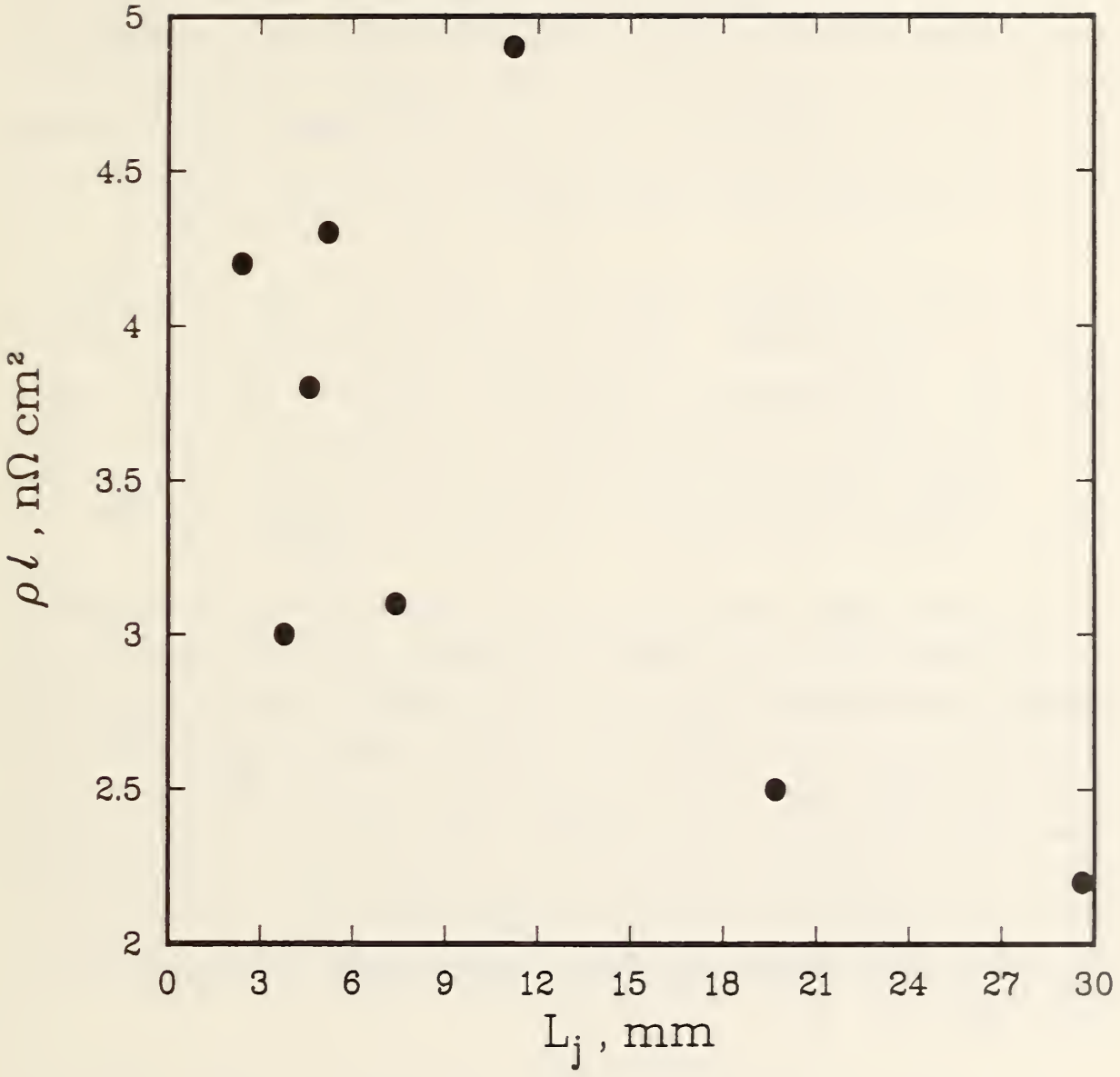

Figure 4.2-4. Product of resistivity and length in the direction of current transfer, $\rho\ell$ for the solder and boundary resistance versus L_j.

which would give a $\rho\ell$ of about 0.2 $n\Omega \cdot cm^2$ for the solder alone. The average was the reciprocal of the sum of the reciprocal thicknesses, which is appropriate for parallel path resistance. This implies that as much as 90% of R1 is due to boundary resistance and the variation in $\rho\ell$ is due to variation in boundary conditions. The wires in the other two joints photographed were tipped. This was indicated by the very different average solder thicknesses: 2 and 34 μm for the 5.4 mm joint, and 5 and 12 μm for the 7.4 mm joint. So for thin solder layers, the solder contribution is a small part of R1.

The boundary resistance between the solder and copper was the main component of $\rho\ell$ (3.5 $\mu\Omega \cdot cm^2$). Not much attention was given to wire surface preparation. The insulation was chemically stripped and the wire surface cleaned with alcohol. This could account for the relatively large variation in $\rho\ell$. Similar results have been reported for the boundary resistance in aluminum stabilized superconductors [4.2-5] where $\rho\ell$ was 3 to 8 $\mu\Omega$ cm^2.

The surface copper resistivity can be computed from R2 for each joint. It is not obvious what area, width, and thickness are appropriate for this resistance extrapolated to zero current. The filament region is not rectangular and has an all copper region in the center. Using the width of the first row of the filament region (0.4 mm) and twice the average distance from the copper layer to the first row of filaments (60 μm) gives the values listed in table 4.2-1 and plotted on figure 4.2-5. The value expected from the resistivity ratio measurement (25 $n\Omega \cdot cm$) is smaller than this value, 53 $n\Omega$ cm. A number of possible sources that would make the copper resistivity appear larger follow:

1. Thickness variation and voids in the solder layer and variation in boundary resistance will cause a nonuniform current density that will effectively decrease the cross-sectional area of the copper layer.

2. Joint misalignment will cause the current to flow a longer distance through the copper.

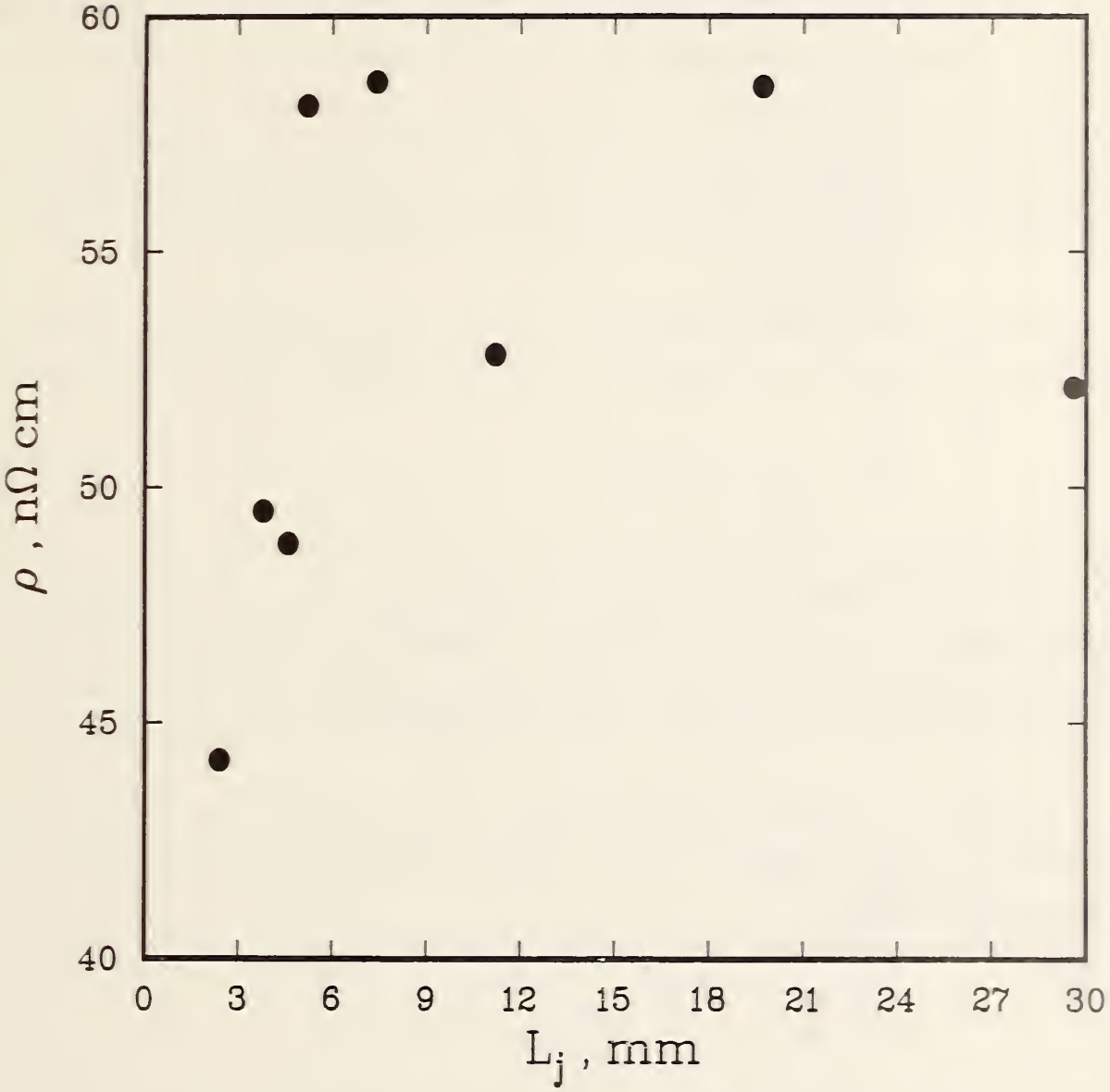

Figure 4.2-5. Surface copper resistivity versus L_j.

3. The fact that the filaments do not form a solid layer will cause the current to focus on each filament.

4. The current will not flow exactly perpendicular to the joint interface, which would make the effective length longer.

These effects are expected to be sufficient to explain the discrepancy. Other effects, like a solder alloyed copper layer or filament boundary resistance, would not be included in R2 due to the magnetoresistance separation method.

The R3 values were determined for each magnetic field using a least-squares fit routine to the emperical current dependence of the joint resistance,

$$R(I) - R0 = R3(I/I_c)^K, \qquad (4.2\text{-}5)$$

where R3 and the exponent, K, were the fitting variables. A linear fit was made of the logarithm of this equation and the fit was restricted to I/I_c values from 0.3 to 0.9. The values of K determined by this fit are shown versus magnetic field for all of the NbTi lap joints in figure 4.2-6. K tended to be smaller for larger magnetic fields and for shorter joints.

In order to find out what information can be obtained from the R3 values, consider the model (Appendix 4.2-A) for the current dependent resistance at the critical current,

$$R3 = \frac{\rho t}{wL} .$$

One way to view this expression is that the average distance that the current penetrates into the filament region of each wire is t/2 when the current is at I_c. For a wire with twisted filaments this model is still valid if the lap-joint length is much smaller than one twist length. For the lap-joint length longer than one twist length, this distance will become half of the transposition thickness. The effective wire thickness can be calculated from the R3 data after an assumption of the value of the effective transverse resistivity. If the transverse resistivity of the filaments is zero, then the

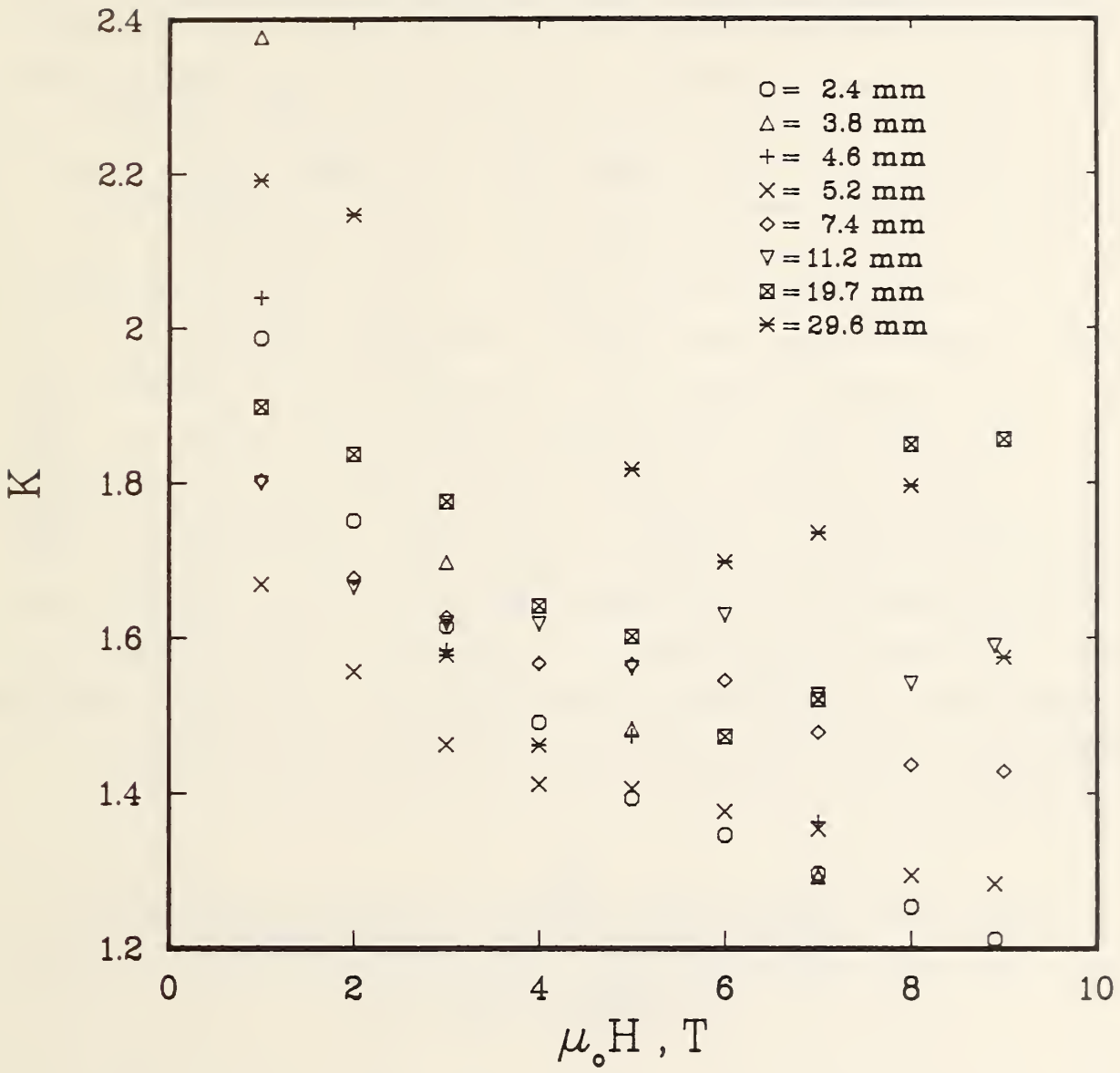

Figure 4.2-6. The exponent, K, of the current dependence versus magnetic fields for all of the NbTi lap joints.

effective transverse resistivity of the filament region would be about one half that of the copper (approximately 1 to 1 copper to superconductor by volume in the filament region). With this assumption, the effective width of the wire can be calculated taking into account the copper layer on the sides and in the center of the conductor. The values for the effective wire thickness are given in table 4.2-2 for all magnetic fields, and on figure 4.2-7 at a magnetic field of 7 T for all eight joints. In table 4.2-2 t_{eff} is almost constant with magnetic field for each joint. A magnetoresistance factor, F, was included in the resistivity of the copper. The only significant departure from this occurred for the shorter joints, at the lower magnetic field (higher current), where the heating was creating a significant temperature rise. The plot of the effective thickness, t_{eff}, illustrates that the expected long joint limit (greater than a twist length) approached the transposition thickness (0.15 mm), the smallest thickness region in which all of the filaments occupy somewhere along the conductor. The 3.8 and 4.6 mm joints were measured embedded with varnish in a fiberglass epoxy groove, so the heating at low field (high current) was significantly more than for the coil geometry. The short joint values of t_{eff}, however, were almost twice the thickness of the filament region (0.44 mm). This is most likely due to the effective resistivity assumption. For the shorter joints, the transverse current density must be large enough that the effective resistivity is closer to that of copper.

Table 4.2-2. Effective wire thickness (in units of mm) for each NbTi lap-joint at various magnetic fields.

L_j (mm)	Magnetic Field (T)								
	1	2	3	4	5	6	7	8	9
2.4	1.48	1.12	1.03	0.93	0.87	0.83	0.81	0.78	0.74
3.8	2.83		1.24		1.04		0.89		
4.6	1.64		0.97		0.89		0.83		
5.2	0.94	0.86	0.86	0.84	0.83	0.82	0.82	0.81	0.76
7.4	0.70	0.64	0.64	0.64	0.63	0.62	0.62	0.62	0.60
11.2	0.39	0.36	0.37	0.37	0.37	0.37	0.36	0.37	0.35
19.7	0.25	0.23	0.24	0.24	0.24	0.24	0.24	0.25	0.25
29.6	0.24	0.20	0.19	0.19	0.19	0.19	0.19	0.19	0.20

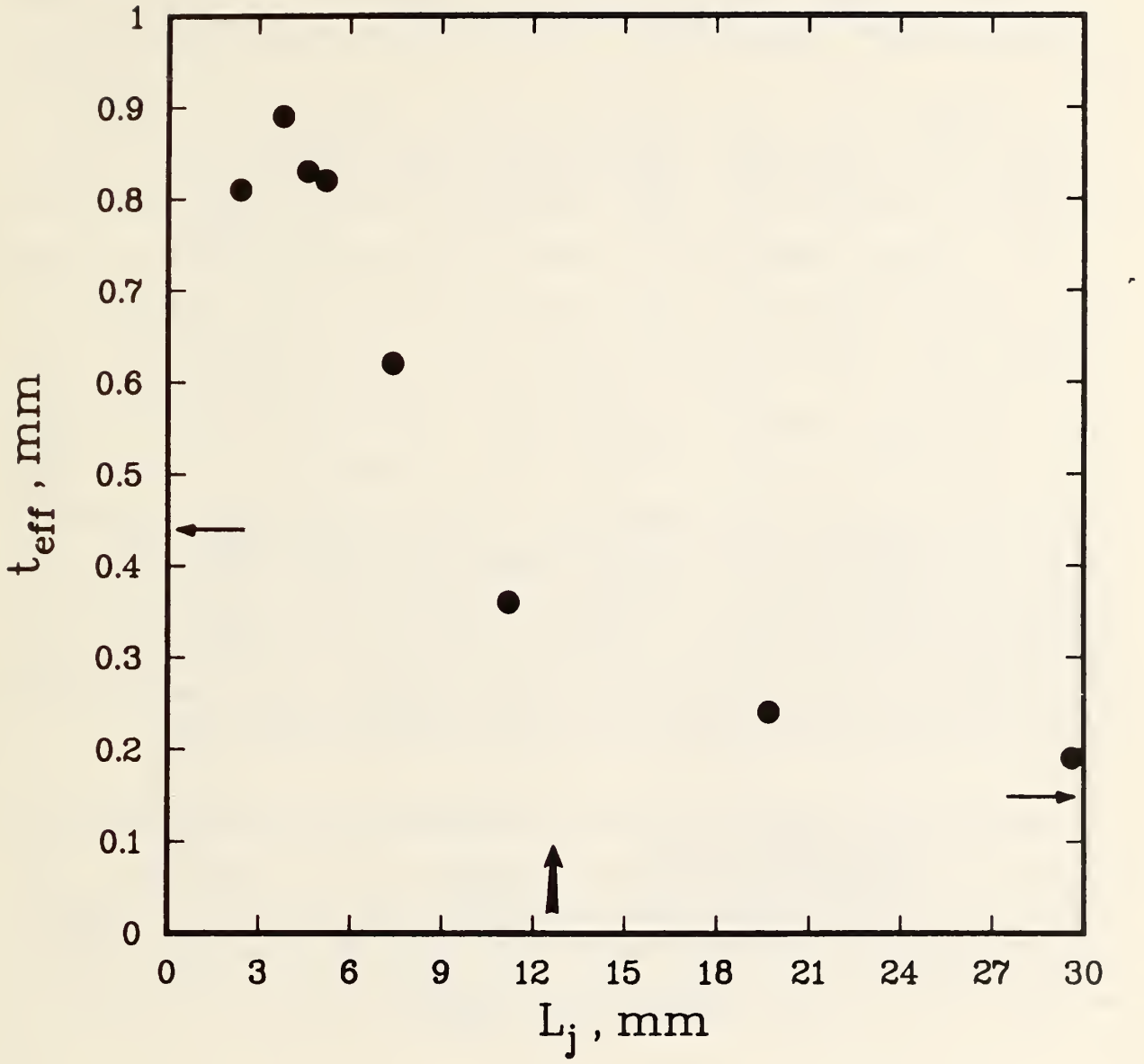

Figure 4.2-7. Effective wire thickness at 7 T for eight joints. The filament twist length is about 12.7 cm. The expected limits for the short and long joints are marked with dashed lines.

Other explanations such as heating would show a stronger magnetic field dependence.

The two straight geometry samples were measured as a function of the orientation of the magnetic field with the joint interface, keeping the magnetic field transverse to the wire axis. The interest was in determining the orientation effect on the magnetoresistance dependence of the joint resistance. The orientation angles are approximate, within a few degrees. The expected symmetry of the results indicated that the orientation was off by 1° to 2°. The zero angle data were taken with the magnetic field in the plane of the joint interface so that the transferring current is in essentially transverse field. The 90° data have the magnetic field perpendicular to the joint interface. The lap-joint resistance was measured as a function of current and magnetic field at 0° and at 90°. The value of R0 was determined for each set of 0° and 90° data. The 0° R0 was separated into R1 and R2 using the assumed magnetoresistance dependence. The R1 was subtracted from R0 for the 90° data. Dividing this difference by R2 gives the F appropriate for longitudinal field. Table 4.2-3 lists the 90° F determined for each joint, along with 0° F for comparison. Figure 4.2-8 is a plot of $\Delta R/R$ versus magnetic field for the two orientations. The longitudinal magnetoresistance does not increase as fast with magnetic field as in the transverse case.

The lap-joint resistance of one of the joints (0.38 cm) was measured as a function of current at 7 T for various magnetic field orientations. The current for each set of data (each orientation) was normalized by measured critical current for that orientation. The change in I_c between 0° and 90° was about 5.2% [4.2-6]. As above, F as a function of angle was determined

Table 4.2-3. Longitudinal magnetoresistance determined using the R0 values for 0° and 90° orientations on two NbTi lap joints.

Magnetic field T	Transverse F	Longitudinal F L_j = 3.8 mm	Longitudinal F L_j = 4.6 mm
1	1.093	1.054	1.058
3	1.382	1.169	1.180
5	1.738	1.308	1.334
7	2.137	1.472	1.482

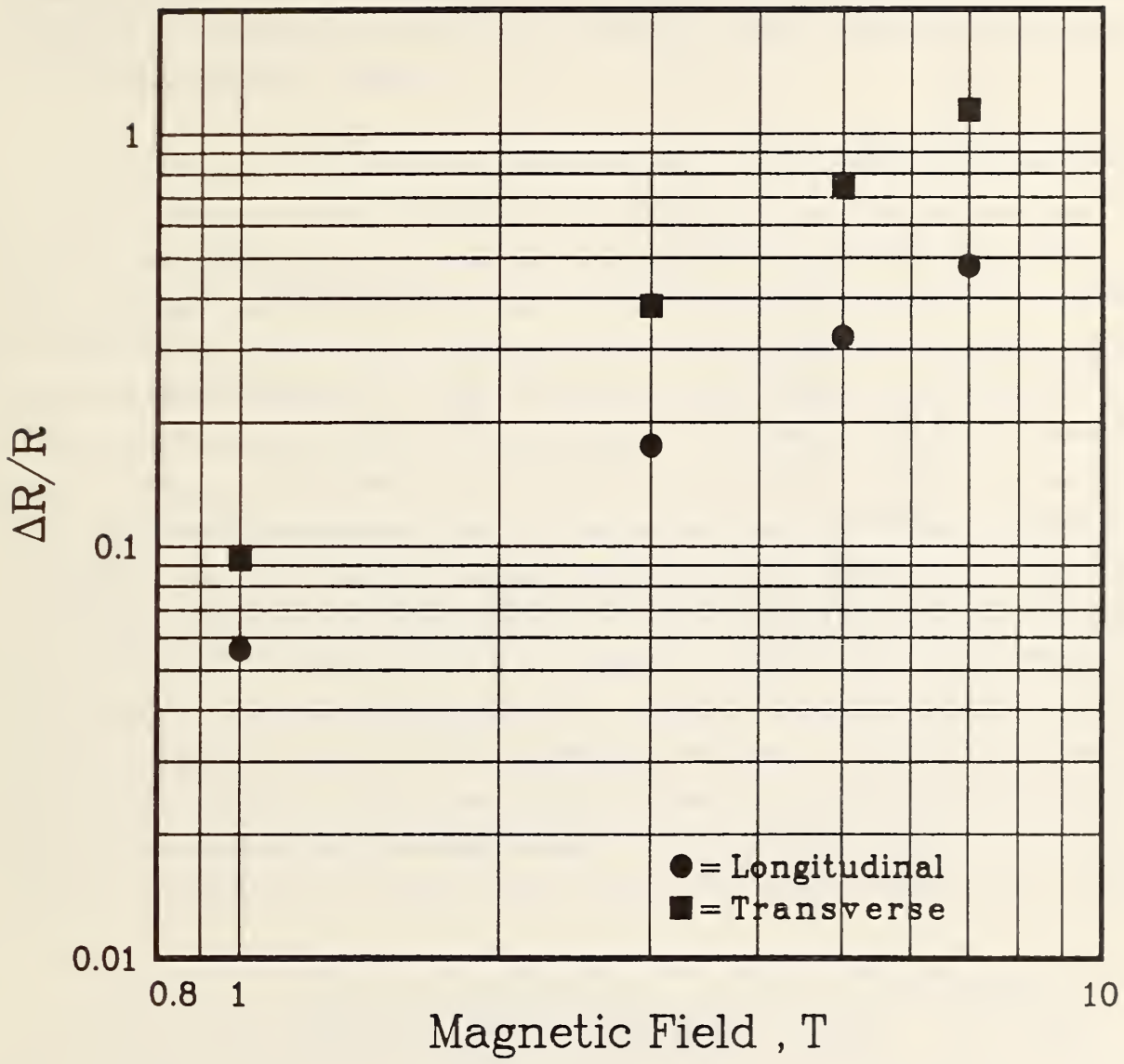

Figure 4.2-8. Magnetoresistance, ΔR/R, versus magnetic field for two lap-joint orientations, 0° transverse and 90°longitudinal.

from R2 (the surface copper component). It was also similarly determined using the transfer resistance component, R3. These values are given in table 4.2-4. The values of F determined from these two resistance components are in good agreement. The difference at 90°, longitudinal, is probably due to differences in the current path in the two regions of the lap joint.

RESULT OF Nb_3Sn JOINTS

The Nb_3Sn joints were made on the coil geometry with a wire that had been wound and reacted on a mandrel with the same diameter as the coil test fixture. The joints were made by cutting the wire in the middle and rotating the two coiled wires so that they overlapped. This overlapped region was then soldered to make the lap joint. The other end of each wire was soldered to each current contact, which was more than 160 cm from the lap joint. Voltage taps were placed 10 cm from each end of the lap joint, whose length was about 250 times the diameter of the filament region, 0.4 mm. With this configuration, the magnetic field was oriented perpendicular to the joint interface. The joint was made this way, keeping both wires on the mandrel surface, so that the wire would not be damaged by an unsupported Lorentz force or by bending it in order to lap with a different orientation. The joint orientation with the magnetic field was not important, however, because the current will flow in many directions in the copper jacket. This is due to the relatively lower resistivity of the copper jacket (20 nΩ·cm) compared to that of

Table 4.2-4. Magnetoresistance as a function of angle determined using R0 and R3 from 7 T data on the 3.8 mm NbTi lap-joint.

Angle (°)	F from R0	F from R3
0	2.160	2.137
20	2.016	2.109
45	1.707	1.846
70	1.497	1.669
90	1.457	1.619
110	1.532	1.664
135	1.738	1.902
-20	2.037	2.081

the interfilament bronze (about 3.4 μΩ cm). The current will flow around in the copper in order to enter the bronze through the whole perimeter. This fact combined with the extra complications of a round wire lap joint made it unreasonable to determine R1 and R2 for the Nb_3Sn joints. Thus, this part of the study concentrated on R3.

Two Nb_3Sn lap joints were measured one at a time in the coil geometry. These joints were 13 and 51 mm long. The lap-joint resistance data as a function of normalized current for various magnetic fields for these two joints are shown on figures 4.2-9 and 4.2-10. The normalizing I_c was about 560 A at 1 T and 93 A at 8 T. This normalization produces a relatively uniform family of curves. The empirical current dependence of resistance is the normalized current raised to the power of 1.6. This is a little higher than for the case of the NbTi joints, but the geometry is different as well. The R0 values were determined for each magnetic field and for each joint, assuming this current dependence for the lower currents (up to 33% fo I_c). The R0 values were then subtracted from the total joint resistance to leave the current dependent part. The current dependent part was then fit from 30% to 90% of I_c to give R3 and the exponent. Those values are given in table 4.2-5 and plotted in figure 4.2-11. The high exponent at 1 T for the shorter joint may be due to heating. The average exponent was 1.62 ± 9% (excluding the 1 T value for the shorter joint).

Table 4.2-5. Effective resistivity of the Nb_3Sn filament region determined from lap-joint data compared to the direct measured value of resistivity.

Magnetic field (T)	L_j = 13 mm		L_j = 51 mm	
	ρ_{eff} (nΩ cm)	$\frac{\rho_{measured}}{\rho_{eff}}$	ρ_{eff} (nΩ cm)	$\frac{\rho_{measured}}{\rho_{eff}}$
1	570	6.0	410	8.3
2	565	6.0	496	6.9
4	583	5.8	532	6.4
6	604	5.6	559	6.1
8	598	5.7	565	6.0

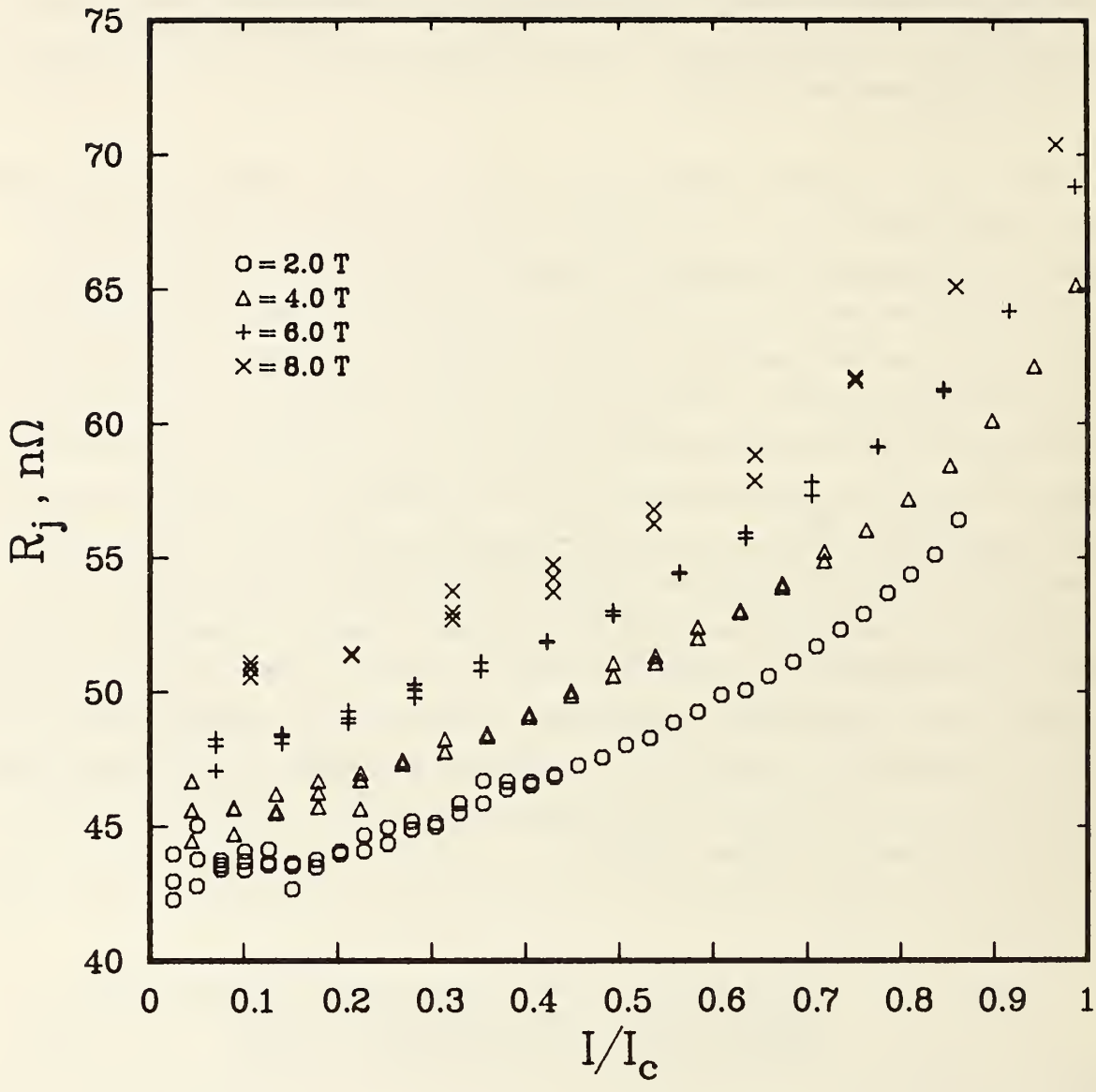

Figure 4.2-9. Lap-joint resistance versus normalized current for the 51 mm long Nb_3Sn joint at various magnetic fields.

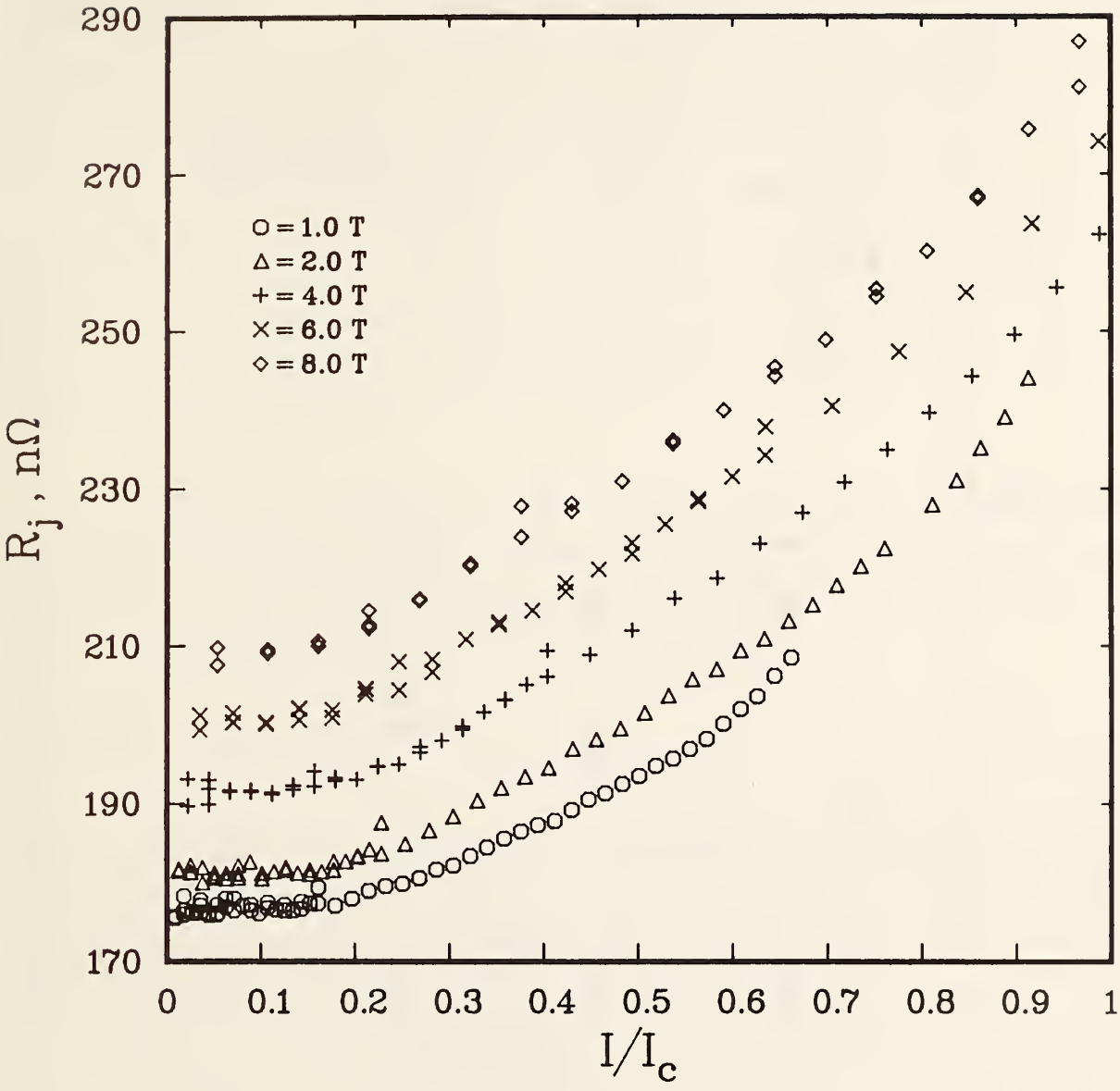

Figure 4.2-10. Lap-joint resistance versus normalized current for the 13 mm long Nb_3Sn joint at various magnetic fields.

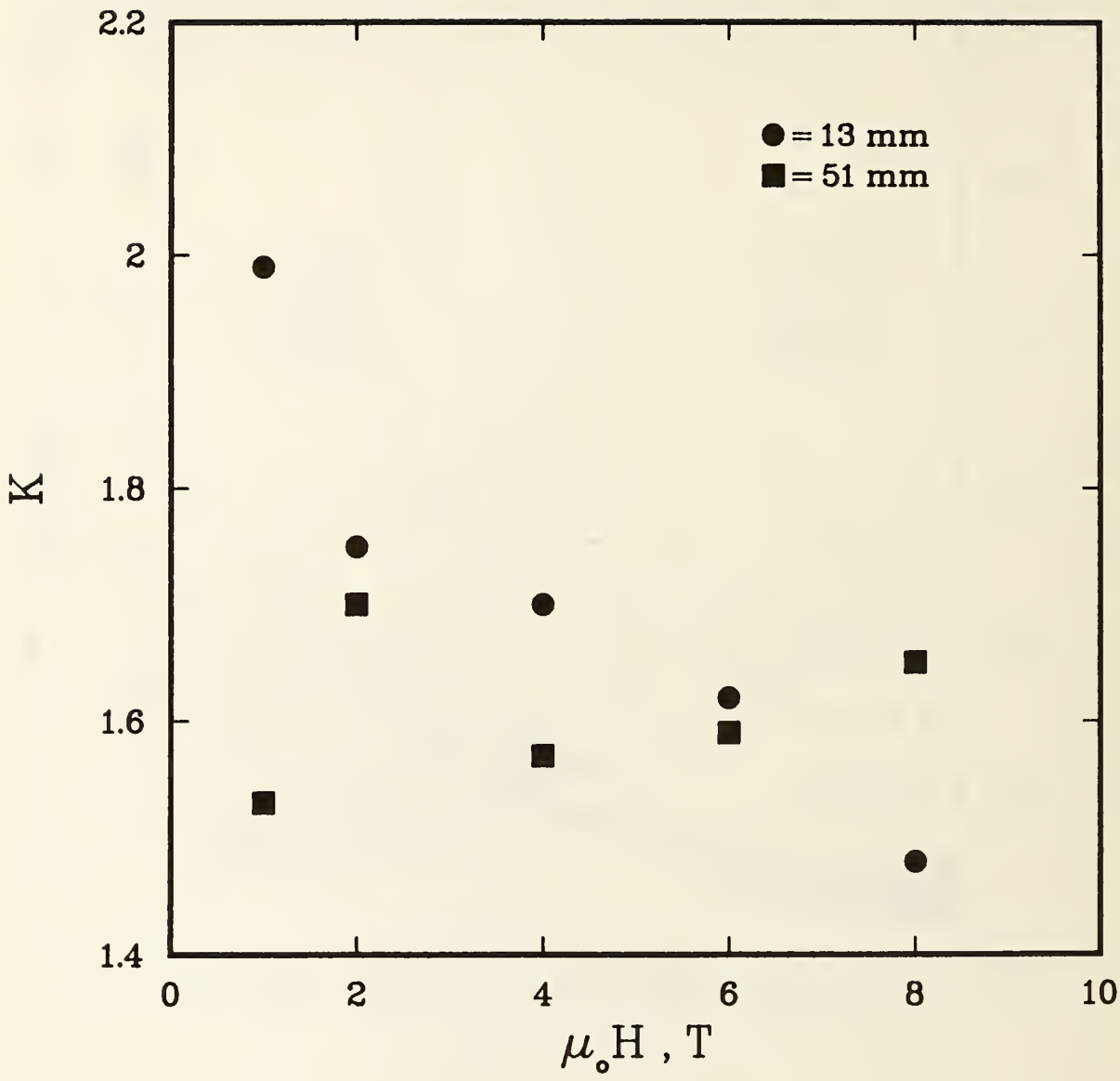

Figure 4.2-11. The exponent of the current dependence versus magnetic field for the two Nb_3Sn joints.

In order to model the transfer resistance, R3, the resistivity of the interfilament bronze has to be estimated. The Nb_3Sn reaction was not complete (30 hours at 730°C), so there might have been as much as 5 wt.% Sn (2.74 at.%) remaining out of the starting 13.5 wt.% bronze alloy. This alloy would have a 4 K resistivity of about 7.3 μΩ·cm [4.2-7]. The low temperature (nonsuperconducting) resistivity of the noncopper part of the wire (bronze, Nb_3Sn, Nb, and Ta) was measured to be 3.4 μΩ·cm. A bronze with that resistivity would be 1.24 atomic percent Sn (2.29 wt.%). The resistivity is directly proportional to impurity concentration. For an unreacted sample, the noncopper low temperature (nonsuperconducting) resistivity was 1.1 μΩ·cm, so it is clear that the Ta and Nb were affecting the measurement. The 3.4 μΩ·cm value will be used here as an estimated value.

The model for R3 (Appendix 4.2-B) is greatly simplified in the case of Nb_3Sn where significant current transfer is known to take place past the end of the joint. Nevertheless, relating the results to a model is necessary in order to extend these results. One way to view R3 is

$$R3 = \frac{\rho_{eff}}{2\pi L} ,$$

where ρ_{eff} is the effective transverse resistivity. The values of ρ_{eff} and the ratio of the estimated ρ and ρ_{eff} are listed in table 4.2-5. This ratio is very high, close to 6, which means that R3 is much lower than expected. Also, notice that the values for the two joints are very close to each other, even though the lap-joint lengths were different by a factor of 3.9. The longer joint shows some magnetoresistance that may be due to current sharing in the copper jacket away from the joint, which was not included in R0. A number of mechanisms that would lower R3 below the model value follow:

1. The transfer is not restricted to the length of the joint. This was known to be true, but an unexpected result was that R3 scaled rather well with the length of the joint for these two joints.

2. The effective transverse resistivity will be smaller because approximately 20% of the non-copper volume (area) is superconducting. Superconducting paths between filaments are not expected.

3. The resistivity of the bronze could be somewhat lower than the measured resistivity of the noncopper material, but the value used was equivalent to a bronze with a Sn content that was half of what was expected.

4. The Sn content of the bronze will be spatially dependent, so the resistivity of the bronze will be lower in the center of the wire than in the ring just inside the Ta barrier.

All of these mechanisms are likely, but the factor of 6 may be beyond these explanations.

DISCUSSION

An earlier report on lap-joint resistance [4.2-1] was based on measurements using a flat bottom hairpin geometry. There was an overlooked effect due to this choice of geometry. The joint was oriented so that the transferring current was in the direction of the applied magnetic field and the resistance separation was based on transverse magnetoresistance of the copper. This caused the $\rho\ell$ to be overestimated, 4.5 $n\Omega \cdot cm^2$ (here 3.3 $n\Omega \cdot cm^2$), and the ρ of the copper to be underestimated as 30.8 $n\Omega \cdot cm$ (here 53 $n\Omega \cdot cm$). Considering this, these two studies are in good agreement.

CONCLUSION

The model and separation scheme seemed to work well for the NbTi lap joints. The added elements of twist length, transverse current density, and variation in solder thickness explain the magnitude differences. The boundary resistance can be as much as 90% of the joint interface resistance. The nonlinear resistivity of the superconducting filaments and their distribution in the cross section are believed to be the cause of the faster than linear dependence of the joint resistance on normalized current. With these additions the model can be used to estimate the lap-joint resistance of NbTi wires.

The model predicted a lap-joint resistance for the Nb_3Sn wires that was about six times higher than the measured value. Part of this discrepancy can be explained with the known limited assumption of the model, but not all of it. The current dependence of the lap-joint resistance was a little stronger than the case of NbTi. This could be due to the round, as opposed to rectangular, wire cross section.

APPENDIX 4.2-A

CURRENT TRANSFER RESISTANCE FOR A RECTANGULAR CONDUCTOR

Some simplifying assumptions are made in order to model the current transfer resistance of a lap joint. These assumptions are:

1. All of the current transfer takes place within the length of the joint, L.

2. The transverse resistivity of the filaments is independent of current and thus the resistivity of the filament regions can be modeled as a variable that is independent of current and position.

3. The filaments have a uniform critical current density, J_c, and a continuous distribution throughout the filament region of the conductor.

With these assumptions, the voltage drop across one filament region of a conductor can be derived and from the functional form of the transfer resistance of a lap joint. The diagram in figure 4.2-A1 defines the geometric variables of one of the conductors in a lap joint. A current, I_o, enters this conductor through the joint area (shaded). The current, I, that is transferred across the conductor is a function of z (the distance into the filament region). This is so because the transverse current will change to longitudinal current up to a current density of J_c until the transverse current reaches zero. The equations for this are:

$$I = I_o - zwJ_c \ ,$$

$$I = I_o - \frac{z}{t} I_c \ ,$$

$$I = I_o \left(1 - \frac{z}{tx}\right) \ ,$$

where x is I_o/I_c. The differential voltage drop across an area with thickness

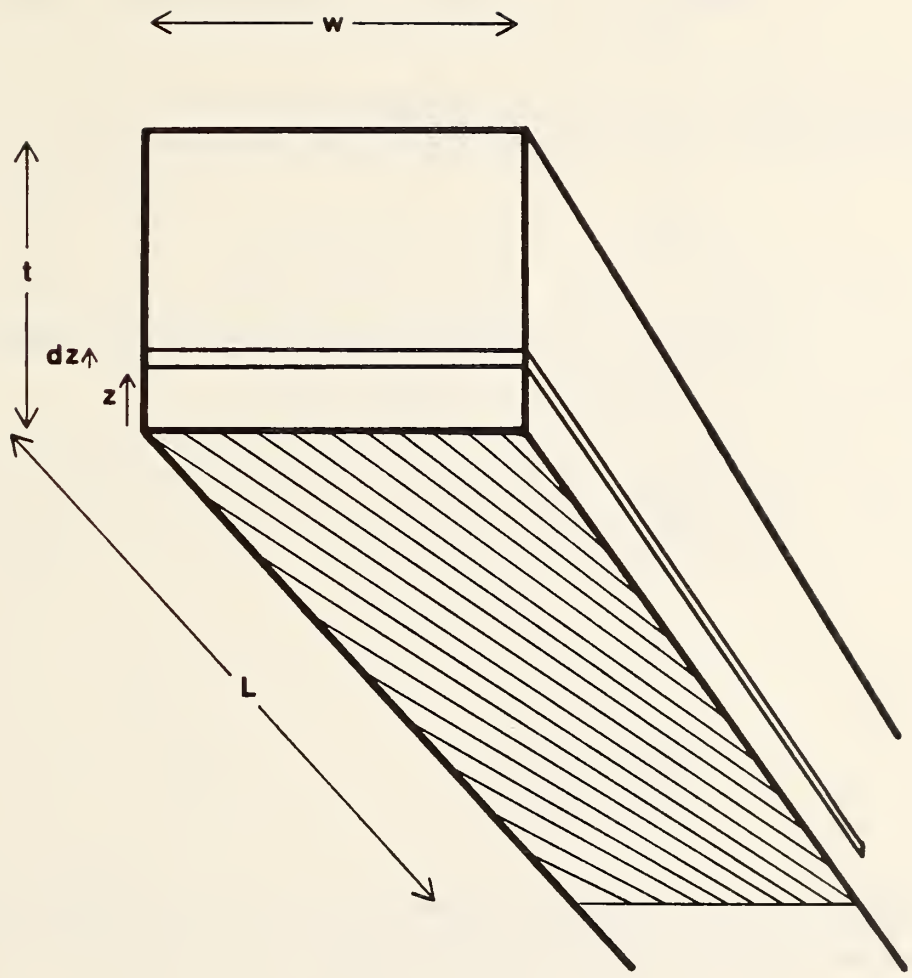

Figure 4.2-A1. Rectangular-conductor lap-joint diagram.

dz is

$$dV = \frac{I\rho}{wL}\, dz.$$

The total voltage drop across this wire is

$$V = \frac{I_o \rho}{wL} \int_o^y \left(1 - \frac{z}{tx}\right) dz,$$

where y is the value of z where the transverse current is zero, which in this geometry is tx. Evaluating the integral gives

$$V = \frac{\rho t}{2wL} \frac{I_o^2}{I_c}$$

and

$$R = \frac{\rho t}{2wL} \frac{I_o}{I_c}.$$

The resistance will increase linearly with current and that the effective transverse distance at the critical current is t/2 (half the thickness of this region). The total resistance of a lap joint will involve two wires, and the factor of 2 will be removed:

$$R(I) = \frac{\rho t}{wL} \frac{I}{I_c}.$$

APPENDIX 4.2-B

CURRENT TRANSFER RESISTANCE FOR A ROUND CONDUCTOR

The same assumptions used for the rectangular conductor, plus one more, will be used here. The additional assumption applies only to a round Nb_3Sn conductor with a copper jacket:

1. The current enters the filament region with a uniform current density along the cylindrical surface area of the joint.

This assumption is due to the relatively low resistivity copper jacket compared to the high resistivity bronze interfilament material. See figure 4.2-A2 for the geometric variables. The equations are analogous to the rectangular conductor's:

$$I = I_o - \pi(a^2 - r^2)\, J_c \ ,$$

$$I = I_o - I_c + \frac{r^2}{a^2} I_c \ ,$$

$$dV = \frac{I\, \rho\, dr}{2\pi r L} \ ,$$

$$V = \frac{-\rho}{2\pi L} \int_a^y \left(\frac{I_o - I_c}{r} + \frac{r\, I_c}{a^2}\right) dr \ ,$$

where $y = a\sqrt{(1-x)}$,

$$R = \frac{\rho}{4\pi L} \left(1 + \frac{(1-x)}{x} \ln (1-x)\right).$$

The second term of this expression is well behaved. It goes to -1 and R goes to zero as x goes to zero. The second term also goes to zero as x goes to 1. R increases faster than linear with current and R at I_c becomes

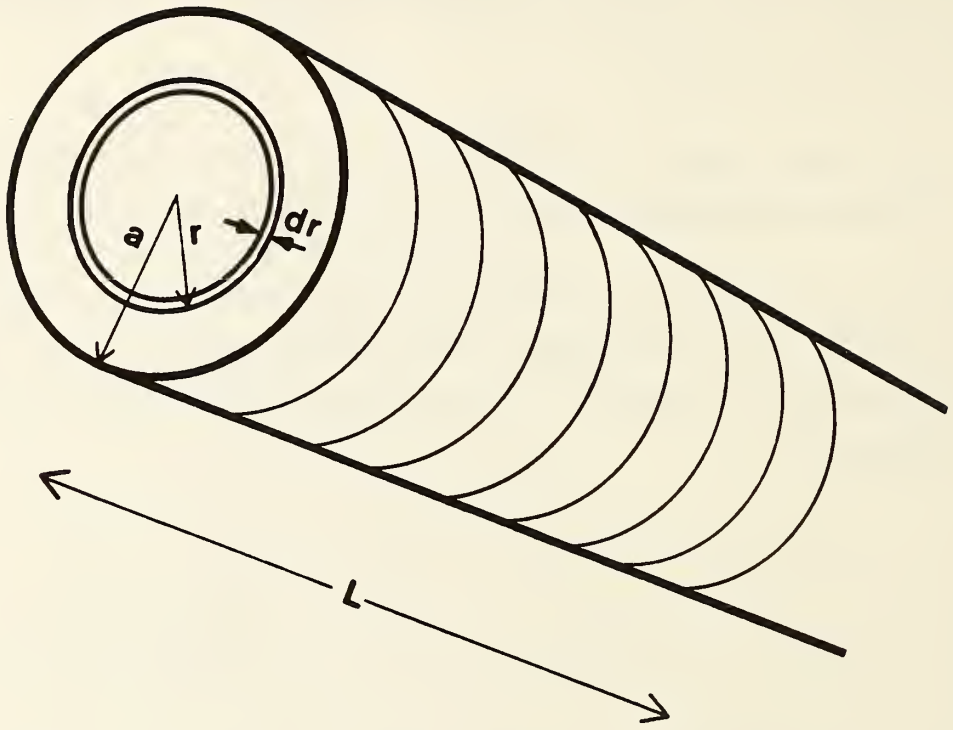

Figure 4.2-A2. Round-conductor lap-joint diagram.

$$R = \frac{\rho}{4\pi L}.$$

Two wires are involved for a lap joint and the resistance at critical current will be

$$R = \frac{\rho}{2\pi L}.$$

4.3 AC Losses

by J. V. Minervini

INTRODUCTION

This writeup is intended to document the principles of the ac loss theory that underlie the experimental apparatus and test conditions to be presented. It is not intended to be a rigorous treatise, but it is designed to give a relatively simple understanding of hysteresis losses in rectangular (one dimensional) and round (two dimensional) superconductors and the methods by which the losses can be experimentally measured.

The focus of this work is to develop an understanding of the loss mechanisms within an individual superconducting filament for two main conditions:

1) dc transport current in an ac external field,

2) ac transport current in a dc external field.

Only hysteresis loss in the filaments will be considered and not coupling or eddy-current losses. The loss will be computed from solution of Maxwell's magneto-quasistatic equations for the field and current distributions within the filament for the two conditions of external field and transport current listed above.

A principal consideration is the form of the field dependence of the critical current density, J_c. In all cases it will be assumed that the Bean-London model applies, i.e., that J_c is constant and independent of the local field H. Although the Kim-Anderson model could be used, in which J_c is inversely proportional to H, the experimental evidence indicates that the Bean-London model is appropriate for most of the operating conditions of interest.

The loss expressions will be developed first for the simple slab model to establish the method and indicate preliminary results. Then the two-dimensional expressions will be developed. However, the exact mathematical formulation for computation of the flux penetration profiles will only be cited since

a complete treatment is given in a previous paper by Minervini [4.3-3].

BASIS OF LOSS MODEL

First we must establish the type of material under consideration. Most present and projected engineering applications use a multifilamentary composite conductor, either in monolithic, cabled or braided form. The materials are primarily NbTi and Nb_3Sn. The loss expressions will be applicable to both types of superconductor and most other nonideal type II superconductors. However, the expressions are probably not suitable for "in situ" type conductors.

There are three well known loss mechanisms in multifilamentary composite superconductors. These are:

1) hysteresis loss in the superconducting filaments,

2) coupling loss due to circulating currents flowing axially through the filaments and returning through the matrix,

3) eddy current loss in the normal matrix material.

In addition there is a surface loss which may be significant at high frequencies in superconducting compounds such as Nb_3Sn which have a reaction layer on the surface of the filaments. The only loss mechanism considered here is the hysteresis loss in the filaments. This is the only significant contributor to the total loss in the composite if the frequency of the field or current change is less than the relaxation time, τ, for coupling currents induced in the matrix given by

$$\tau = \frac{\mu_0 \, \sigma_\perp}{2} \left(\frac{L_t}{2\pi}\right)^2 ,$$

where $\mu_0 = 4\pi \times 10^{-7}$, H/m

$\sigma_\perp$ = conductivity normal to the filament axis, A/(V·m)

L_t = twist pitch of the filaments, m.

Under these conditions the eddy current flow is dominated by the composite resistance, and the reaction field of the eddy currents is ignored. No shielding takes place and all the superconducting filaments are subjected to the same changing field and thus to the same hysteresis loss. The total loss for the wire is just the hysteresis loss for one filament multiplied by all the filaments in the composite. Since the loss is hysteretic and therefore frequency independent, the loss expressions are good for any time dependence of the field or current change.

ONE-DIMENSIONAL FLUX PENETRATION: NO TRANSPORT CURRENT

A one-dimensional slab of nonideal type II superconductor is often used as a simple model to illustrate the fundamentals of the hysteresis loss calculation. Consider the slab of thickness d in figure 4.3-1 to be of infinite extent in the y and z directions. If a uniform external field, H_e, oriented parallel to the sides of the slab in the y direction is increased from 0 to a value above H_{c1}, flux will begin to penetrate the material. For our purposes assume H_{c1} is very small so that we can ignore the Meissner state. Just how small is small will be determined later. As the flux penetrates from both surfaces bulk screening currents are induced to flow near the surfaces to screen the interior region of the conductor. If we assume the material to be in the critical state as in the Bean-London model then the screening currents flow just at the critical current density, J_c, and are independent of the local field variation.

The field and current distribution will be given by solution of the Maxwell equation $\vec{\nabla} \times \vec{H} = \vec{J}$ with the boundary condition that $H = H_e$ at the surfaces. The solution has the form

$$H = H_e + J_c(x - d/2), \quad x > 0. \tag{4.3-1}$$

The field penetrates to a point X_p given by

$$x_p = d/2 - H_e/J_c. \tag{4.3-2}$$

The slab is fully penetrated when $H_e = H_p$, the full-penetration field, where

$$H_p = J_c d/2. \tag{4.3-3}$$

The field and current distributions that correspond to flux penetration for the Bean-London model are shown in figures 4.3-1a through 4.3-1c for an increasing external field and figures 4.3-1d through 4.3-1g for a decreasing external field. The hysteresis inherent in the superconductor is illustrated by the trapped flux remaining in the slab when the external field is reduced to zero (fig. 4.3-1e). As long as $H_{c1} << H_p$, the effects of the Meissner state can be ignored.

The magnetization of the slab is given by

$$M = \frac{1}{d}\left[\int_{-d/2}^{+d/2} H\, dx\right] - H_e\ , \tag{4.3-4}$$

and the magnetization curve for a complete cycle to the upper critical field limit of H_{c2} is shown in figure 4.3-2. A more complete treatment of the computation of the magnetic moment as a function of the applied field is given in Appendix 4.3-A. The energy loss per cycle per unit volume is easily computed from the area under the magnetization curve and given by

$$W_h = \int_{\text{volume}} \left[\oint_{\text{cycle}} M\, dH\right] dV\ . \tag{4.3-5}$$

Carrying out the integration we get for the loss per unit volume per cycle,

$$\frac{W_h}{V} = \frac{2}{3}\mu_0 H_p^2 \left(\frac{H_m}{H_p}\right)^3 \qquad H_m \leq H_p \tag{4.3-6a}$$

and

$$\frac{W_h}{V} = \frac{2}{3}\mu_0 H_p^2 \left[3\left(\frac{H_m}{H_p}\right)-2\right] \qquad H_m \geq H_p, \tag{4.3-6b}$$

where H_m is the maximum external field for the loop.

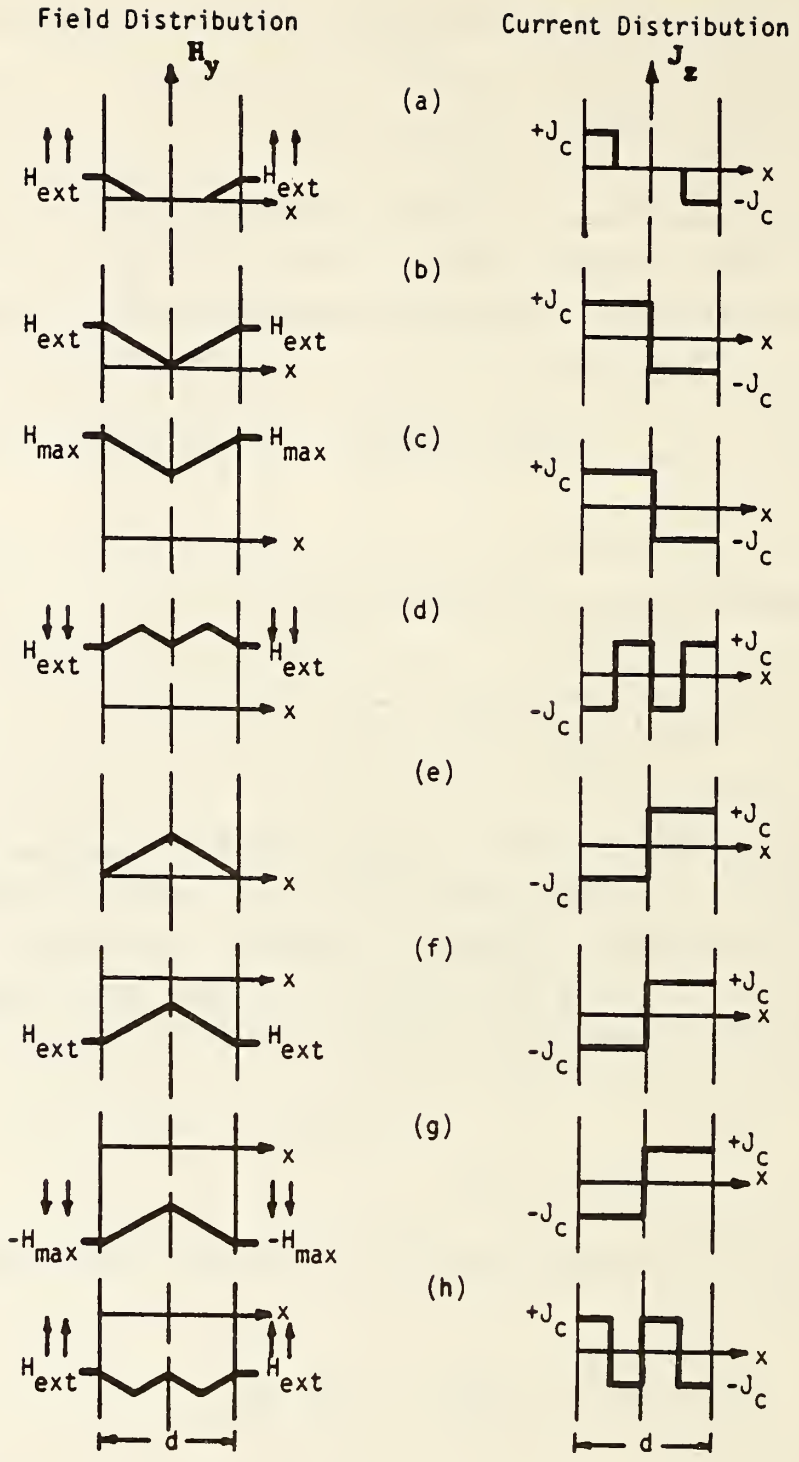

Figure 4.3-1. Field and current distribution in a type II superconducting slab of thickness d with external field applied parallel to the slab surfaces.

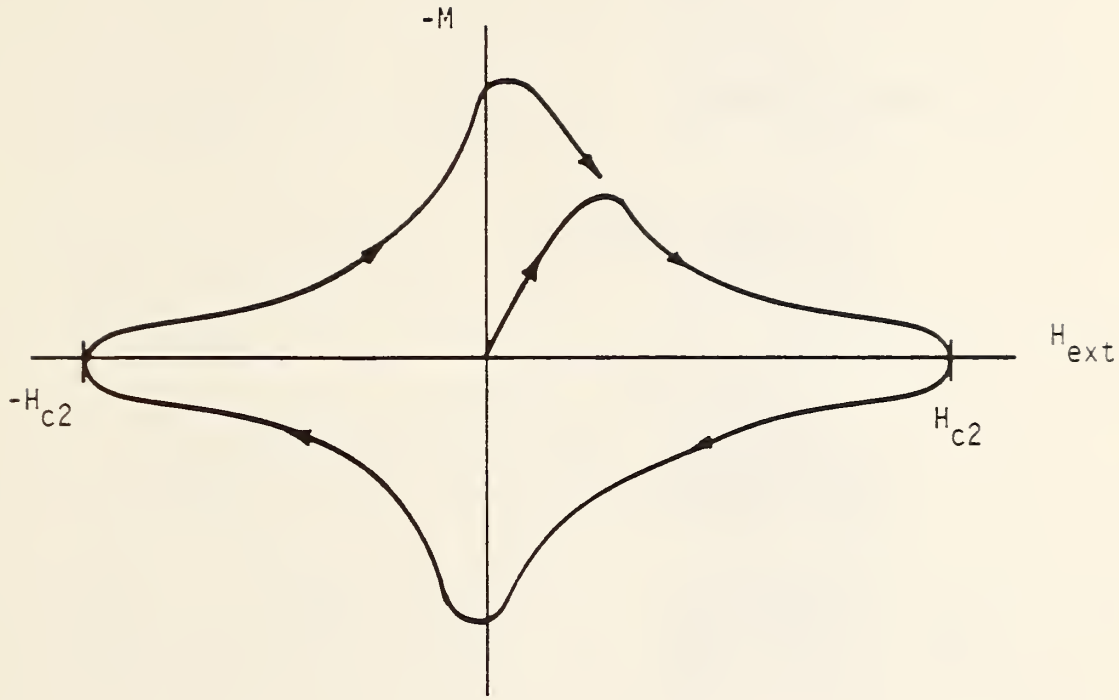

Figure 4.3-2. Magnetization curve for a type II superconducting slab.

We can normalize field values to the full penetration field H_p and losses to the full penetration field loss given by

$$\frac{W_0}{V} = \frac{2}{3} \mu_0 H_p^2$$

to get the reduced results:

$$\frac{W_h}{W_0} = \left(\frac{H_m}{H_p}\right)^3 \qquad \frac{H_m}{H_p} \leq 1 \tag{4.3-7a}$$

and

$$\frac{W_h}{W_0} = \left[3\left(\frac{H_m}{H_p}\right)-2\right] \qquad \frac{H_m}{H_p} \geq 1, \tag{4.3-7b}$$

and, if $H_m/H_p >> 1$,

$$\frac{W_h}{W_0} \cong 3\left(\frac{H_m}{H_p}\right). \tag{4.3-7c}$$

These results were originally derived by London.

ONE-DIMENSIONAL EFFECT OF TRANSPORT CURRENT

Consider the one-dimensional slab to be in a uniform external field and carrying a transport current I_t in the z direction. Let I_t be a fraction of the critical current I_c such that $0 < i < 1$, where $i = I_t/I_c$. The current and field distributions for the slab are shown in figure 4.3-3. The current flows everywhere in the cross section at the critical current density $\pm J_c$ which has been assumed to be a constant as per the Bean-London model. The net current flowing through the slab will always be given by i as can be seen by summing the positive and negative current-carrying areas and dividing by the total area. If the external field, H_e, is cycled by an amount $\pm H_m$ about the

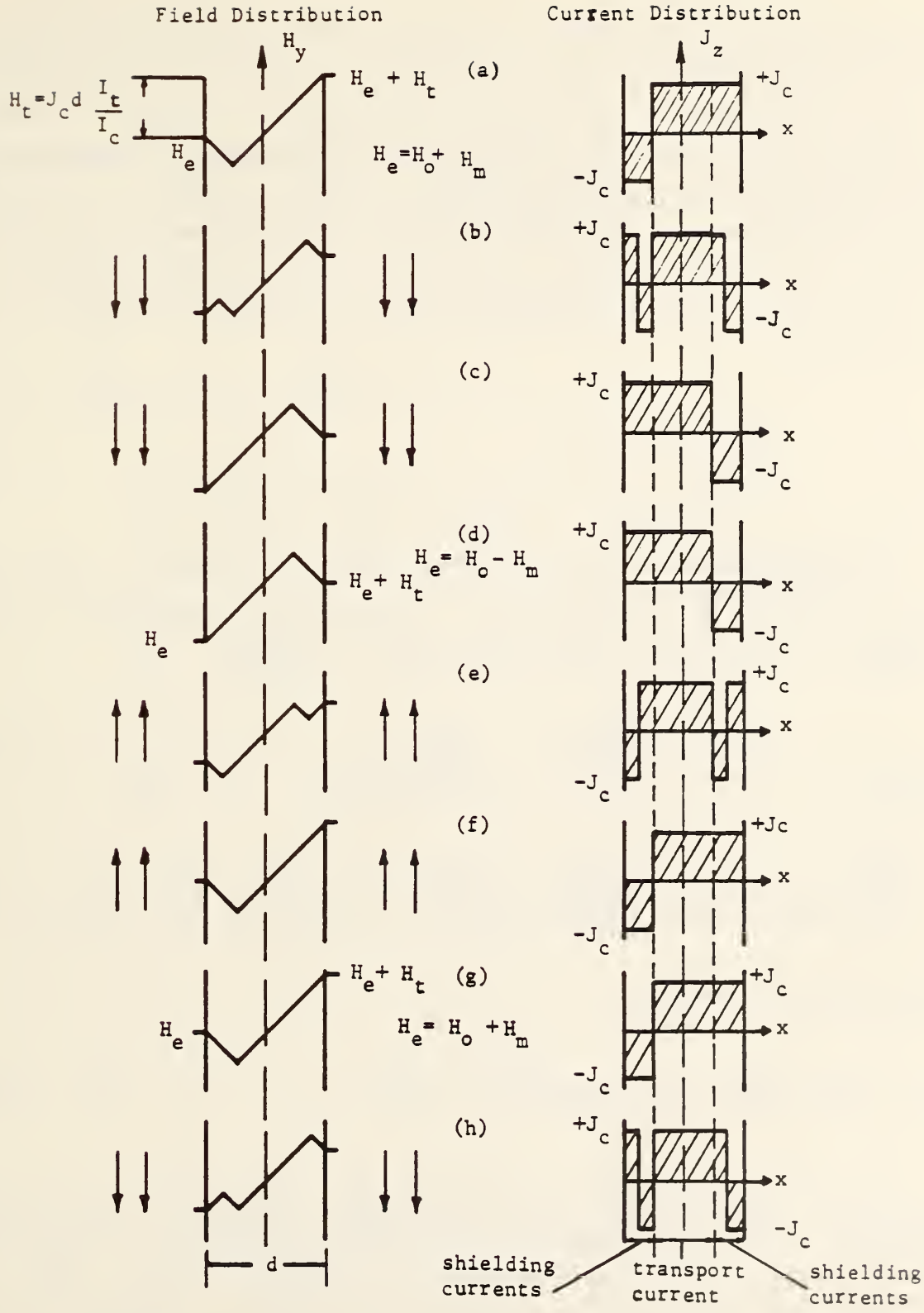

Figure 4.3-3. Bean model of field and current distribution in a slab carrying a transport current, $I_t/I_c = 0.5$.

value H_0 the current and field distributions will be as shown in figures 4.3-3a through 4.3-3h.

Since one can picture the central region of the slab as being occupied by the transport current, the field required to fully penetrate to this region, $H_p(i)$, will be less than the field required to penetrate to the center of the slab for zero transport current. That is, $H_p(i) < H_p(0)$, where $H_p(0) = J_c d/2$. The full penetration field now depends upon the fraction of transport current and is given by

$$\frac{H_p(i)}{H_p(0)} = (1 - i). \tag{4.3-8}$$

The magnetization and the hysteresis loss can be computed as before from eqs (4.3-4) and (4.3-5), respectively. The results are given below in normalized form for the energy loss per unit volume per cycle:

$$\frac{W_h(i)}{W_0} = \left(\frac{H_m}{H_p(0)}\right)^3, \qquad \frac{H_m}{H_p(i)} \leq 1 \tag{4.3-9a}$$

$$\frac{W_h(i)}{W_0} = (1 - i)^3 + 3\left[\left(\frac{H_m}{H_p(0)}\right) - \left(\frac{H_p}{H_p(0)}\right)\right](1 + i^2), \qquad \frac{H_m}{H_p(i)} > 1 \tag{4.3-9b}$$

where now W_0/V is given by

$$\frac{W_0}{V} = \frac{2}{3}\mu_0 H_p^2(0). \tag{4.3-10}$$

If $i = 0$, eqs (4.3-9a) and (4.3-9b) reduce to eqs (4.3-7a) and (4.3-7b), respectively. It is interesting to note that if H_m is less than $H_p(i)$ the hysteresis loss is totally unaffected by the transport current. This is so because the flux front does not penetrate deep enough into the slab to reach the central transport current carrying region during any portion of the cycle.

One of the most significant features of this model is that the loss during a cyclic field change is partly due to flux motion in the portion of the conductor carrying screening currents and partly due to flux motion in the portion of the conductor carrying the transport current. The two components of the loss are additive and can be computed separately. The results are given below. For partial penetration the total loss is identical to that given in eq (4.3-9a).

For $\frac{H_m}{H_p(i)} \leq 1$ or $\frac{H_m}{H_p(0)} \leq (1 - i)$:

$$\frac{W_h(i)}{W_0} = \frac{W_s(i)}{W_0} + \frac{W_t(i)}{W_0} = \left(\frac{H_m}{H_p(0)}\right)^3 \qquad \text{Total Loss} \qquad (4.3\text{-}11a)$$

$$\frac{W_s(i)}{W_0} = \left(\frac{H_m}{H_p(0)}\right)^3 \qquad \text{Shielding Loss} \qquad (4.3\text{-}11b)$$

$$\frac{W_t(i)}{W_0} = 0 \qquad \text{Transport Loss} \qquad (4.3\text{-}11c)$$

For $\frac{H_m}{H_p(i)} \geq 1$ or $\frac{H_m}{H_p(0)} \geq (1 - i)$, the full penetration loss is given by:

$$\frac{W_h(i)}{W_0} = \frac{W_s(i)}{W_0} + \frac{W_t(i)}{W_0} = (1 - i)^3 + 3\left[\left(\frac{H_m}{H_p(0)}\right) - \frac{H_p(i)}{H_p(0)}\right](1 + i^2) \qquad \text{Total Loss} \qquad (4.3\text{-}11d)$$

$$\frac{W_s(i)}{W_0} = (1 - i)^3 + 3\left[\left(\frac{H_m}{H_p(0)}\right) - \frac{H_p(i)}{H_p(0)}\right](1 - i^2) \qquad \text{Shielding Loss} \qquad (4.3\text{-}11e)$$

$$\frac{W_t(i)}{W_0} = 6\left[\left(\frac{H_m}{H_p(0)}\right) - \left(\frac{H_p(i)}{H_p(0)}\right)\right] i^2 \qquad \text{Transport Loss} \qquad (4.3\text{-}11f)$$

The normalized hysteresis loss per cycle per unit volume versus maximum external field change is shown in figure 4.3-4 with the transport current as a parameter. The shielding and transport loss components are shown as a function of the transport current in figures 4.3-5 and 4.3-6, respectively, and the total loss in figure 4.3-7. The maximum field change is the parameter. It is clear that the transport current does not affect the loss unless the field change is large enough to penetrate into the transport current region, which for the slab occurs when $H_m/H_p(0) > (1 - i)$.

The two loss components can be measured separately because the shielding loss component is provided by the external field source power supply and the transport current loss is provided by the transport current power supply. For a summary of the loss expressions see Appendix 4.3-A.

AC TRANSPORT CURRENT IN A DC FIELD: SLAB MODEL

Consider the case of a slab carrying an alternating transport current while in a dc background field. For simplicity, let us assume there are two adjacent slabs, side by side, carrying the same transport current in series opposition, as illustrated in figures 4.3-8a and 4.3-8b. The net field surrounding the slabs will be zero while the field between the slabs will be the sum of the self field of each slab carrying a transport current i, the fraction of critical current. The field and current distributions are shown in figures 4.3-8a and 4.3-8b, respectively. The field has penetrated to x_p which is just i d. Figures 8c and 8d show a sequence of field profiles for decreasing current and increasing current, respectively. Again we have assumed that the slabs are in a large uniform dc bias field parallel to the surfaces and also that the Bean-London model applies.

The magnetic moment as a function of the transport current can be computed as before by application of eq (4.3-4), giving the results for increasing current,

$$\frac{M_{\uparrow}}{H_p(0)} = \frac{1}{2} i_m^2 \left[-1 + 2 \left(\frac{i}{i_m}\right) + \left(\frac{i}{i_m}\right)^2\right] \qquad (4.3\text{-}12a)$$

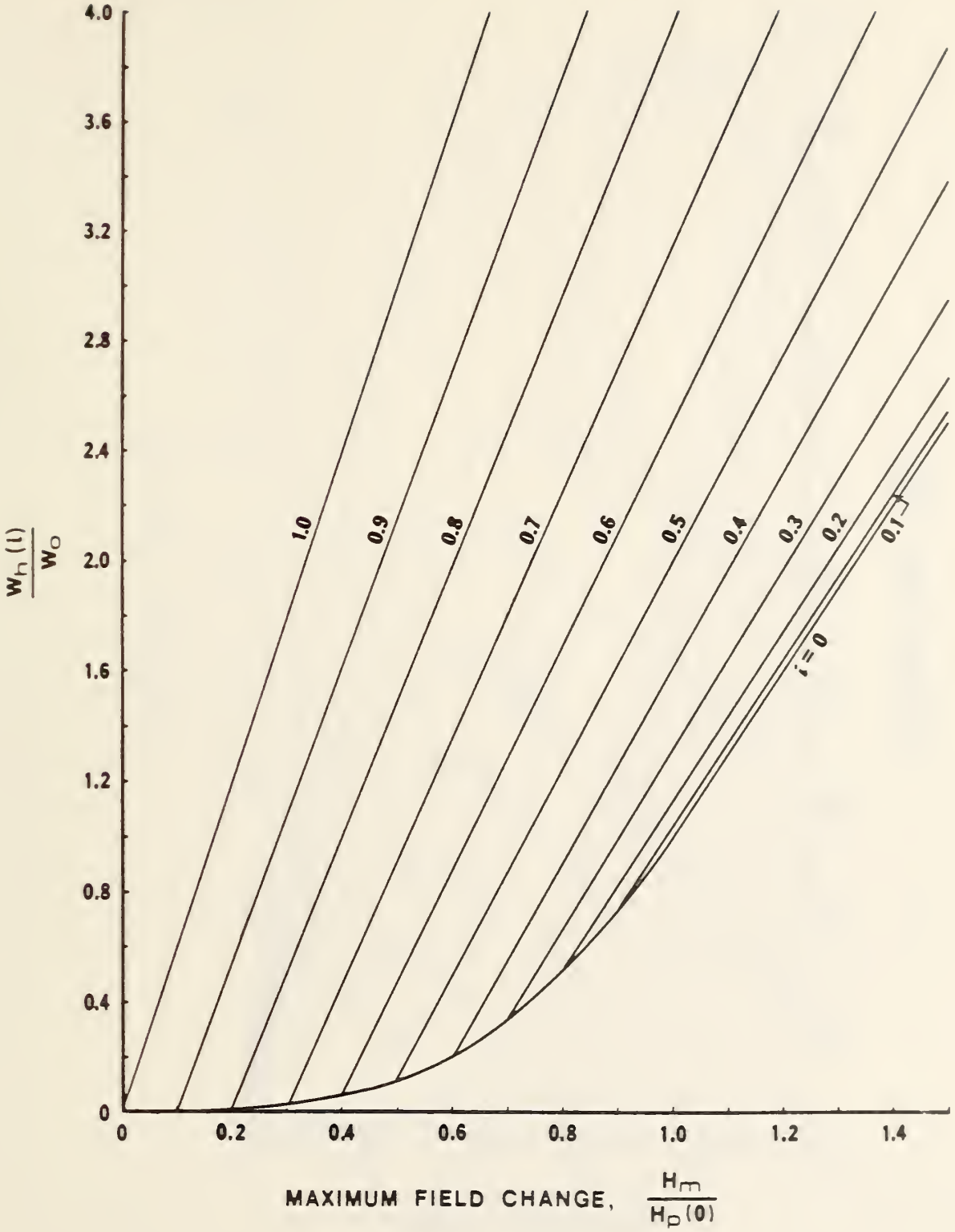

Figure 4.3-4. Total hysteresis loss in a slab as a function of the maximum field change for different values of transport current.

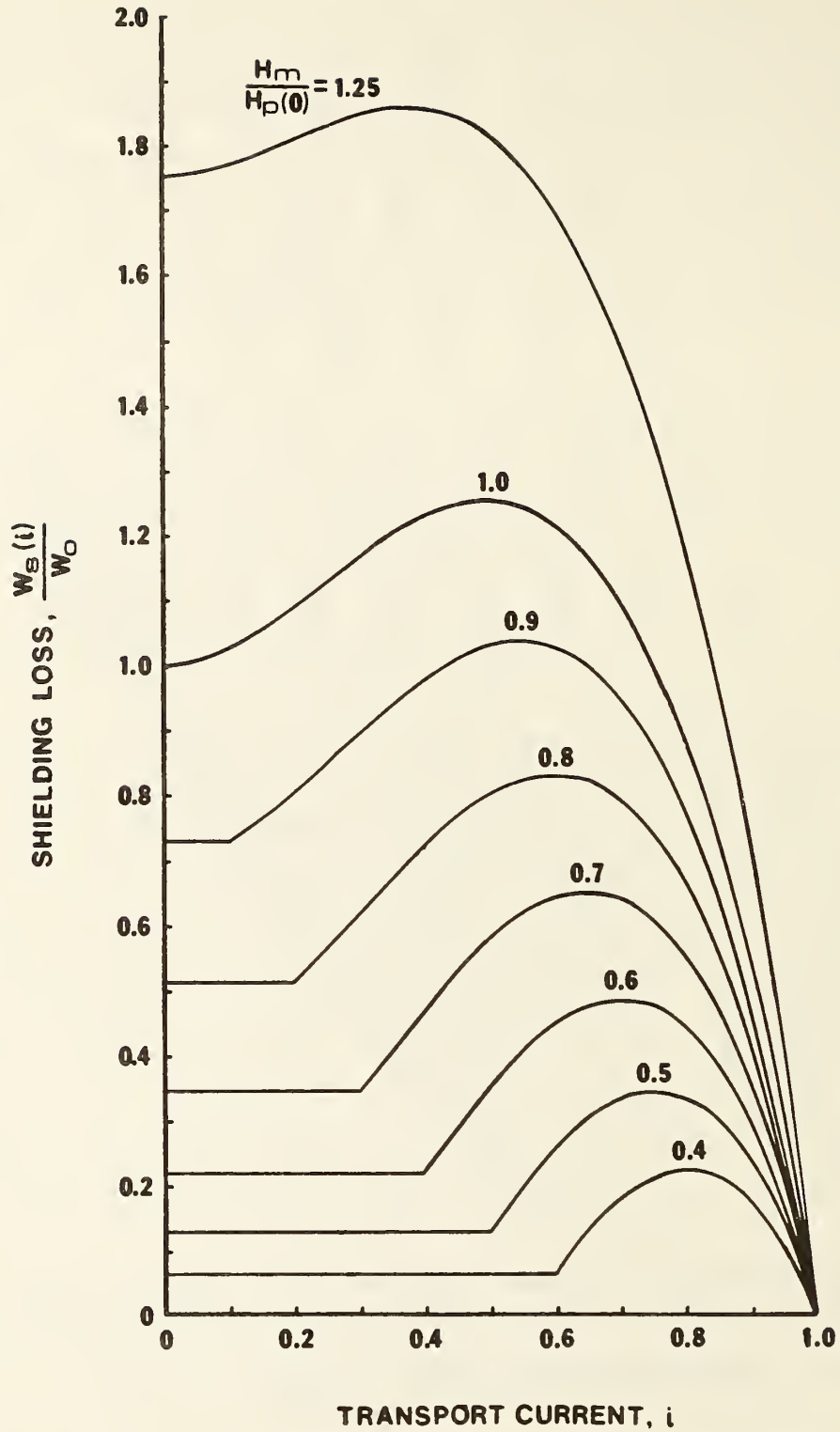

Figure 4.3-5. The shielding loss in a slab as a function of the transport current with maximum field change as a parameter.

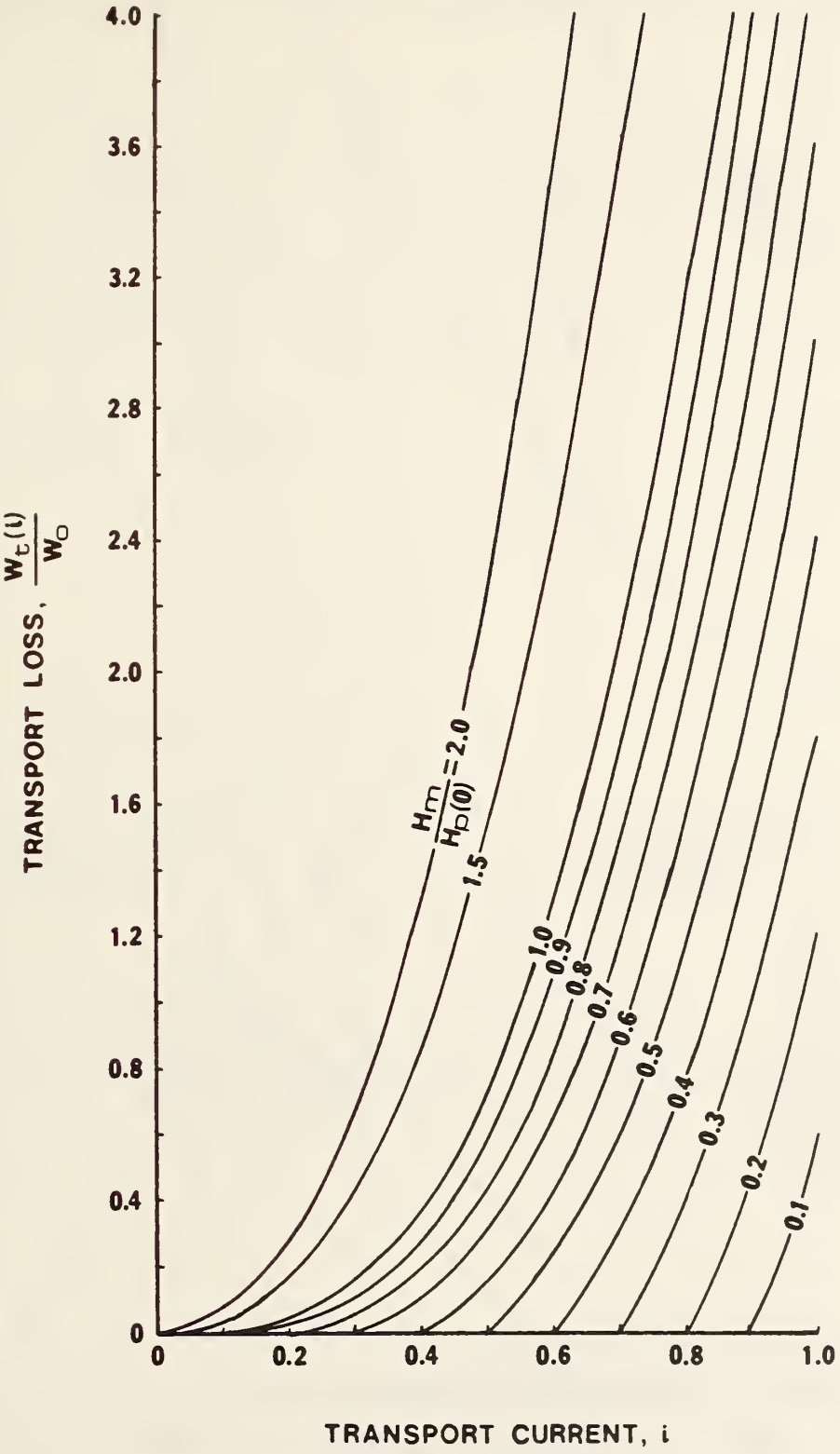

Figure 4.3-6. The transport loss in a slab as a function of transport current with maximum field change as a parameter.

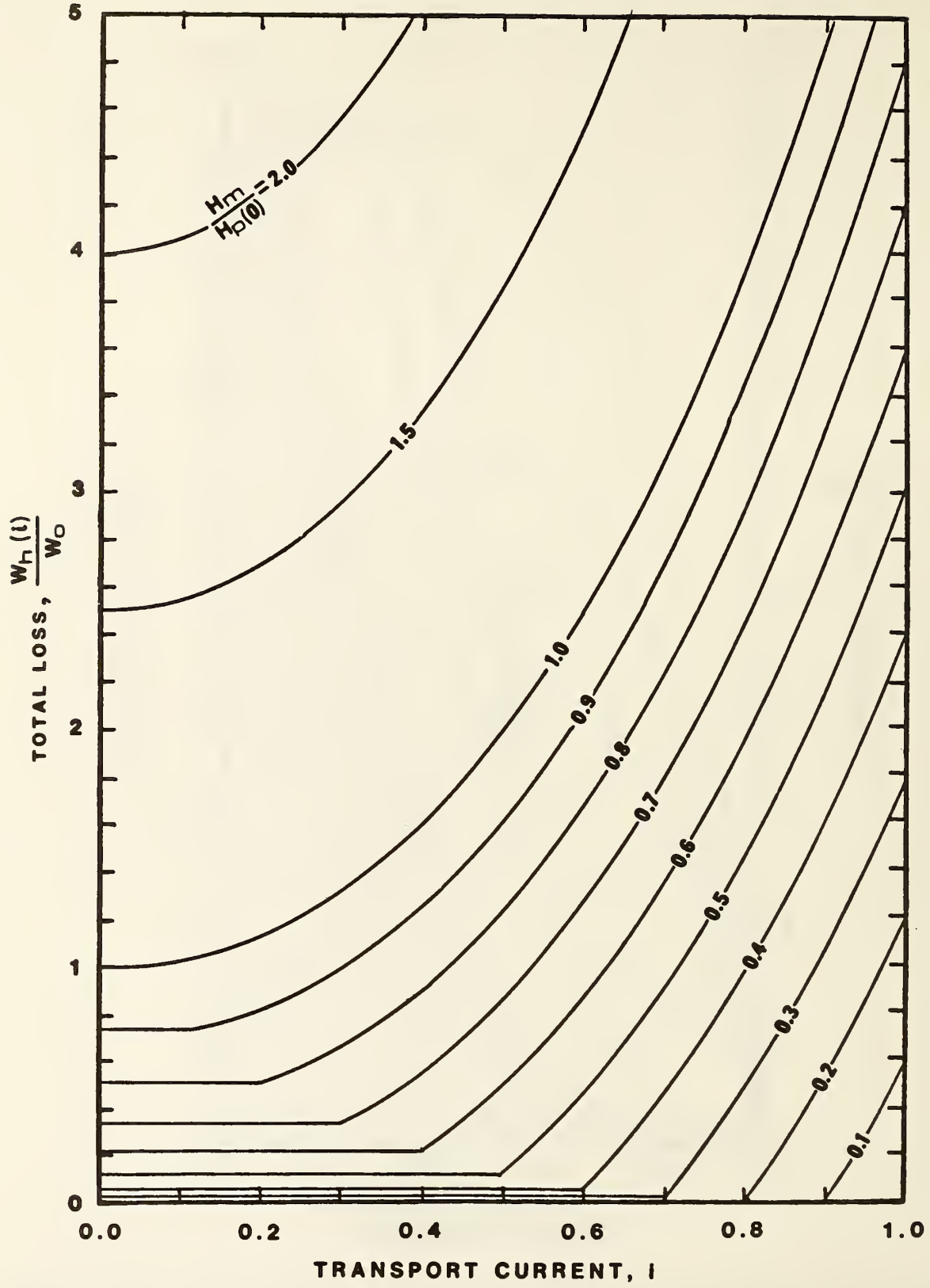

Figure 4.3-7. Total hysteresis loss in a slab as a function of transport current with maximum field change as a parameter. These data are the same as that in Figure 4.3-4.

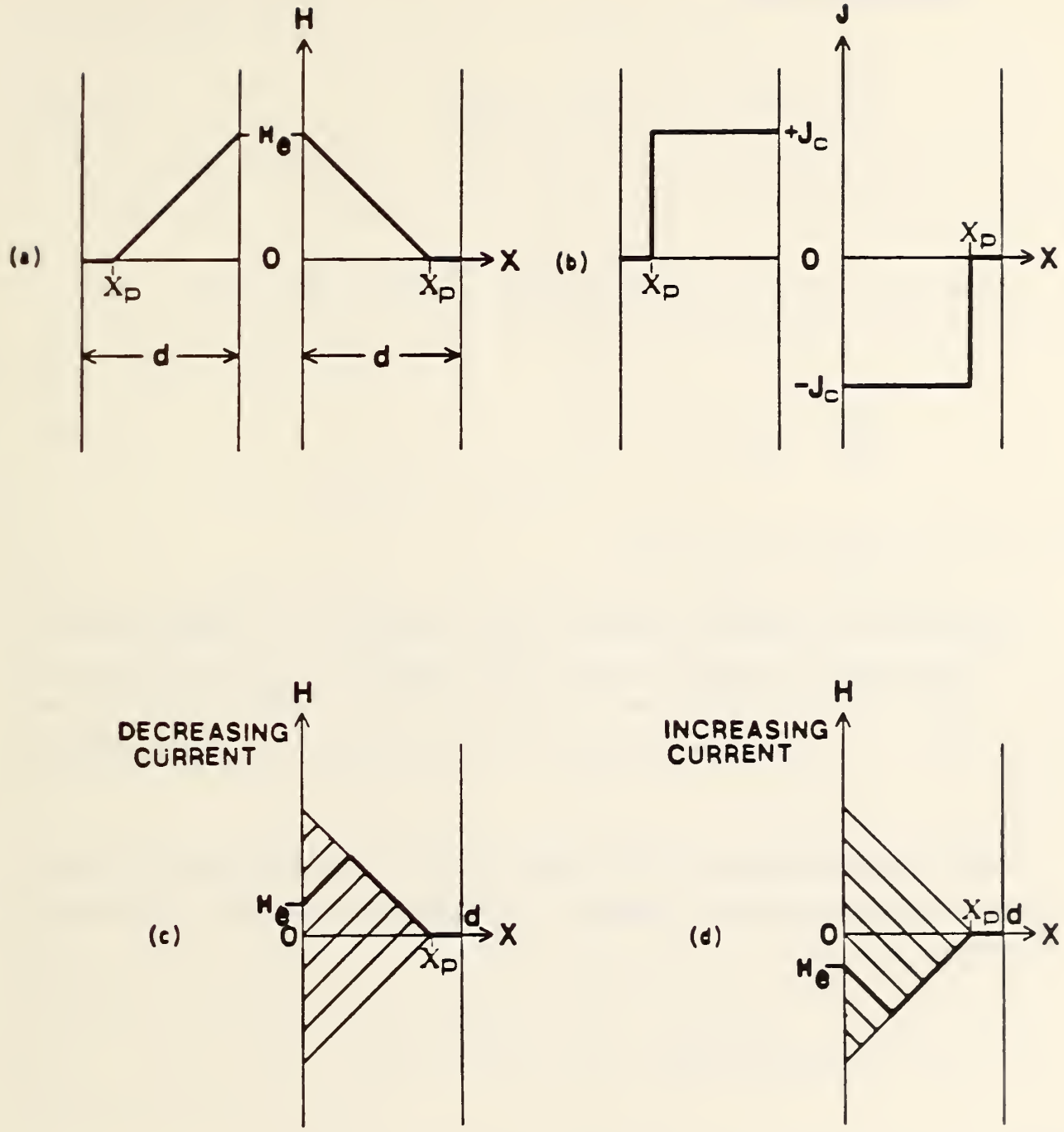

Figure 4.3-8. a) Field and b) current distributions in a slab carrying an alternating current in a constant background field; c) and d) are sequences of field profiles for decreasing and increasing current, respectively.

and for decreasing current,

$$\frac{M_{\downarrow}}{H_p(0)} = \frac{1}{2} i_m^2 [1 + 2 (\frac{i}{i_m}) - (\frac{i}{i_m})^2] \qquad (4.3\text{-}12b)$$

where i_m is the maximum value of $i \leq 1$, and $H_p(0)$ is as previously defined.

Integration of the magnetization around a cyclic change of the transport current yields for the normalized hysteresis loss per cycle per unit volume

$$\frac{W_h}{W_0} = 4 i_m^3 \quad , \qquad (4.3\text{-}13)$$

where W_0/V is given in eq (4.3-10).

This result is similar to that for a slab carrying zero transport current in a changing external field (eq (4.3-7a)). Note that i_m cannot exceed 1. For a current change i_m that gives an equivalent field change $H_m \leq J_c d/2$, then the loss due to a changing current is half the loss due to a changing external field.

Some interesting results can be obtained if we note that the total flux in the filament is just the integral of the field distribution across the filament,

$$\phi = \mu_0 \ell \int_0^d H \, dx \quad ,$$

where ℓ is the length of the sample and the induced voltage is

$$V = \frac{-d\phi}{dt}.$$

Assuming a sinusoidal time dependence of the current with frequency ω,

$$i = i_m \sin(\omega t) , \tag{4.3-14}$$

we get the terminal voltage as a function of time for increasing current,

$$\frac{V_{\uparrow}}{V_0} = -\cos(\omega t)[1 + \sin(\omega t)] \tag{4.3-15a}$$

and for decreasing current,

$$\frac{V_{\downarrow}}{V_0} = -\cos(\omega t)[1 - \sin(\omega t)] \tag{4.3-15b}$$

where $V_0 = \mu_0 H_p(0)\, d\ell\, i_m^2\, \omega$. The voltage and current as a function of time are shown plotted in figure 4.3-9, and voltage versus current in figure 4.3-10. These theoretical curves are useful to compare with measured waveforms.

TWO-DIMENSIONAL FLUX PENETRATION IN A CYLINDRICAL FILAMENT

The loss calculations of the previous sections have all been computed based upon the one-dimensional slab model. Until recently these solutions were all that was available due to the complexity of solving the two-dimensional field equations. A mathematical technique has been developed to determine the two-dimensional contours of flux penetration into cylindrical shaped superconducting filaments exposed to a transverse ac external field [4.3-1, 4.3-2, 4.3-3]. These solutions have been found for both circular and elliptic shaped cylinders.

The problem is to compute the region of flux penetration in a cylindrical, type-II superconducting filament. The model is based upon the following assumptions: (a) the constant bias field is uniform, transverse to the filament and much greater than $H_p(0)$, the field required to fully penetrate the filament at zero transport current, and (b) the filament is in the critical state and the Bean-London model holds.

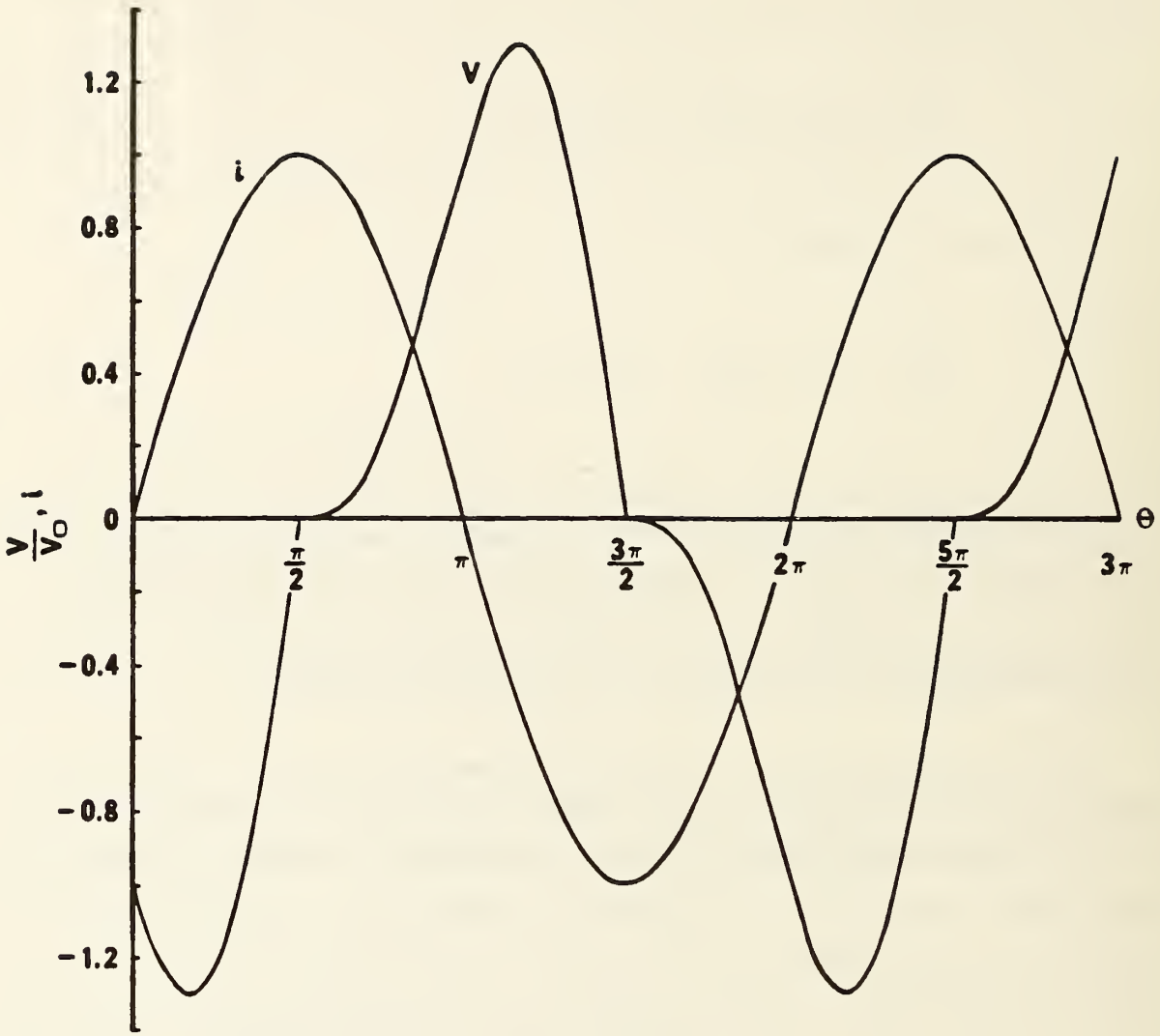

Figure 4.3-9. Terminal voltage, V, if a slab carrying an alternating current, i, in a constant background field as a function of time.

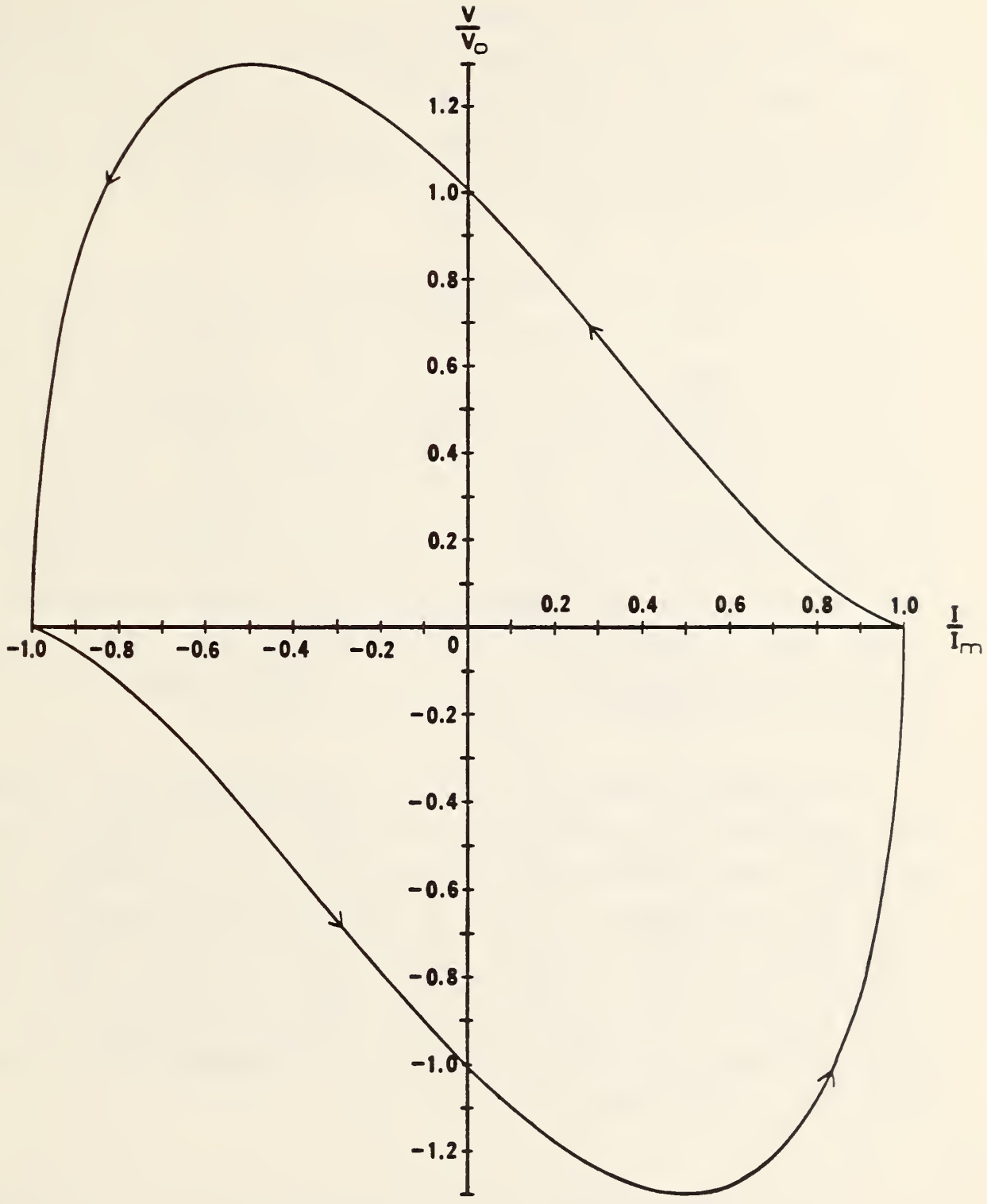

Figure 4.3-10. Terminal voltage of a slab as a function of the alternating transport current.

Consider the filament to be in a transverse field, H_e. The induced current distribution creates a uniform magnetic field in an interior region that is equal in magnitude and antiparallel to the external field so that the interior region is completely shielded. The net magnetic field distribution is just the superposition of the external field and the reaction field generated by the induced current distribution.

As the external field is decreased from the fully penetrated condition (fig. 4.3-11a) the flux exits from the surface, reversing the current distribution in the region where the flux has decreased. The boundary that separates the shielded region from the flux change region penetrates deeper into the filament as the external field is further decreased (figs. 4.3-11b and 4.3-11c). Once the flux front reaches the center of the filament it is considered to be fully penetrated (fig. 4.3-11e). At this point the filament can no longer shield itself. Thus, if the field is increased beyond this point, the current distribution will remain constant as the flux continues to penetrate uniformly. After a complete cycle the current distribution will return to that pictured in figure 4.3-11a. Reversal of the field change before full penetration will begin a second flux front (fig. 4.3-11d).

The sequence of flux fronts shown in figure 4.3-11 is only schematic. The actual shapes of the flux front profiles have been computed by the mathematics of complex variables and an iterative numerical technique [4.3-1, 4.3-2, 4.3-3]. Figure 4.3-12 shows the computed flux front profiles for a circle (fig. 4.3-12a), an ellipse of aspect ratio 0.5 (fig. 4.3-12b), and an ellipse of aspect ratio 0.5 (fig. 4.3-12c). The numbers on the curves refer to the ratio of the external field change to the full penetration field of the circular filament at zero transport current. This value of the full penetration field has been computed to be

$$H_p(0) = \frac{J_c\, d}{\pi} \tag{4.3-16}$$

where d is the diameter of the filament.

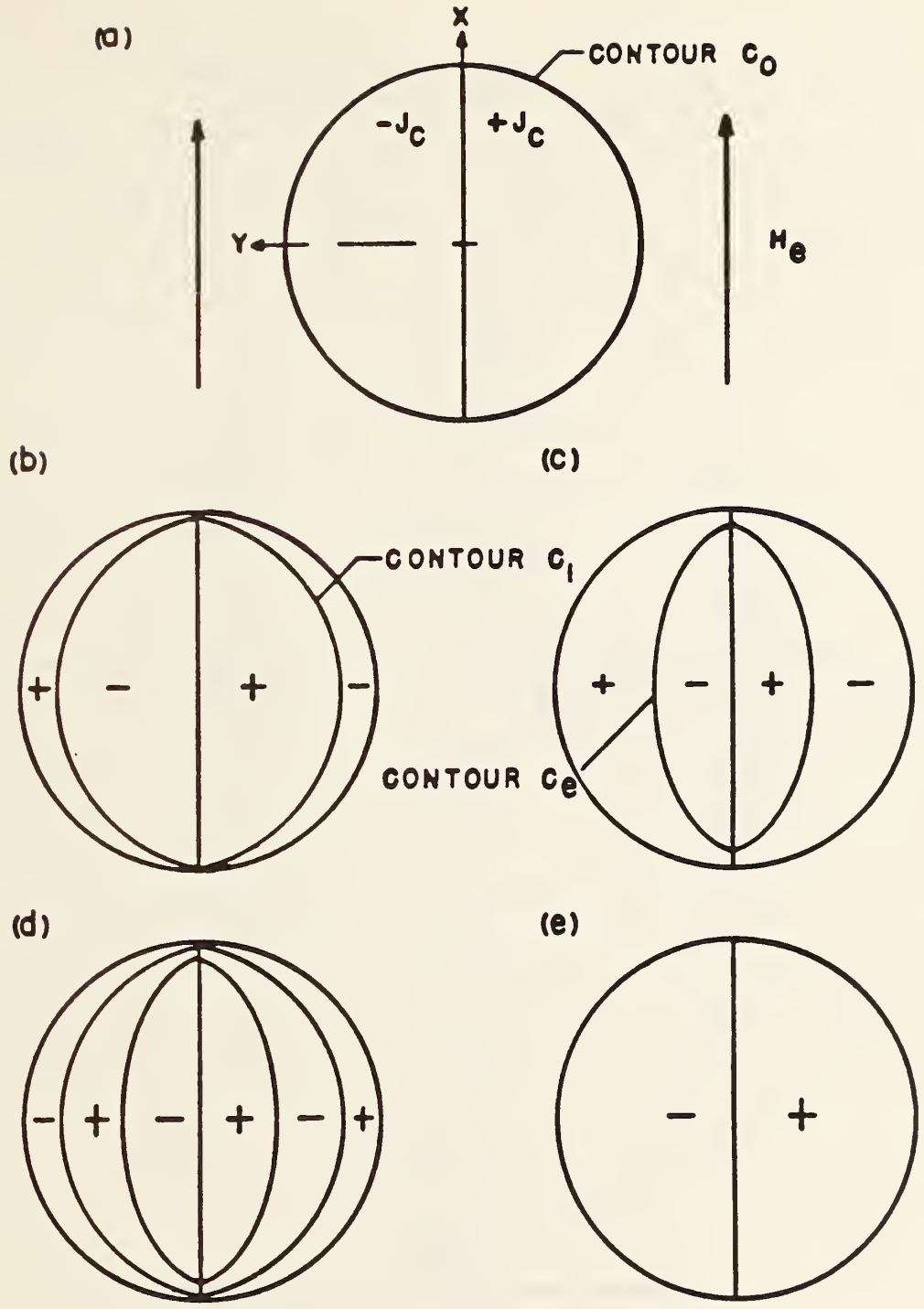

Figure 4.3-11. a) Initial condition at $H_0 + \Delta H_e$. b) Field reduced to $H_0 + \Delta H_e - \Delta H_1$. c) Lower limit of field change $H_0 - \Delta H_e$. d) Field increased to $H_0 - \Delta H_e + \Delta H_2$. e) End of half cycle with $H_0 + \Delta H_e$. Note: currents bounded by contour C shield $\Delta H/2$.

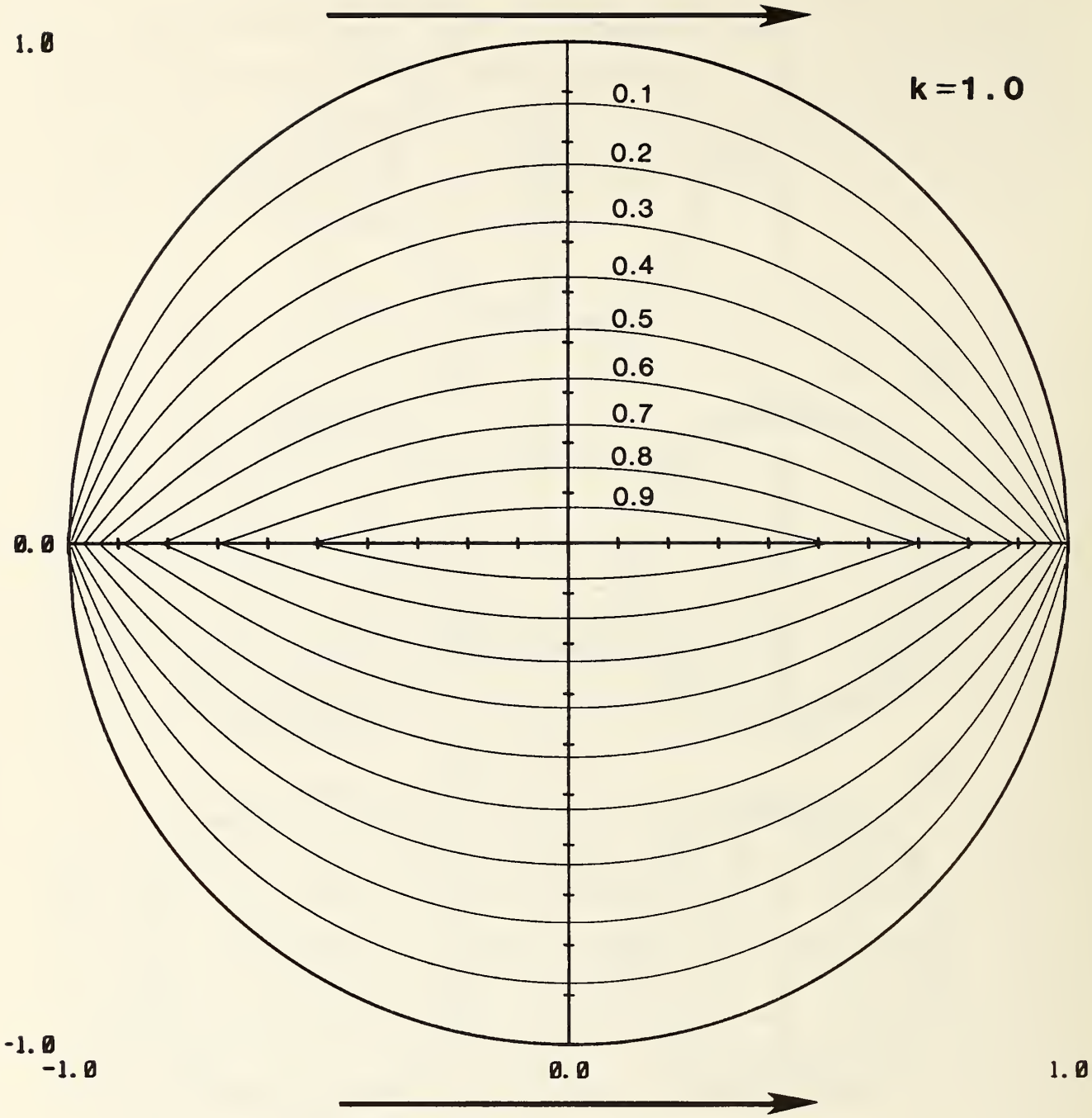

Figure 4.3-12. a) Limits of transverse flux penetration into cylindrical filaments of circular cross section for different values of the external field change $\Delta H_e/H_p(0)$.

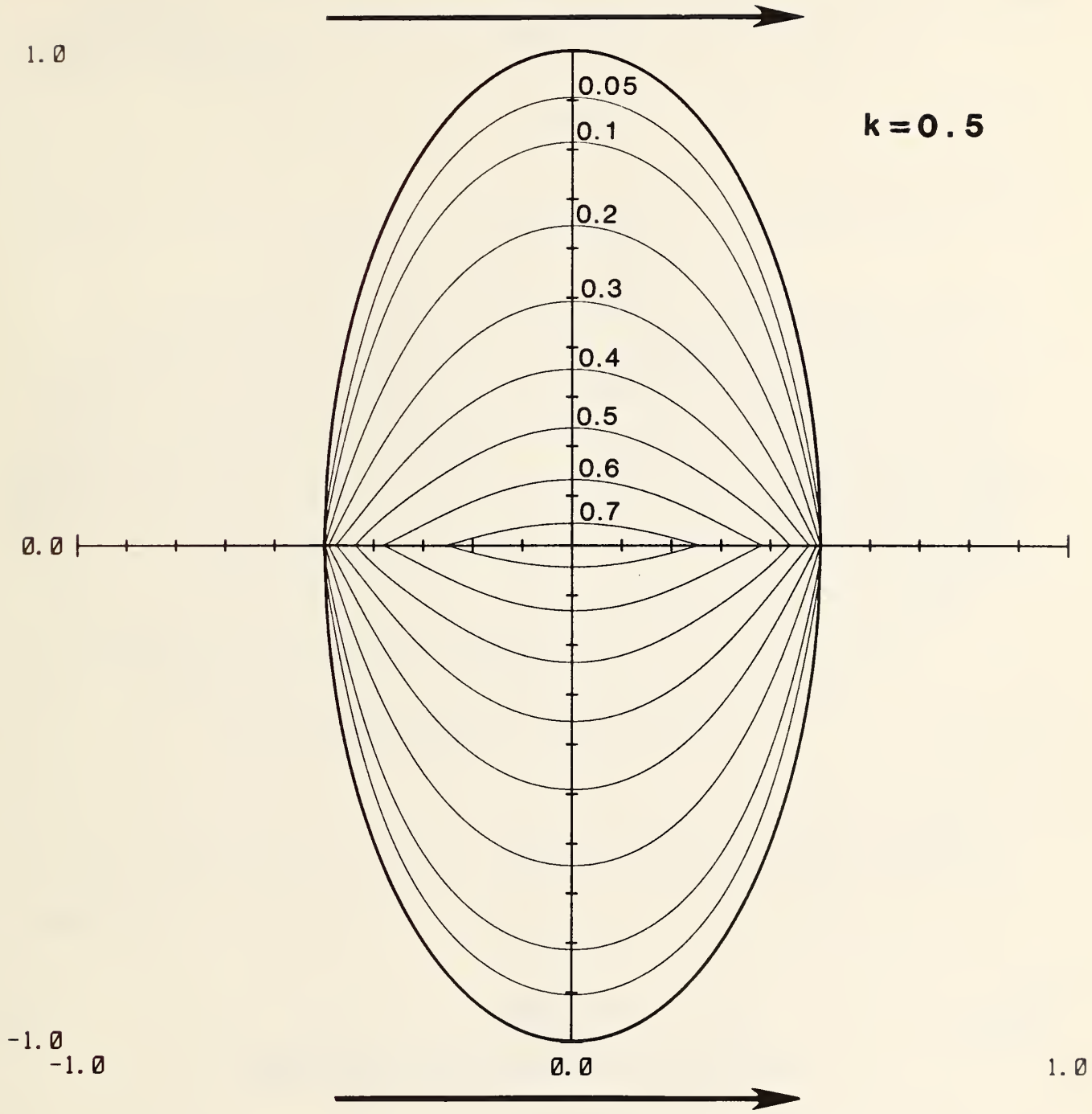

Figure 4.3-12 b) Limits of transverse flux penetration into cylindrical filaments of elliptical cross section for different values of the external field change $\Delta H_e/H_p(0)$ along the minor axis.

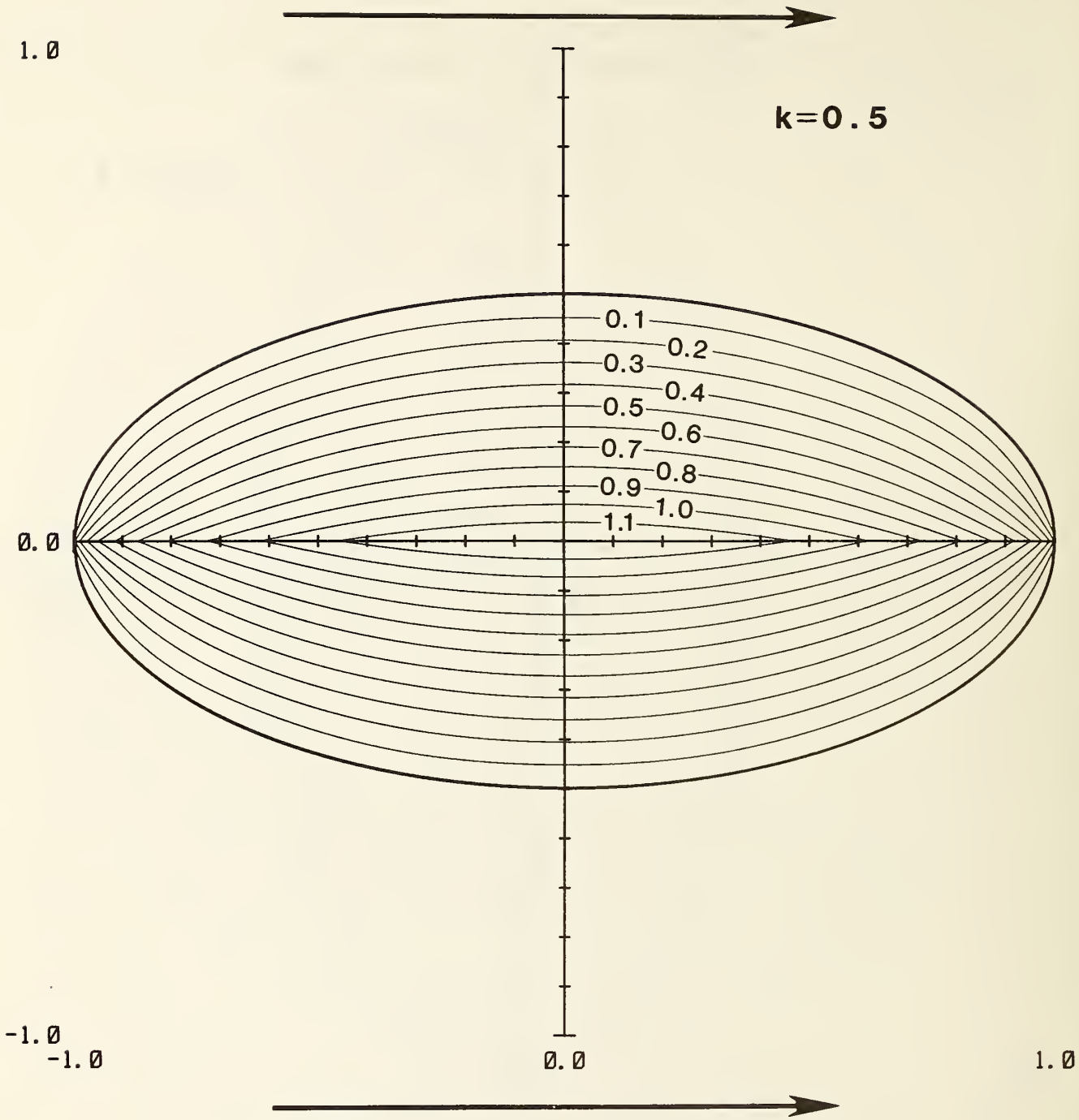

Figure 4.3-12 c) Limits of transverse flux penetration into cylindrical filaments of elliptical cross section for different values of the external field change $\Delta H_e/H_p(0)$ along the major axis.

The curves of flux penetration illustrated in figure 4.3-12 were generated by assuming their shape to be in the form of an even polynomial, i.e.,

$$y = f(x) = a_0 + a_2x^2 + a_4x^4 + a_6x^6 + a_8x^8 \quad , \tag{4.3-17}$$

where the coefficients a_n were determined by iteration to satisfy the boundary conditions of the governing equations for each value of external field.

The analytic form of the flux penetration curves allows the calculation of the filament magnetization for a discrete number of field points. Since at a given value of the external field the current distribution in the filament is known, the magnetization at a point due to this current distribution is given by [4.3-4]

$$\vec{m} = \frac{1}{2} (\vec{r} \times \vec{J}) \tag{4.3-18}$$

and the average magnetization is given by

$$\vec{M} = \frac{1}{2V} \int (\vec{r} \times \vec{J}) \, dV \tag{4.3-19}$$

The current density J is just $\pm J_c \cdot \vec{i}_z$ and the average value of the y-directed magnetization component is zero by symmetry. Thus, eq (4.3-19) reduces to

$$M = \frac{4}{\pi a^2 \ell} \left[\int_0^{\ell} dz \int_0^{a} dx \int_{f(x)}^{a\sqrt{1-(x/a)^2}} (y \, J_c) \, dy \right] \tag{4.3-20}$$

which in nondimensional form becomes

$$\frac{M}{H_p(0)} = 2\left[\int_0^{1} dx' \int_{f(x')}^{\sqrt{1-x'^2}} y' \, dy' \right] \tag{4.3-21}$$

where all primed dimensions have been normalized to the filament radius a and the form of f(x) is given by eq (4.3-17). Evaluation of eq (4.3-21) for the curves shown in figure 4.3-12a gives values for the magnetization which can be closely approximated by the following expression [4.3-5]

$$\frac{M}{H_p(0)} = \left[\frac{2}{3}\left(\frac{\Delta H_e}{H_p(0)}\right)^3 - 2\left(\frac{\Delta H_e}{H_p(0)}\right)^2 + 2\left(\frac{\Delta H_e}{H_p(0)}\right)\right], \quad \frac{\Delta H_e}{H_p(0)} \leq 1 \qquad (4.3\text{-}22)$$

The expression for M in eq (4.3-22) gives the magnetization for an initial increase of ΔH_e from zero. The complete hysteresis curve can be constructed by noting that once the filament is fully penetrated, any change in external field must induce a shielding current change of magnitude $2J_c$ to reverse the current distribution in the shielding current region (fig. 4.3-11). The complete hysteresis curve is shown in figure 4.3-13.

TWO DIMENSIONAL LOSS: NO TRANSPORT CURRENT

The hysteresis loss per cycle per unit volume can be computed by integration of the magnetization over a complete cycle. This must be done for two conditions: partial penetration and full penetration. The partial penetration loss W_{p0} results from substitution of eq (4.3-22) for the magnetization into eq (4.3-5) to give

$$\frac{W_{p0}}{W_0} = 2\left(\frac{\Delta H_e}{H_p(0)}\right)^3 - \left(\frac{\Delta H_e}{H_p(0)}\right)^4 , \qquad (4.3\text{-}23)$$

where $W_0/V = (4/3)\,\mu_0\,H_p^2(0)$ is the loss per unit volume for $\Delta H_e = H_p(0)$.

To compute the full penetration loss W_{fp0} we note that the current distribution cannot change once the full penetration field $H_p(0)$ has been exceeded. Thus the field penetrates uniformly. The total loss over one cycle is the sum of the partial penetration loss plus the loss that occurs when ΔH_e exceeds $H_p(0)$ and is given by

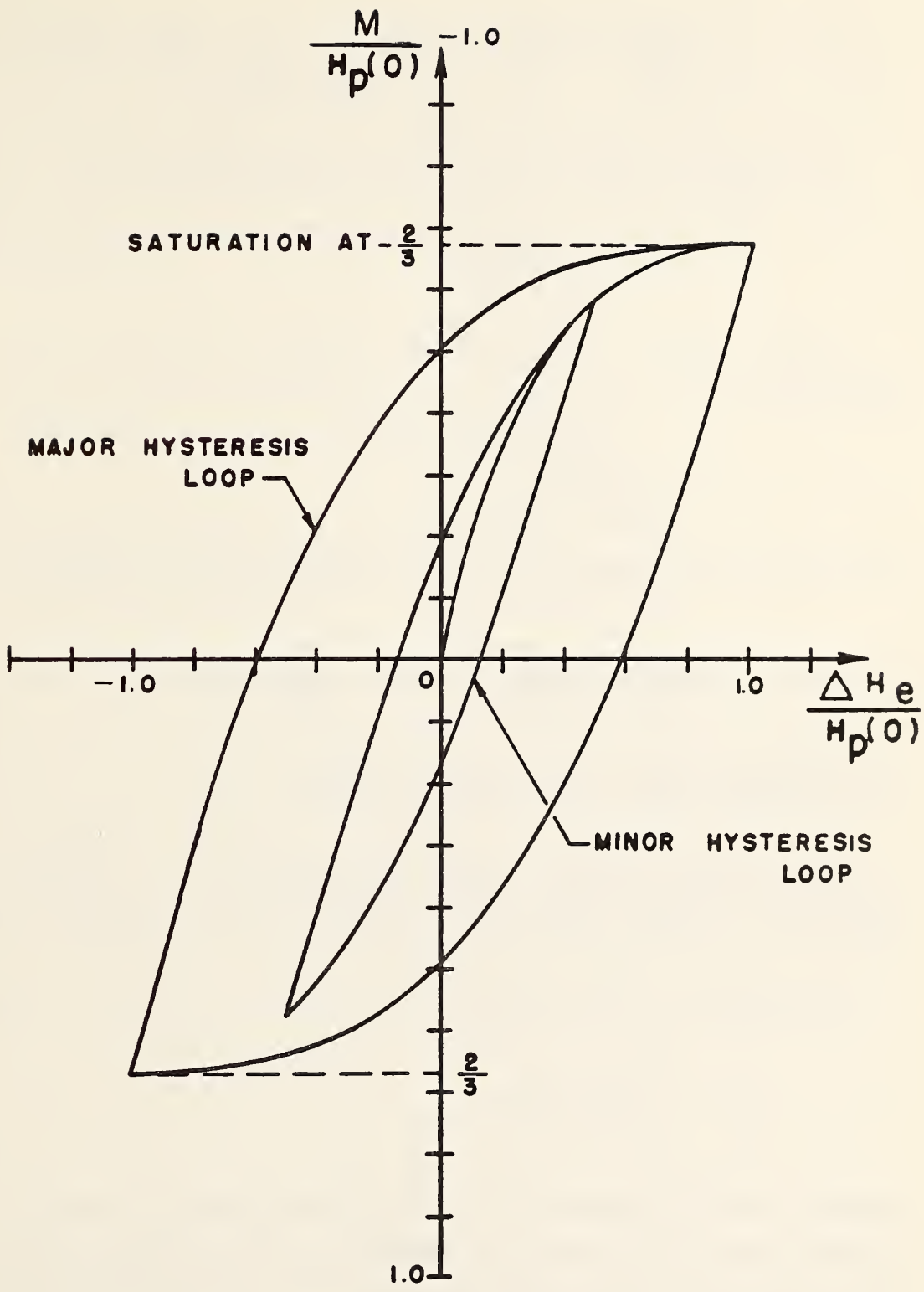

Figure 4.3-13. Magnetization loop for circular superconducting filament.

$$\frac{W_{fp0}}{W_0} = \frac{W_{p0}(H_p(0))}{V} + \frac{1}{V}\left[\int_{\text{volume}} \S \int_{\text{cycle}} (\vec{J}\cdot\vec{E})\, dt\, dV\right]. \qquad (4.3\text{-}24)$$

The electric field E is found from the Maxwell equation,

$$\nabla \times \vec{E} = -\mu_0 \frac{d(\vec{H}_c)}{dt} \qquad (4.3\text{-}25)$$

and given by

$$E_z = -\mu_0 \dot{H} \frac{y}{2} \qquad (4.3\text{-}26)$$

Carrying out the integration in eq (4.3-24) gives for the loss per cycle,

$$\frac{W_{fp0}}{W_0} = \left[2\left(\frac{\Delta H_e}{H_p(0)}\right) - 1\right], \qquad \frac{\Delta H_e}{H_p(0)} \geq 1. \qquad (4.3\text{-}27)$$

TWO DIMENSIONAL LOSS: WITH TRANSPORT CURRENT

The transport current destroys the symmetry of the problem due to the addition of the self field of the filament. In the previous case the net current in the filament was zero whereas now the current must sum to the transport current. The following condition must always be satisfied:

$$i = \left(\frac{A_+ - A_-}{A_+ + A_-}\right) \quad , \qquad (4.3\text{-}28)$$

where $A_\pm$ = area of $\pm J_c$, and $i = (I_t/I_c)$ is the ratio of transport to critical current. In addition, the field required to fully penetrate the filament must become a function of the transport current such that $H_p(i) \leq H_p(0)$ where $H_p(i)$ is a function yet to be determined.

Assume that the filament carries a normalized transport current i, $0 < i < 1$, in a uniform external field $H_0 >> H_p(i)$. The problem is to compute the

current distribution as the external field is cycled between $H_0 \pm \Delta H_e$ while the transport current remains constant for two cases: (1) $\Delta H_e \leq H_p(i)$ and (2) $\Delta H_e \geq H_p(i)$. The exact initial current distribution is not known. In fact, we cannot assume any one specific initial state since the current pattern is determined by the most recent history of current and field change. The crucial element in this reasoning process is that only the most recent history of change is important.

After several cycles of external field change with constant transport current the initial current distribution will be wiped out or, more accurately, rearranged. The process is guided by three requirements:

1) flux can enter or leave only from the filament surface,
2) current can only flow at $\pm J_c$, and
3) the condition of eq (4.3-28) must always be satisfied.

This reasoning will result in a time-dependent steady-state current distribution as shown in figure 4.3-14 with the transport current redistributed into a central core of the filament surrounded by positive and negative shielding currents near the outer surface. The exact number of cycles required to completely rearrange the current distribution is not known but must be a function of i and ΔH_e. If there are many cycles of external field change the details of the transition stage will have an insignificant effect on the loss.

This type of current distribution in a circular filament is analogous to that in a slab under similar conditions as indicated in figure 4.3-3. The shielding currents will alternate in sign in a region near the surface while screening the transport current in the core while $\Delta H_e \leq H_p(i)$. Thus, the definition of the full-penetration field as a function of transport current $H_p(i)$ follows in that it is just the magnitude of the external field change, ΔH_e, that, if exceeded, will no longer change the current distribution in the filament. The curves that define the boundary between shielding currents and transport current are also known. They are the same curves that define the field penetration profiles for the case when i = 0. This is so because the current distributions defined by these profiles totally shield the region within them.

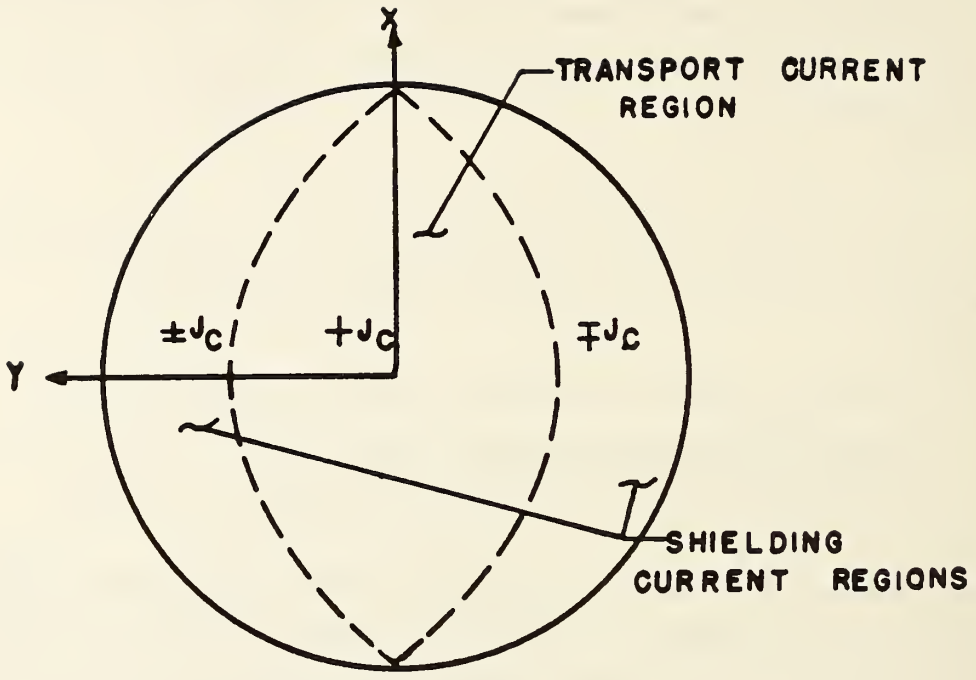

Figure 4.3-14. Current distribution in a circular filament showing the shielding current region and the transport current region.

A curve of $H_p(i)$ versus i was computed from the previously determined shielding profiles (fig. 4.3-12a). At each value of applied field the shielding currents surround an area which is proportional to the transport current i. The integration to determine this area is trivial since the curves that define this boundary are simple polynomials. The fraction of transport current is then

$$i = \frac{4}{\pi}\left(a_0 x_m + a_2 \frac{x_m^3}{3} + a_4 \frac{x_m^5}{5} + a_6 \frac{x_m^7}{7} + a_8 \frac{x_m^9}{9}\right) \qquad (4.3\text{-}29)$$

where the polynomial coefficients a_n and the x-axis intercept, x_m, were previously computed for several values of applied field. The full penetration field versus current is shown in fig. 4.3-15. At zero transport current $H_p(0)$ is equal to $J_c d/\pi$ while at $i = 1$ $H_p(1)$ goes to zero since the entire filament is filled with transport current and thus cannot carry any shielding currents.

To compute the loss for the case of partial penetration with transport current W_{pt} is quite simple. The current distribution and the full penetration field are given in figures 4.3-14 and 4.3-15, respectively. The transport current contributes nothing to the loss since it is completely shielded from the external field change throughout the cycle. Thus, the loss is identical to that for the case of partial penetration without transport current as long as the condition $\Delta H_e \leq H_p(i)$ holds, i.e.,

$$\frac{W_{pt}}{W_0} = 2\left(\frac{\Delta H_e}{H_p(0)}\right)^3 - \left(\frac{\Delta H_e}{H_p(0)}\right)^4. \qquad (4.3\text{-}30)$$

Full penetration occurs when ΔH_e exceeds $H_p(i)$. At this point the flux penetrates the filament uninhibited by shielding currents and the energy dissipation for this cycle W_{fpt} is given by

$$\frac{W_{fpt}}{V} = \frac{W_{pt}(H_p(i))}{V} + \frac{1}{V}\left[\int_{\text{volume}} \S \; (J \cdot E)\, dt\, dv\right]_{\text{cycle}} \qquad (4.3\text{-}31)$$

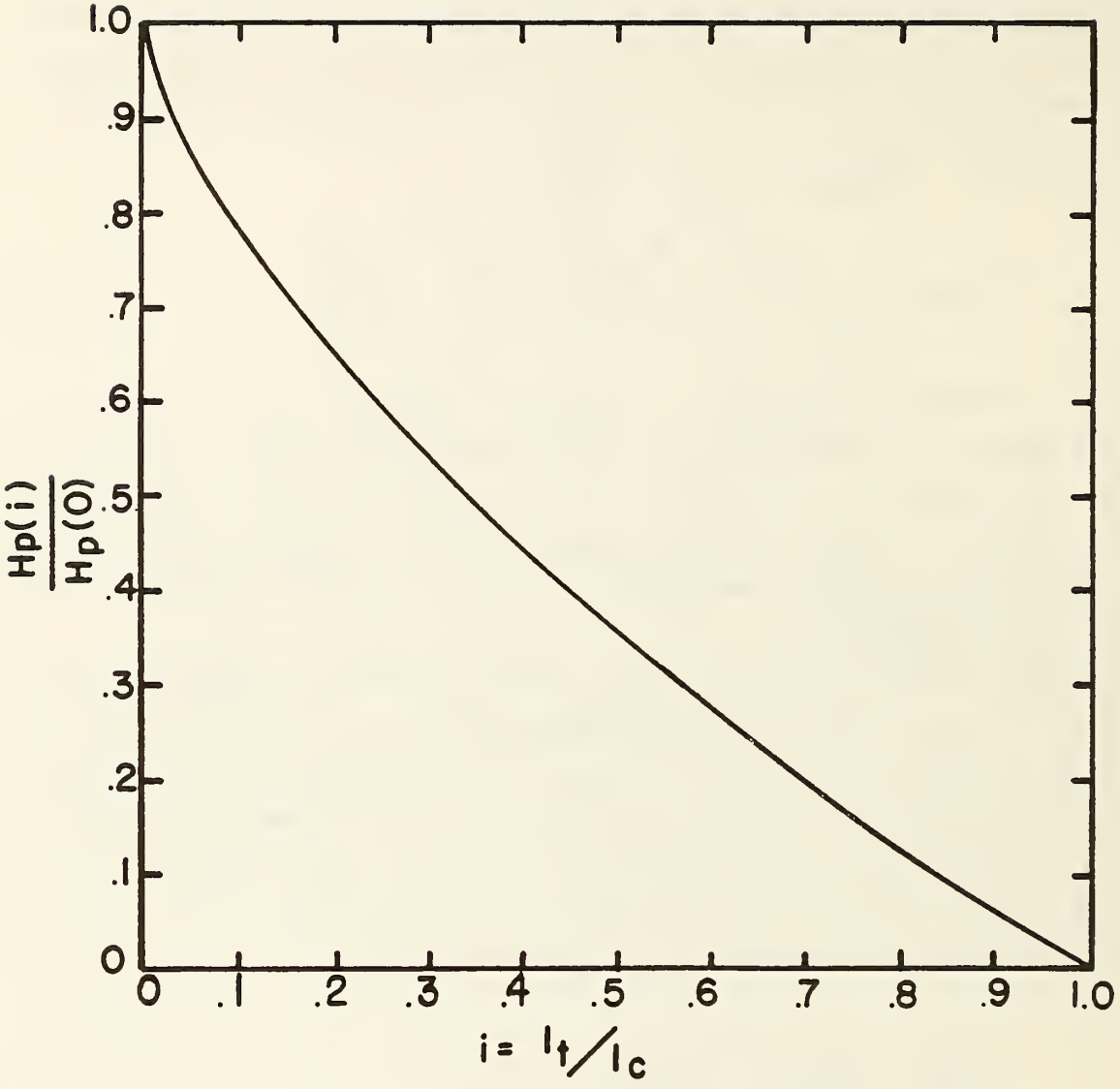

Figure 4.3-15. Full penetration field as a function of the transport current.

The electric field E is determined from eq (4.3-26), but the computation is more complicated than the zero current case because the position of zero electric field no longer lies on a line of symmetry along the x axis. It now coincides with the boundary separating regions of positive and negative current. This boundary is a function of the transport current and its shape is given by the appropriate curve in figure 4.3-12a for $\Delta H_e = H_p(i)$. Thus E is given by

$$E_z = -\mu_0 |\Delta \dot{H}_e| y \frac{d}{2} \qquad \text{for } -1 < x < -x_m \text{ and } x_m < x < 1 \qquad (4.3\text{-}32a)$$

and

$$E_z = -\mu_0 |\Delta \dot{H}_e| \frac{d}{2}[y - f(x)] \qquad \text{for } -x_m < x < x_m \ , \qquad (4.3\text{-}32b)$$

where x and y are normalized to the filament radius a = d/2, and f(x) is the function defining the transport current region boundary (eq (4.3-17)). See figure 4.3-16.

The effect can be summed up as follows. The magnetic flux penetrates uniformly into the filament from both sides inducing a positive electric field in regions of positive current and a negative electric field in regions of negative current. No flux crosses the surface separating the two regions and thus E = 0 along this boundary. The power dissipation is given by $J_c \cdot E$ and can be separated into two contributions: one from the shielding currents and the other from the transport current. The external field source supplies the energy dissipated by the shielding currents and the current source provides the energy dissipated by the transport current.

Substituting eq (4.3-32) into eq (4.3-31) and carrying out the integration over a complete cycle gives the loss per unit volume for $\Delta H_e > H_p(i)$:

$$\frac{W_{fpt}}{W_0} = \{2[\frac{H_p(i)}{H_p(0)}]^3 - [\frac{H_p(i)}{H_p(0)}]^4\} + 2\{[\frac{\Delta H_e}{H_p(0)}] - [\frac{H_p(i)}{H_p(0)}]\} \gamma(i) \ . \qquad (4.3\text{-}33)$$

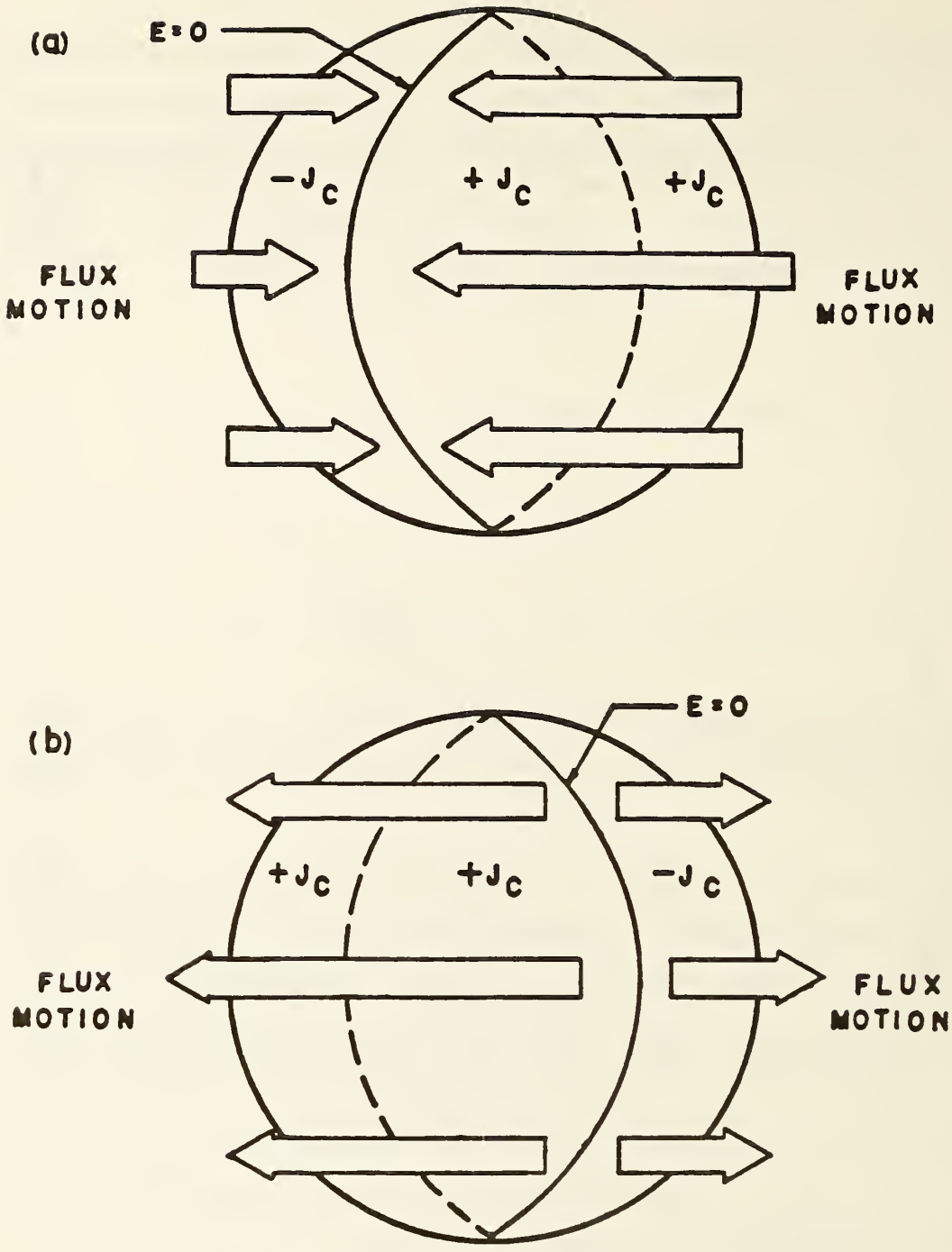

Figure 4.3-16. Full penetration flux motion for a) increasing external field, and b) decreasing external field.

The non-dimensional function $\gamma(i)$ is shown in figure 4.3-17. The two-dimensional loss expression in eq (4.3-33) is very similar to the one-dimensional loss expression, eq (4.3-9b). The first term on the right side of each expression is the portion of the loss that occurs when the conductor is partially penetrated. The second term on the right side of each expression is the portion of the loss that occurs when the conductor is fully penetrated. The factor $\gamma(i)$ for the two-dimensional case is directly analogous to the $(1+i^2)$ term for the slab loss. However, it cannot be expressed analytically but must be computed numerically for each of the flux penetration curves of figure 4.3-12a.

Just as in the slab model, a portion of the loss occurs in the transport current region and a portion in the shielding current region during the part of the cycle when ΔH_e exceeds $H_p(i)$. Thus, $\gamma(i)$ can be written as $\gamma(i) = \alpha(i) + \beta(i)$, where $\alpha(i)$ represents the fraction of the loss that occurs in the shielding current region and $\beta(i)$ represents the fraction of the loss in the transport current region. The functions α and β are shown along with γ as functions of current in figure 4.3-17. They can be computed from the following expressions:

$$\alpha(i) = \frac{3}{4}\{4\left[\int_{-x_m}^{1} dx \int_{0}^{\sqrt{1-x^2}} y\, dy\right] + 2\left[\int_{0}^{x_m} dx \int_{f(x)}^{\sqrt{1-x^2}} (y-f(x))\, dy\right]$$

$$- 2\left[\int_{0}^{x_m} dx \int_{-\sqrt{1-x^2}}^{-f(x)} (y - f(x))\, dy\right]\} \qquad (4.3\text{-}34a)$$

and

$$\beta(i) = \frac{3}{4}\{2\left[\int_{0}^{x_m} dx \int_{f(x)}^{-f(x)} (y - f(x))\, dy\right]\}. \qquad (4.3\text{-}34b)$$

The shapes of these curves are not unexpected since at zero transport current the loss is all shielding loss, $\alpha(0)=1$, and no transport loss, $\beta(0)=0$.

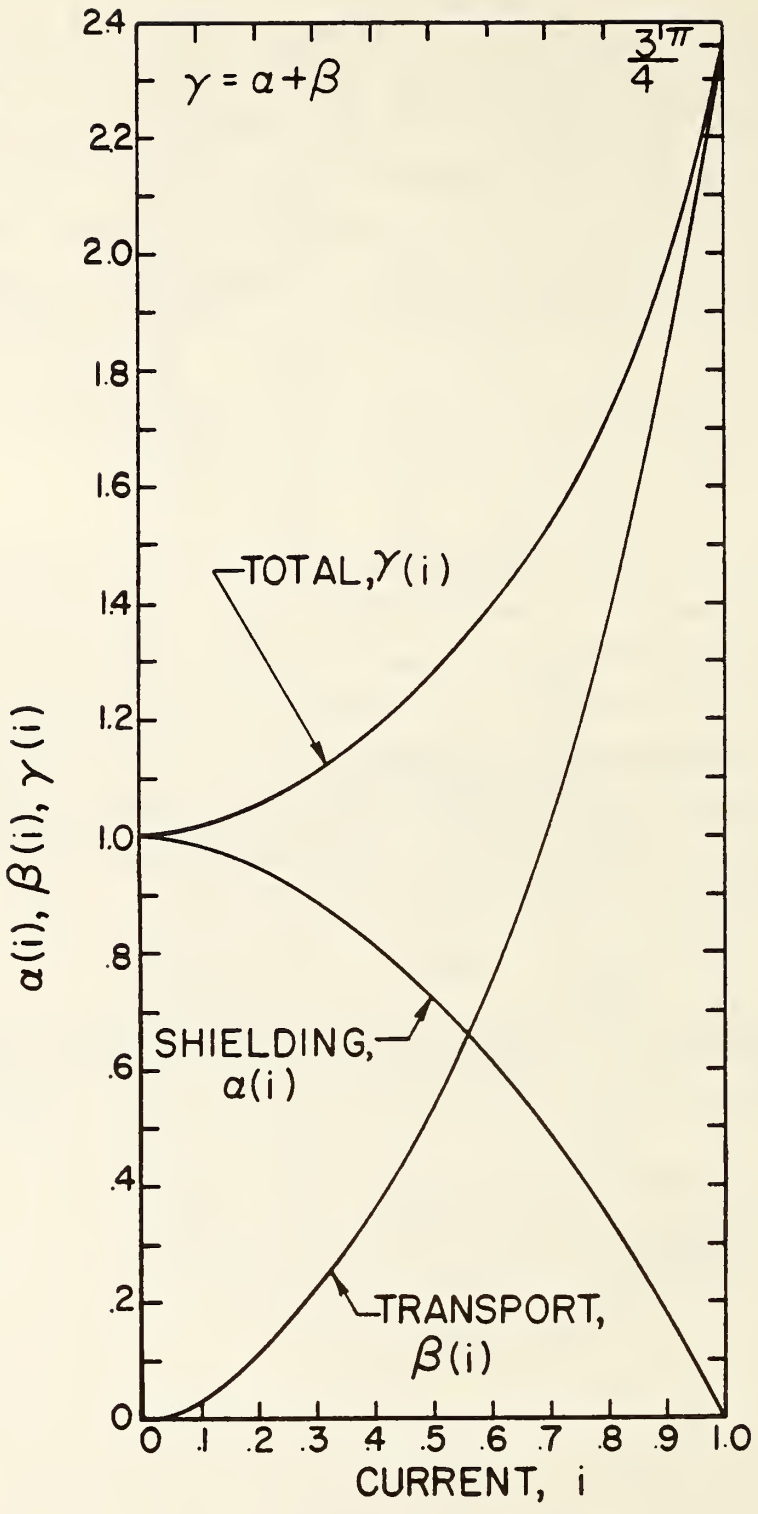

Figure 4.3-17. Functions α, β, and γ as functions of transport current.

As i is increased $\alpha(i)$ must decrease and $\beta(i)$ must increase since a greater area of the filament is filled with transport current, leaving less area for shielding currents until the filament is totally filled with transport current at i=1. The two-dimensional factors $\alpha(i)$ and $\beta(i)$ are analogous to the slab factors $(1-i^2)$ and i^2, respectively.

The total loss can be separated into two components and summarized as follows:

$$\frac{W_{ft}}{W_0} = \frac{W_s}{W_0} + \frac{W_t}{W_0} \quad , \tag{4.3-35a}$$

where, for $\Delta H_e \leq H_p(i)$,

$$\frac{W_s}{W_0} = 2\left(\frac{\Delta H_e}{H_p(0)}\right)^3 - \left(\frac{\Delta H_e}{H_p(0)}\right)^4 \quad , \tag{4.3-35b}$$

$$\frac{W_t}{W_0} = 0 \tag{4.3-35c}$$

and for $\Delta H_e > H_p(i)$

$$\frac{W_s}{W_0} = \left\{2\left(\frac{H_p(i)}{H_p(0)}\right)^3 - \left(\frac{H_p(i)}{H_p(0)}\right)^4\right\} + 2\left\{\left(\frac{\Delta H_e}{H_p(0)}\right) - \left(\frac{H_p(i)}{H_p(0)}\right)\right\} \alpha(i) \quad , \tag{4.3-35d}$$

$$\frac{W_t}{W_0} = 2\left\{\left(\frac{\Delta H_e}{H_p(0)}\right) - \left(\frac{H_p(i)}{H_p(0)}\right)\right\} \beta(i) \quad . \tag{4.3-35e}$$

The shielding, transport, and total losses are shown as functions of the transport current with external field change as a parameter in figures 4.3-18, 4.3-19, and 4.3-20, respectively. The two-dimensional loss expressions are summarized in Appendix 4.3-B.

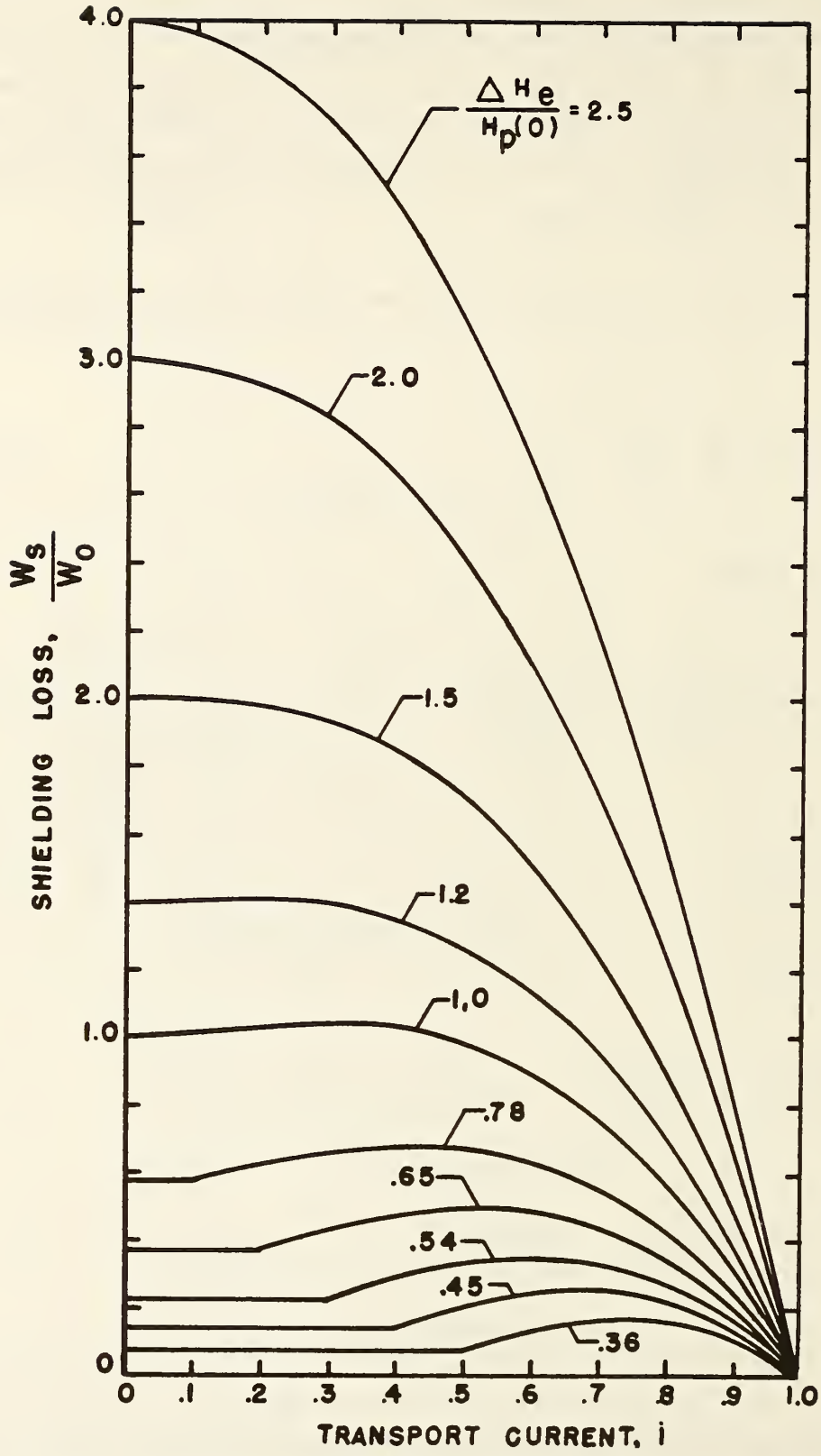

Figure 4.3-18. Shielding loss versus transport current for different values of external field change.

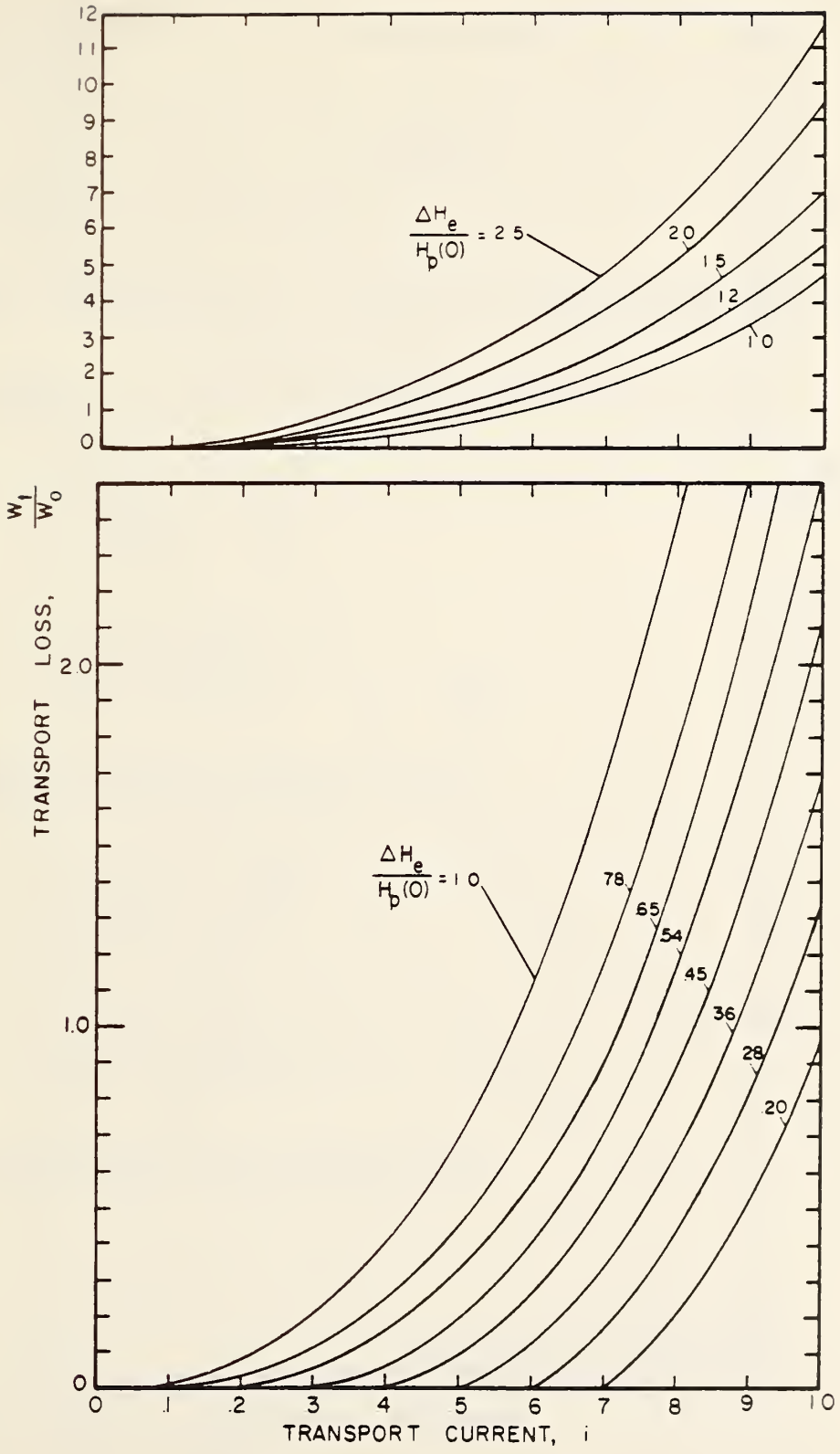

Figure 4.3-19. Transport loss versus transport current for different values of external field change.

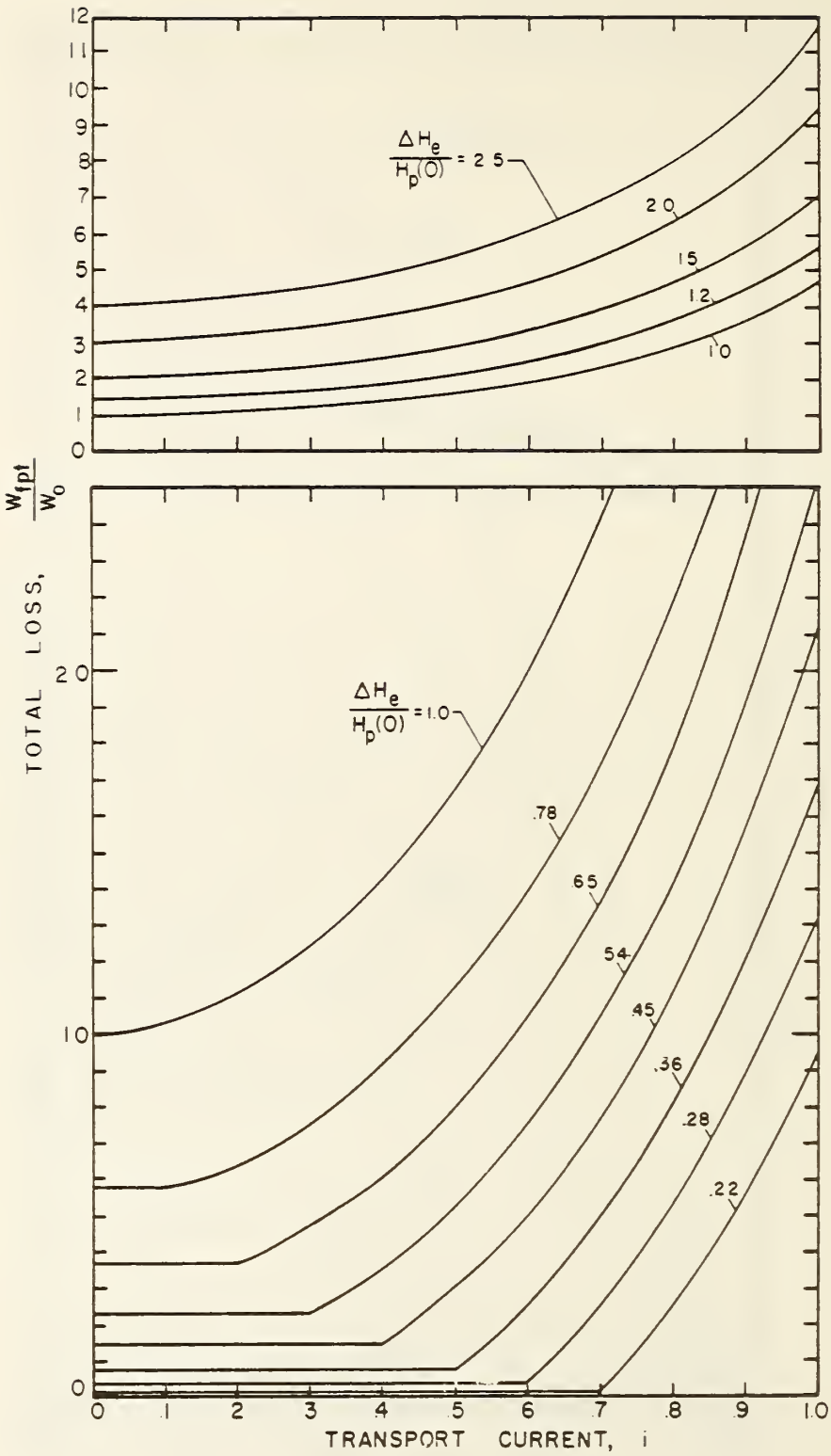

Figure 4.3-20. Total loss versus transport current for different values of external field change.

APPENDIX 4.3-A

SUMMARY OF ONE-DIMENSIONAL LOSS FORMULA

All losses are given as a normalized loss per unit volume per cycle.

CONDITIONS: Changing external field with constant transport current.

Partial Penetration Without Transport Current

$$\frac{H_m}{H_p(0)} \leq 1, \quad i=0$$

$$\frac{W_{p0}}{W_0} = \left(\frac{H_m}{H_p(0)}\right)^3$$

Full Penetration Without Transport Current

$$\frac{H_m}{H_p(0)} > 1, \quad i=0$$

$$\frac{W_{fp0}}{W_0} = \left[3\left(\frac{H_m}{H_p(0)}\right)-2\right]$$

Partial Penetration With Transport Current

$$\frac{H_m}{H_p(0)} \leq 1, \quad 0 \leq i \leq 1$$

$$\frac{W_{pt}}{W_0} = \left(\frac{H_m}{H_p(0)}\right)^3$$

Full Penetration With Transport Current

$$\frac{H_m}{H_p(0)} > 1, \quad 0 \leq i \leq 1$$

$$\frac{W_{fpt}}{W_0} = \left(\frac{H_p(i)}{H_p(0)}\right)^3 + 3\left[\left(\frac{H_m}{H_p(0)}\right) - \left(\frac{H_p(i)}{H_p(0)}\right)\right] (1 + i^2)$$

W_{fpt}/W_0 is the total loss. It can be further broken down into a shielding current loss, W_s/W_0 and a transport current loss, W_t/W_0.

$$\frac{W_{fpt}}{W_0} = \frac{W_s}{W_0} + \frac{W_t}{W_0}$$

where

$$\frac{W_s}{W_0} = \left(\frac{H_p(i)}{H_p(0)}\right)^3 + 3\left[\left(\frac{H_m}{H_p(0)}\right) - \left(\frac{H_p(i)}{H_p(0)}\right)\right] (1 - i^2)$$

and

$$\frac{W_t}{W_0} = 6\left[\left(\frac{H_m}{H_p(0)}\right) - \left(\frac{H_p(i)}{H_p(0)}\right)\right] i^2$$

if $H_m >> H_p(0)$

$$\frac{W_{fpt}}{W_0} \cong 3\left(\frac{H_m}{H_p(0)}\right) (1 + i^2)$$

Note (1): These losses are for a constant transport current, $i=I_t/I_c$ and for an alternating external field, H_e, given by

$$H_e = H_0 \pm H_m(t)$$

where H_0 is the uniform background field.

$$H_0 >> H_p(0)$$

$$H_p(0) = \frac{J_c d}{2}$$

$$\frac{W_0}{V} = \frac{2}{3} \mu_0 H_p^2(0)$$

Note (2): The partial penetration field as a function of transport current, $H_p(i)$, is given by

$$\frac{H_p(i)}{H_p(0)} = (1 - i)$$

CONDITIONS: Constant External Field With Alternating Transport Current

Loss expression

$$0 \leq i_m \leq 1$$

$$\frac{W_h}{W_0} = 4 i_m^3$$

$$i_m = \frac{I_{max}}{I_c}$$

$$\frac{W_0}{V} = \frac{2}{3} \mu_0 H_p^2(0)$$

$$H_p(0) = \frac{J_c d}{2}$$

Additional Formulas

for $i = i_m \sin(\omega t)$

increasing current

magnetization $$\frac{M_{\uparrow}}{H_p(0)} = \frac{1}{2} i_m^2 \left[-1 + 2\left(\frac{i}{i_m}\right) + \left(\frac{i}{i_m}\right)^2\right]$$

terminal voltage $$\frac{V_{\uparrow}}{V_0} = -\cos(\omega t)\,[1 + \sin(\omega t)]$$

decreasing current

magnetization $$\frac{M_{\downarrow}}{H_p(0)} = \frac{1}{2} i_m^2 \left[1 + 2\left(\frac{i}{i_m}\right) - \left(\frac{i}{i_m}\right)^2\right]$$

terminal voltage $$\frac{V_{\downarrow}}{V_0} = -\cos(\omega t)\,[1 - \sin(\omega t)]$$

where: $V_0 = \mu_0 H_p(0)\, d\, \ell\, \omega\, i_m^2$

d = slab thickness

ℓ = slab length

ω = frequency

APPENDIX 4.3-B

SUMMARY OF TWO-DIMENSIONAL LOSS FORMULA

All losses are given as a normalized loss per unit volume per cycle.

Partial Penetration Without Transport Current

$$\frac{\Delta H_e}{H_p(0)} \leq 1, \quad i=0$$

$$\frac{W_{p0}}{W_0} = 2\left(\frac{\Delta H_e}{H_p(0)}\right)^3 - \left(\frac{\Delta H_e}{H_p(0)}\right)^4$$

Full Penetration Without Transport Current

$$\frac{\Delta H_e}{H_p(0)} > 1, \quad i=0$$

$$\frac{W_{fp0}}{W_0} = 2\left(\frac{\Delta H_e}{H_p(0)}\right) - 1$$

Partial Penetration With Transport Current

$$\frac{\Delta H_e}{H_p(i)} \leq 1, \quad 0 \leq i \leq 1$$

$$\frac{W_{pt}}{W_0} = 2\left(\frac{\Delta H_e}{H_p(0)}\right)^3 - \left(\frac{\Delta H_e}{H_p(0)}\right)^4$$

Full Penetration With Transport Current

$$\frac{\Delta H_e}{H_p(i)} > 1, \quad 0 \leq i \leq 1$$

$$\frac{W_{fpt}}{W_0} = \left[2\left(\frac{H_p(i)}{H_p(0)}\right)^3 - \left(\frac{H_p(i)}{H_p(0)}\right)^4\right] + 2\left[\left(\frac{\Delta H_e}{H_p(0)}\right) - \left(\frac{H_p(i)}{H_p(0)}\right)\right] \gamma(i)$$

W_{fpt}/W_0 is the total loss. It can be further broken down into a shielding current loss, W_s/W_0 and a transport current loss, W_t/W_0.

$$\frac{W_{fpt}}{W_0} = \frac{W_s}{W_0} + \frac{W_t}{W_0}$$

where

$$\frac{W_s}{W_0} = \left[2\left(\frac{H_p(i)}{H_p(0)}\right)^3 - \left(\frac{H_p(i)}{H_p(0)}\right)^4\right] + 2\left[\left(\frac{\Delta H_e}{H_p(0)}\right) - \left(\frac{H_p(i)}{H_p(0)}\right)\right] \alpha(i)$$

and

$$\frac{W_t}{W_0} = 2\left[\left(\frac{\Delta H_e}{H_p(0)}\right) - \left(\frac{H_p(i)}{H_p(0)}\right)\right] \beta(i)$$

If $\Delta H_e >> H_p(0)$

$$\frac{W_{fpt}}{W_0} \cong 2\left(\frac{\Delta H_e}{H_p(0)}\right) [\alpha(i) + \beta(i)] = 2\left(\frac{\Delta H_e}{H_p(0)}\right) \gamma(i)$$

Note (1): These losses are for a constant transport current, $i = I_t/I_c$ and for an alternating external field, H_e, given by

$$H_e = H_0 \pm \Delta H_e$$

where H_0 is the uniform background field.

$$H_0 >> H_p(0)$$

$$H_p(0) = \frac{J_c d}{\pi}$$

$$W_0 = \frac{4}{3} \mu_0 H_p^2(0)$$

Note (2): The partial penetration field as a function of transport current $H_p(i)$, is given in figure 4.3-15.

Note (3): $\gamma(i) = \alpha(i) + \beta(i)$
The coefficients $\alpha(i)$, $\beta(i)$, and $\gamma(i)$ are given in figure 4.3-17. The losses W_s/W_0, W_t/W_0, and W_{fpt}/W_0 are given in figures 4.3-18, 4.3-19, and 4.3-20, respectively.

4.4 References

[4.1-1] M. N. Wilson, Rutherford Lab. Report SMR/1, Chilton, Oxfordshire, England, 1977 (unpublished).

[4.1-2] J. W. Ekin, J. Appl. Phys. 49, 3406 (1978).

[4.1-3] L. Dresner, Cryogenics 18, 285 (1978).

[4.1-4] L. F. Goodrich and F. R. Fickett, Cryogenics 22, 225 (1982).

[4.1-5] J. W. Ekin, private communication.

[4.1-6] L. F. Goodrich, J. W. Ekin, and F. R. Fickett, Advances in Cryogenic Engineering - Materials 28, 571 (1982).

[4.1-7] L. F. Goodrich, IEEE Trans. Magn. MAG-19, to be published.

[4.1-8] A. F. Clark, L. F. Goodrich, F. R. Fickett, and J. V. Minervini, NBSIR 82-1678, National Bureau of Standards, Boulder, Colorado (July 1982).

[4.2-1] L. F. Goodrich and J. W. Ekin, "Lap Joint Resistance and Intrinsic Critical Current Measurements on a NbTi Superconducting Wire," IEEE Trans. Magn. MAG-17, 69 (1981).

[4.2-2] F. R. Fickett, "Electrical Properties," Chapter 5 in: Materials at Low Temperatures, edited by R. P. Reed and A. F. Clark (American Society for Metals, Ohio, 1983).

[4.2-3] F. R. Fickett, private communication.

[4.2-4] M. Kobayashi, M. Mruzek, and W. Craddock, "Electrical and Mechanical Properties of Lead/Tin Solders and Splices at 4.2 K," presented at the International Cryogenic Materials Conference, May 11-14, 1983, Kobe, Japan (unpublished).

[4.2-5] D. Yu, Y. M. Eyssa, and P. Zollikei, "Electrical Boundary Resistance in an Aluminum-Stabilized Superconductor," Adv. Cryog. Eng. - Materials, 28, 701 (1981).

[4.2-6] L. F. Goodrich and F. R. Fickett, "Critical Current Measurements: A Compendium of Experimental Results," Cryogenics 22, 225 (1982).

[4.2-7] F. R. Fickett, "Electric and Magnetic Properties of CuSn and CuNi Alloys at 4 K," Cryogenics 22, 135 (1982).

[4.3-1] R. A. Beth, J. Appl. Phys. 38 (12), 4689 (1967).

[4.3-2] J. V. Minervini, Adv. Cryo. Eng. 28, 587 (1982).

[4.3-3] J. V. Minervini, "Analysis of loss mechanisms in superconducting windings for rotating electric generators," Ph.D. Thesis, Department of Mechanical Engineering, Massachusetts Inst. of Technology, Cambridge, MA (1981).

[4.3-4] J. D. Jackson, "Classical Electrodynamics," John Wiley and Sons, New York, 146 (1967).

[4.3-5] C. Y. Pang, P. G. McLaren, and A. M. Campbell, in: Proceedings of the Eighth International Cryogenic Engineering Conference, IPC Science and Technology Press, Guildford, Surrey, England (1980).

APPENDIX A

PUBLICATIONS AND PRESENTATIONS

1. A. F. Clark and J. W. Ekin, "Defining Critical Current," IEEE Trans. Mag. MAG-13, 38-40 (1977).

2. R. L. Powell and A. F. Clark, "Definitions of Terms for Practical Superconductors, 1. Fundamental States and Flux Phenomena," Cryogenics 17, 697-701 (1977).

3. R. L. Powell and A. F. Clark, "Definitions of Terms for Practical Superconductors, 2. Critical Parameters," Cryogenics 18, 137-141 (1978).

4. J. W. Ekin, "Current Transfer in Multifilamentary Superconductors. I. Theory," J. Appl. Phys. 49, 3406-3409 (1978).

5. J. W. Ekin, A. F. Clark, and J. C. Ho, "Current Transfer in Multifilamentary Superconductors. II. Experimental Results," J. Appl. Phys. 49, 3410-3412 (1978).

6. A. F. Clark, J. W. Ekin, R. Radebaugh, and D. T. Read, "The Development of Standards for Practical Superconductors," IEEE Trans. Mag. MAG-15, 224-227 (1979).

7. F. R. Fickett and A. F. Clark, "Development of Standards for Superconductors, Annual Report FY 79," NBSIR 80-1629, National Bureau of Standards, Boulder, Colorado (Dec. 1979).

8. F. R. Fickett and A. F. Clark, "Standards for Superconductors," Prof. 1979 Mech. and Mag. Energy Storage Contractors' Review Meeting, Conf-790854, U.S. Dept. of Energy, Washington, DC (Dec. 1979).

9. D. T. Read, J. W. Ekin, R. L. Powell, and A. F. Clark, "Definitions of Terms for Practical Superconductors: 3. Fabrication, Stabilization, and Transient Losses," Cryogenics 19, 327-332 (1979).

10. F. R. Fickett and A. F. Clark, "Development of Standards for Superconductors," Prof. 8th Int'l. Cryo. Eng. Conf. (ICEC8), IPC Science and Technology Press (1980) pp. 494-498.

11. F. R. Fickett and L. F. Goodrich, "NBD Superconductor Standardization Program," Prof. 1980 Superconducting MHD Magnet Design Conference A. M. Dawson, ed., (Report published by Bitter National Magnet Laboratory, MIT, Oct. 1981) p. 87-89.

12. F. R. Fickett, S. B. Kaplan, R. L. Powell, R. Radebaugh, and A. F. Clark, "Definitions of Terms for Practical Superconductors: 4. Josephson Phenomena," Cryogenics 20, 319-325 (1980).

13. G. Fujii, J. W. Ekin, R. Radebaugh, and A. F. Clark, "Effect of Thermal Contraction of Sample Holder Material on Critical Current," Adv. Cryog. Eng. Vol. 26, Plenum Press, New York (1980) p. 589-598.

14. G. Fujii, "Present Practices in Japan for the Measurement and Definition of Various Superconducting Parameters," Tech. Report ISSP Univ. of Tokyo, Ser. A, No. 1063 (July 1980).

15. G. Fujii, J. W. Ekin, R. Radebaugh, and A. F. Clark, "Effect of Thermal Contraction of Sample-Holder Material on Critical Current," Tech. Report ISSP Univ. of Tokyo, Ser. A, No. 1074 (Aug. 1980).

16. A. F. Clark, "Development of Standards for Practical Superconductors," Proc. Superconductivity Technical Exchange Meeting, IAPG, PIC-ELE-SC 209/1 (1980), p. 103 (presentation only).

17. L. F. Goodrich and J. W. Ekin, "Lap Joint Resistance and Intrinsic Critical Current Measurements on a NbTi Superconducting Wire," Proc. 1980 Applied Superconductivity Conference, IEEE Trans. Mag. MAG-17, 69-72 (1981).

18. R. Radebaugh, G. Fujii, D. T. Read, and A. F. Clark, "A Standards Program for ac Losses in Superconductors," Proc. IVth Int'l. Congress on Refrigeration (1980), Comm. A 1/2-10 (1980)., pp. 1-4.

19. G. Fujii, "Present Practices in Japan for the Measurement and Definition of Various Superconducting Parameters," Cryogenics 21, 21-38 (1981).

20. H. R. Segal, Z. J. J. Stekley, and T. A. DeWinter, "Development of Critical Current Measurement Standards," Prof. 1980 Applied Superconductivity Conference, IEEE Trans. Mag. MAG-17, 73-76 (1981).

21. G. Fujii, M. A. Ranney, and A. F. Clark, "Thermal Expansion of Nb_3Sn and V_3Ga Multifilamentary Superconducting Cables, Fiberglass-Epoxy and Cotton-Phenolic Composite Materials," Jap. J. Appl. Phys. 20, L267-L270 (1981).

22. L. F. Goodrich, J. W. Ekin, and F. R. Fickett, "Effect of Twist Pitch on Short-Sample V-I Characteristics of Multifilamentary Superconductors," Adv. Cryog. Eng. - Materials, Vol. 28, Plenum Press, New York (1981), p. 571-580.

23. A. F. Clark, G. Fujii, and M. A. Ranney, "The Thermal Expansion of Several Materials for Superconducting Magnets," IEEE Trans. Mag. MAG-17, 2316-2319 (1981).

24. F. R. Fickett, L. F. Goodrich, and A. F. Clark, "Development of Standards for Superconductors: Annual Report FY 80," NBSIR 80-1642, National Bureau of Standards, Boulder, Colorado (Dec. 1980).

25. L. F. Goodrich and F. R. Fickett, "Critical Current Measurements: A Compendium of Experimental Results," Cryogenics 22, 225-241 (1982).

26. A. F. Clark, L. F. Goodrich, F. R. Fickett, and J. V. Minervini, "Development of Standards for Superconductors, Interim Report Oct. 80 to Jan. 82," NBSIR 82-1678, National Bureau of Standards, Boulder, Colorado (July 1982).

27. Standard Definitions of Terms Relating to Superconductors, Annual Book of ASTM Standards, ASTM B713-82, Part 2.03, pp. 591-594, American Society for Testing and Materials, Philadelphia, PA (1983).

28. Standard Test Method for D-C Critical Current of Composite Superconductors, Annual Book of ASTM Standards, ASTM B714-82, Part 2.03, pp. 595-98, American Society for Testing and Materials, Philadelphia, PA (1983).

29. L. F. Goodrich, "The Effect of Field Orientation on Current Transfer in Multifilamentary Superconductors," IEEE Trans. Mag. MAG-19, 244-247 (1983).

30. L. F. Goodrich, E. S. Pittman, and A. F. Clark, "Critical Current Measurements on Standard Reference Material," presented at the Int'l. Cryog. Materials Conf., August 15-19, 1983, Colorado Springs, Colorado.

31. A. F. Clark, L. F. Goodrich, and F. R. Fickett, "Experience in Standardizing Superconductor Measurements," J. Physique 45(C1), 379-382 (1984).

32. L. F. Goodrich, D. F. Vecchia, E. S. Pittman, J. W. Ekin, and A. F. Clark, "Critical Current Measurements on an NbTi Superconducting Wire Standard Reference Material," NBS Special Publication 260-91 (1984).

APPENDIX B

EFFECT OF TWIST PITCH ON SHORT-SAMPLE V-I CHARACTERISTICS OF MULTIFILAMENTARY SUPERCONDUCTORS*

L. F. Goodrich, J. W. Ekin, and F. R. Fickett

Electromagnetic Technology Division, National Bureau of Standards, Boulder, Colorado

INTRODUCTION

Precise determination of the critical current of practical superconductors requires measurement of the voltage-current (V-I) characteristic of the conductor at various magnetic fields. The measurement usually requires the detection of quite small voltages since very sensitive critical current criteria are necessary for the design of practical devices. Furthermore, most laboratories have only relatively small-bore solenoidal magnets, leading to the common use of very short sample lengths for routine critical current measurements. This situation may lead to some difficulties, as we show here.

Data taken on short samples of commercial multifilamentary superconductors have uncovered anomalous V-I characteristics. A voltage was detected at currents well below the sharp upturn in the V-I characteristic near I_c. It was apparently due to current transfer, but larger in magnitude than would be expected from previous current-transfer analyses.[1] Further data indicated that the voltage was strongly dependent on the voltage tap location. In fact, the voltage measured below I_c in the current direction between some taps was negative. In all cases, as I_c was approached, the V-I characteristic returned to "normal." Extensive experiments have shown that there are two extreme anomalous shapes of the V-I curves. These are illustrated in Fig. 1. Depending on the test geometry, the magnitude of many of these anomalous voltages can be on the order of commonly used critical-current criteria and may significantly affect the determination of I_c.

*Partially funded by the Department of Energy.

571

Adv. Cryog. Eng. - Materials, Vol. 28,

Plenum Press, New York (1982), 571-580.

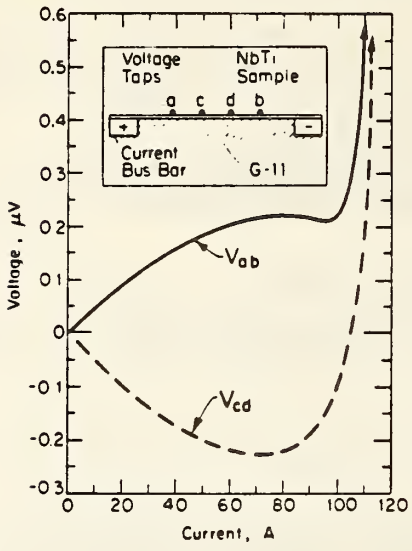

Fig. 1. Experimental data at 8 T showing anomalous V-I characteristic of short NbTi sample ($\ell_{ab} \approx 1.5$ cm, 2.5 filament twists between current contact centers). The horizontal dimensions of the inset are approximately to scale.

In this paper, the experimental investigation of the anomalous behavior and a phenomenological model developed to account for the observations are presented. Several techniques are discussed that minimize the effect and, thus, allow precise critical current determination in short samples.

APPARATUS AND SAMPLE PREPARATION

The apparatus used in this experiment was typical for a short, straight sample critical current measurement. It consisted of the following: a Dewar with a 9-T superconducting solenoid (3.8-cm bore), a cryostat with 600-A vapor-cooled leads, a series-regulated 600-A battery current supply, an analog nanovoltmeter, and an X-Y recorder. The magnetic field measurements were made to a precision of 0.1% with a calibration accuracy of 0.2%. The voltage and current measurements had an accuracy of 2% and 0.4% and a precision of 1% and 0.2%, respectively. Typical noise voltages were ±5 nV. Thermal voltages were checked at zero current and usually did not vary by more than ±10 nV. The sample holder was made of NEMA G-11 epoxy-fiberglass. Superconducting bus bar current contacts were set flush with one surface of the G-11 (see the inset in Fig. 1) such that the Lorentz force on the sample could be supported by the G-11, either directly or by a thin layer of varnish. Small slots were routed into the G-11 for voltage taps on the underside of the wire where needed.

The measurements were made principally on two samples: a twisted multifilamentary NbTi (twist pitch 1.27 cm, Cu:NbTi of 1.8:1, RRR of the copper ~70, 0.53 x 0.68 mm, 180 filaments) and an

untwisted multifilamentary Nb_3Sn (0.70-mm diameter, 2869 filaments). The Nb_3Sn wire had an outer copper jacket separated by a tantalum diffusion barrier from the core of bronze, niobium, and Nb_3Sn.

Sample preparation was typical for short sample testing except for the two following techniques. A technique was developed to spot-solder a pair of voltage taps directly across the wire from each other to allow measurement of transverse voltages. The alignment of these taps was checked by measuring the room temperature resistivity and the voltage polarity of the pair and thus deducing the approximate misalignment. The worst case misalignment was ~0.2 mm, but more usually $\lesssim$ 0.1 mm. The other special technique was selective etching of the copper jacket from the Nb_3Sn wire. This was accomplished using an enamel insulating paint as a mask and a nitric acid etch. Small copper islands were left on the sample for ease in soldering voltage taps and current contacts.

EXPERIMENT

To investigate the anomalous voltage seen on the NbTi critical current sample as described in the Introduction, tests were made with two pairs of voltage taps spaced 0.5 and 1.5 cm apart. The V-I characteristics are shown in Fig. 1. Here the voltage definition $V_{ab} = V_a - V_b$ was used. These curves were reproducible and reversible to within 1%.

It was observed that both V_{ab} and V_{cd} changed sign when the current was reversed, but not when the field direction was reversed. There were slight differences (~10%) in the magnitudes of these voltages, especially close to I_c, as the direction of the current and the field were changed. These are attributed to the Hall effect and are discussed below, but they do not significantly affect the unusual shape of the V-I characteristics.

During the development of the phenomenological model, experiments were made using several unique sample configurations of both the twisted NbTi and the untwisted Nb_3Sn. These data and the voltage tap and current lead arrangements are presented in the appropriate places in our discussion of the model.

PHENOMENOLOGICAL MODEL AND SUPPORTING DATA

The unusually shaped V-I characteristics may be understood in terms of the interaction between current transfer and the twist pitch of the superconductor. Filaments nearest the current contacts carry current near their critical current density and exhibit a flux-flow resistivity. Conversely, filaments on the opposite side of the superconductor from the current contacts carry very little current because the resistive matrix separates them from the

point of current injection. Therefore, it is possible for a voltage tap to be sampling either a resistive or nonresistive group of filaments and, thus, the voltage between taps may be quite different, depending on the relationship of tap spacing to twist pitch. Also, significant transverse voltages should be observed across the wire.

Results of transverse voltage measurements made on the NbTi sample are shown in Fig. 2. Notice that these curves are similar in shape and size to those in Fig. 1 except near I_c. As I_c is approached, the transverse voltage tends to go to zero as the current distribution among the filaments becomes more uniform. The distance between current injection points (approximately center to center) for the data shown in Fig. 2 was 2.6 times the twist pitch. Thus, the group of filaments nearest to the current bus bar on one end of the sample are not the same as the group nearest to the bus bar at the other end. Current must therefore transfer between the two groups of filaments by flowing through the resistive matrix material of the wire. This generates the large transverse voltages. The unusual V-I characteristics shown in Fig. 1 are simply the sum of the usual flux-flow V-I characteristic and

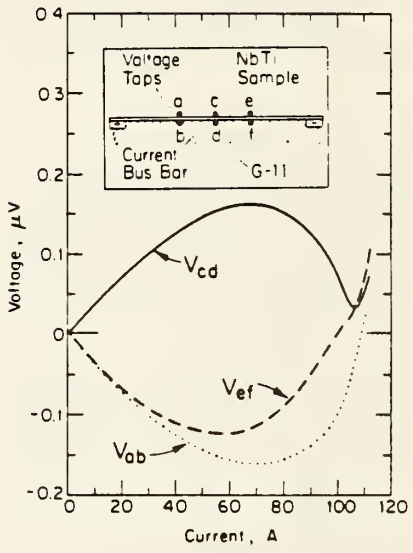

Fig. 2. Experimental data at 8 T on transverse voltages of short NbTi sample (ℓ_{ae} ≈ 1.25 cm, 2.6 filament twists between current contact centers).

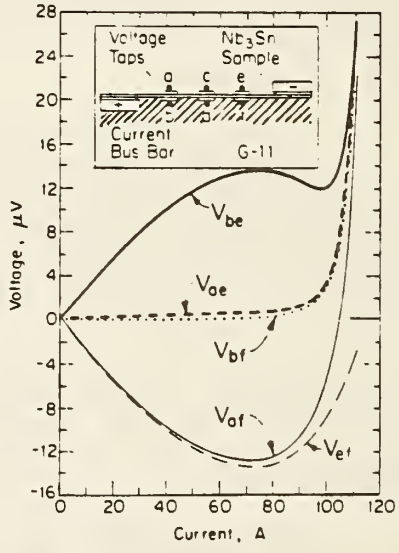

Fig. 3. Experimental data at 9 T on a selectively etched Nb_3Sn conductor (ℓ_{ae} ≈ 1.25 cm, no filament twists). Note the bus bar locations.

the transverse voltages caused by current transfer through the resistive matrix from one group of filaments to another.

Understanding of the effect is simplified considerably if the conductor used to obtain the V-I characteristics in Figs. 1 and 2 is untwisted. In this arrangement one current bus bar was placed on top, the other on the bottom to provide a half-integral number of twists between the current injection points. Data were obtained on the untwisted Nb_3Sn conductor in this geometry and are shown in Fig. 3. These data can be explained by the model shown in Fig. 4. Note that in multifilamentary conductors the equipotential lines at low currents are much more closely aligned with the conductor axis than in a conductor with an isotropic resistivity. The voltage between taps e and f starts from zero at $I \ll I_c$ (Fig. 4A), rises in magnitude as I increases (Fig. 4B), and decreases toward zero as all the filaments become resistive near I_c (Fig. 4C). Similarly, the voltage between taps a and f starts from zero at $I \ll I_c$ (Fig. 4A), rises in magnitude to a negative peak at an intermediate value of I (Fig. 4B), and then becomes positive as the entire conductor becomes resistive at $I \cong I_c$ (Fig. 4C). The voltage between taps b and e rises from a low value at $I \ll I_c$ to an intermediate high at an intermediate value of I, back to a low value as the

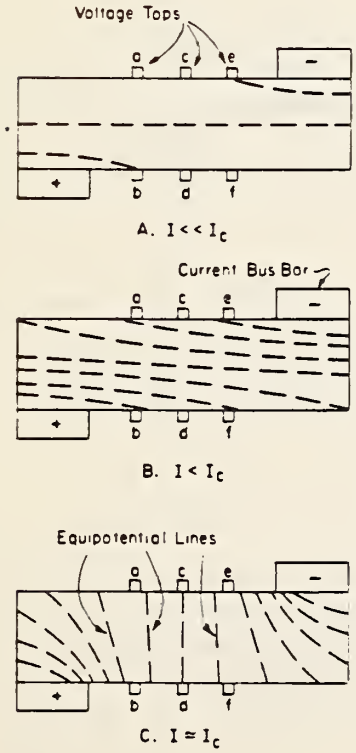

Fig. 4. Model of equipotential lines in a superconductor with an odd half-integral number of filament twists between the current contacts: (A) current much less than I_c; (B) intermediate currents less than I_c; and (C) current near I_c.

resistivity becomes more isotropic at $I \approx I_c$, and finally to a high value as I exceeds I_c. Note that the curves in Fig. 3 have about the same shape as those in Fig. 1.

In Fig. 3 it is easy to separate the anomalous V-I characteristics (V_{be}, V_{af}) into an essentially intrinsic characteristic (V_{bf}, V_{ae}) and an anomalous current-transfer characteristic (transverse voltages V_{ab}, V_{ef}). These separations, $V_{be} = V_{bf} - V_{ef}$ and $V_{af} = V_{ae} + V_{ef}$, were demonstrated experimentally with agreement of about 1% ±10 nV. So it is possible to have V-I characteristics with these shapes (and everything in between) depending on voltage tap location. Remember that this discussion and the data shown in Figs. 1, 2, and 3 correspond to a sample with a half-integral number of twist lengths between the points of current injection.

When there is an integral number of twist lengths between the points of current injection, the current transfer pattern is altered. Data obtained on the NbTi conductor with a current contact spacing of about two twist lengths are shown in Fig. 5. In this geometry, the V-I characteristic of the resistive filament,

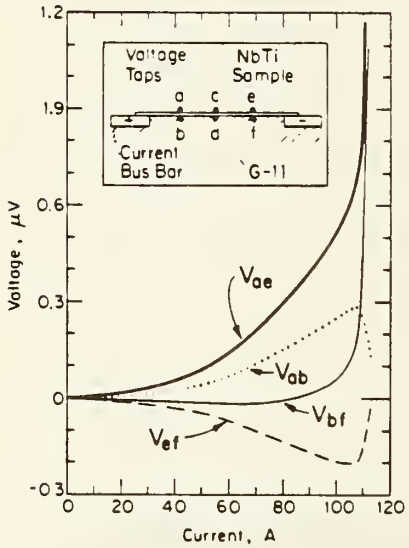

Fig. 5. Experimental data at 8 T on a NbTi conductor ($\ell_{ae} \approx 1.25$ cm, 2 filament twists between current contact centers).

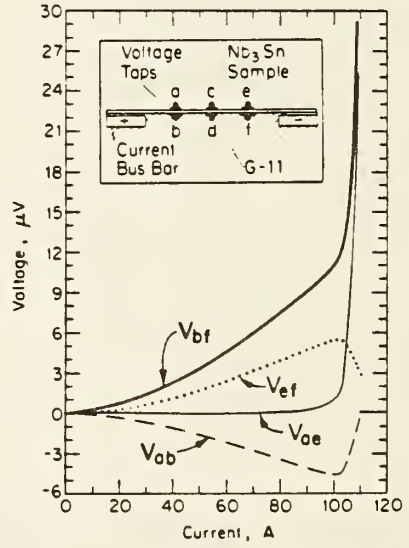

Fig. 6. Experimental data at 9 T on a selectively etched Nb_3Sn conductor ($\ell_{ae} \approx 1.25$ cm, no filament twists).

V_{ae}, is the sum of the V-I characteristics of nonresistive filaments, V_{bf} (essentially intrinsic characteristic), and the transverse voltages, V_{ab}, V_{ef} (anomalous current-transfer characteristic). The equation $V_{ae} = V_{bf} + V_{ab} - V_{ef}$ was demonstrated experimentally with an agreement of about 1.5% ±15 nV. Data obtained on the Nb_3Sn conductor in this geometry are shown in Fig. 6. Note that these curves are very similar in shape to the curves in Fig. 5 and can also be separated into an intrinsic V-I characteristic and an anomalous current-transfer characteristic, $V_{bf} = V_{ae} + V_{ef} - V_{ab}$, with experimental agreement of about 1% ±10 nV. The model for this configuration is shown in Fig. 7. The current is injected and extracted from the same group of filaments. The voltage between taps b and f is indicative of this group of filaments and rises much more rapidly than the voltage between taps a and e. Current does not transfer through the matrix to the far group of filaments sampled by taps a and e until I approaches I_c. In fact, the voltage taps on the top of the conductor remain at about the same potential until I reaches I_c.

TECHNIQUES TO MINIMIZE THE ANOMALOUS CURRENT TRANSFER VOLTAGE

Note from the above discussion that these unusually shaped V-I characteristics result from nonsymmetric current injection. If the

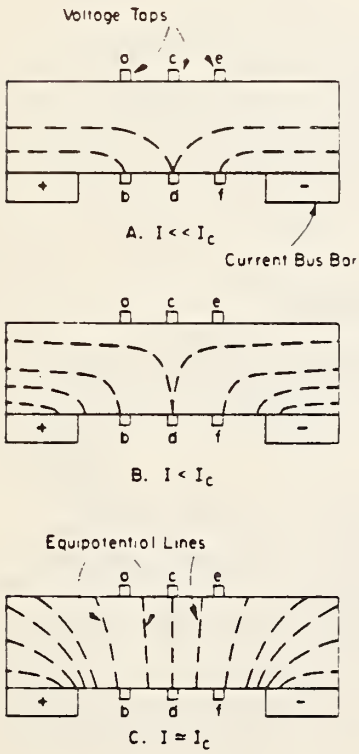

Fig. 7. Model of equipotential lines in a superconductor with an integral number of filament twists between current contacts: (A) current much less than I_c; (B) intermediate current less than I_c; and (C) current near I_c.

current is uniformly introduced around the circumference of the superconductor, the current transfer voltage should be independent of twist pitch considerations and reduced in magnitude.

There are at least two possible methods of making the current injection symmetric in short sample testing. One method is to make the solder joint at the current contact longer, at least one twist length, so that the current is introduced into all of the outer filaments. In the second method, current injection is made more uniform by having a symmetric current contact. Both of these techniques have been shown experimentally to reduce the anomalous voltages greatly, thus permitting a more accurate determination of the critical current.

The long current contact method was tested on the twisted NbTi wire. First the voltages were measured with the current contacts covering more than one twist length, then the wire was cut to shorten the current contact, and the same voltage taps were measured again. The current-transfer voltages were about a factor of 10 lower for the long current contacts and of a magnitude consistent with symmetric current-transfer analysis.[1]

Measurements on the Nb_3Sn wire with the copper jacket intact illustrate the second method. The copper jacket gives a more uniform injection of the current into the superconducting filament region because of the relatively high resistivity of the bronze in that region. The results are shown in Fig. 8. The magnitude of the current transfer voltage is reduced over that of V_{bf} in Fig. 6, again consistent with symmetric current-transfer analysis. Also, the voltage drop along the top filaments is about the same as that along the bottom filaments, which indicates a removal of the twist pitch dependence.

A COMMENT ON GALVANOMAGNETIC EFFECTS

Observations of strange voltages in a current-carrying conductor at low temperatures in a high magnetic field are often explained by arguments involving one or more of the many classical galvanomagnetic effects. It is our contention that, although several of these effects are present in our data, none of them cause the unusual shape of the V-I curves. Most of the effects are seen only in metals where the product of the cyclotron frequency, ω, and the electron collision time, τ, is quite large, usually ~100. Even in the copper stabilizer on our wires, $\omega\tau \lesssim 2.4$ at 4 K and 10 T. Furthermore, large effects are most common to single crystals and our metals are highly polycrystalline.

Two galvanomagnetic effects do appear in our data: the Hall effect and transverse magnetoresistance. Of these, only the former

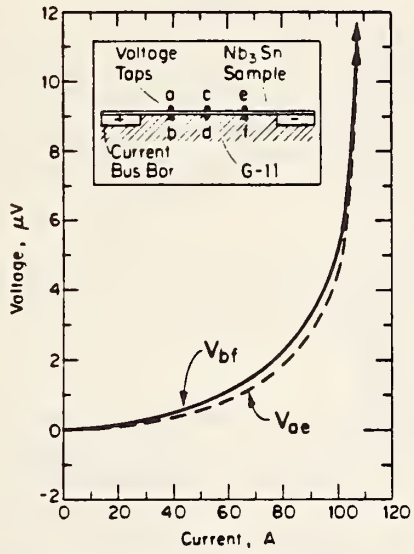

Fig. 8. Experimental data at 9 T on Nb_3Sn conductor with copper jacket giving uniform current injection (ℓ_{ae} = 1.25 cm, no filament twists).

can be seen directly in I-V curves made at fixed field. The Hall voltages appear most strongly on the probe pairs transverse to the current. They reverse with both field and current and are developed almost entirely in the normal metal components of the wire. In the wires measured here, at currents well below I_c, we noted Hall voltages of ~10 nV in the NbTi at 8 T (on top of a ~200 nV current transfer voltage) and ~100 nV in the Nb_3Sn at 9 T (on top of a ~15 μV transfer voltage). These values appear to be consistent with the known Hall coefficients for the matrix materials[2] and the other parameters, but even an order of magnitude calculation requires a much more detailed model than we have space for. Suffice it to say that the Hall effect, although observable, represents only a small contribution to the measured transverse voltages.

Magnetoresistance is an even effect, it does not depend on current and does not reverse with field, thus it does not affect the shape of the V-I curves. It shows up most strongly in measurements on voltage taps along the sample as an increase in the resistance of the relatively pure copper stabilizer as the field is increased. For our wires this effect causes the zero field resistivity of the stabilizer at 4 K to increase by about a factor of 3 in going to 9 T.

CONCLUSIONS

Anomalous voltages may be observed in short sample critical current tests on multifilamentary superconductors. These voltages may in some instances even be negative, but in any case they can interfere with the correct determination of I_c (even for NbTi) especially when using sensitive (but realistic) electric field or resistivity criteria.

All of the observed behavior can be adequately explained by use of a model that considers the combined effects of the twist pitch of the filaments and the details of current injection and transfer within the sample.

The anomalous voltages can be reduced in short sample testing by insuring that the current is injected symmetrically into the conductor by long (at least one twist pitch) current contacts or by symmetric current contacts. The current-transfer voltages then will be independent of twist pitch and reduced in magnitude, making the usual methods of treating current-transfer voltages applicable.[1]

ACKNOWLEDGMENTS

The authors have benefited greatly from numerous discussions with A. F. Clark. E. Pittman has been most helpful in the care and feeding of the instrumentation. Ms. V. Grove prepared the manuscript--many times. Our thanks to them all.

REFERENCES

1. J. W. Ekin, J. Appl. Phys. 49:3406 (1978).
2. C. M. Hurd, "The Hall Effect in Metals and Alloys," Plenum Press, New York (1972).

THE EFFECT OF FIELD ORIENTATION ON CURRENT TRANSFER IN MULTIFILAMENTARY SUPERCONDUCTORS*

L. F. Goodrich
National Bureau of Standards
Boulder, Colorado 80303

Abstract

Experimental data and discussion are presented on the current distribution along the length of a superconducting wire when subjected to multiple parallel and perpendicular magnetic fields. The experimental data were taken on a rectangular pancake coil with the applied magnetic field in the plane of the coil. These data indicate that significant current transfer occurs in the first and last perpendicular magnetic field sections and little transfer occurs between these two sections. The implication for superconducting magnet design will also be discussed.

Introduction

Results of recent measurements[1] on current transfer in hairpin and long straight critical current geometries showed curious effects in multiple parallel and perpendicular field sections on the current transfer in multifilamentary superconductors. These two critical current geometries are illustrated on Fig. 1. In the hairpin geometry, the sample axis changes along its length from parallel, to perpendicular, to a return parallel with respect to the relatively uniform applied magnetic field. In the long geometry, the sample traverses several magnetic field regions; from low, to gradient, to relatively uniform perpendicular, to gradient, and then to low again. All of the measurements reported and discussed here were made on the same material. A cross-sectional view of this material is given in Fig. 2. It is a commercial multifilamentary Nb_3Sn superconductor with a diameter of 0.7 mm, 2869 filaments, and a copper to non-copper ratio of 1.7. Its critical current is about 75 A at 8 T, 4 K using an electric field criterion of 1 nV/cm.

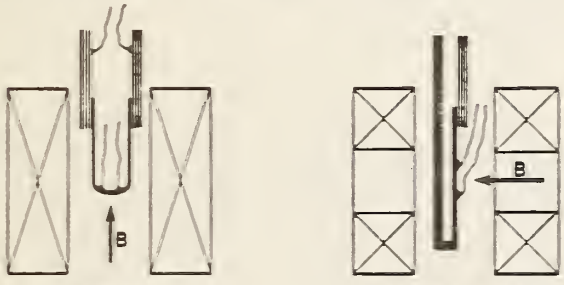

Figure 1. Schematic representation of the hairpin and long straight critical current measurement geometries.

The following experimental observations on the symmetry of current transfer were made on both the hairpin and the long straight geometries. The current contacts were made at the surface of the wire and the copper jacket ensured that the current entering the core of the conductor was nearly radially symmetric. The length of the sample in the parallel or low field region was long enough that the current transfer caused by the low or parallel field critical current density was essentially completed before the wire

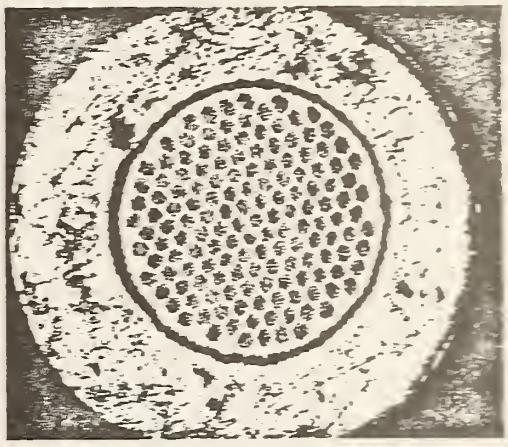

Figure 2. Cross section of the superconducting sample with an outer copper jacket separated by a tantalum diffusion barrier from the core of bronze, Nb, and Nb_3Sn.

enters the perpendicular, high-field region. This was indicated by the profile of the current transfer electric field, E_z, with distance from the current contact, x. E_z close to the current contact was a few uV/cm and it had decreased to less than 1 nV/cm before the perpendicular high-field region was reached. Thus, assuming the E_z continues monotonically decreasing with x, and that there is a finite current density, J_c^*, below which the superconducting filament resistivity is zero, then the current distribution among the filaments must have essentially reached the distribution that the conductor would have in a parallel or low field if the current contact were an infinite distance away. This postulate only states that the effect would be observed and would have about the same magnitude if the current contact were an infinite distance away. The electric field profile of each end of the sample in parallel or low field was symmetric, implying that the transfer into the conductor occurs in the same way as the transfer out. In the absence of a perpendicular-field region, no additional transfer (in) would take place at this current. However, additional transfer does take place when the current enters the perpendicular, high-field region because the lower critical current density forces the current distribution among the filaments to be more uniform. This transfer results in E_z's as high as 100 nV/cm. These transfer electric fields were symmetric about the center of the magnetic field just as in the low or parallel field region. This implies that the current starts to transfer to the outer filaments on the other side of center, symmetric with the transfer in.

A logical extension of these results is to ask what would happen if there were multiple parallel and perpendicular field sections? Would the current transfer in and out among the filaments on every perpendicular field section? If it did, this would have a serious implications for superconducting magnet design in cases where the windings are such that the magnitude or angle of the magnetic field cycles many times. It would affect the persistence, refrigeration load, and the stability of the system. The experiment below was designed to answer these questions.

*Work supported in part by the Department of Energy, Division of High Energy Physics, and the Office of Fusion Energy.

Manuscript received November 30, 1982

0018-9464/83/0500-0243$01.00 © 1983 IEEE

Experimental

The special shape sample for this study was formed prior to its reaction, in a rectangular pancake coil as illustrated in Fig. 3. The bends in the sample have a radius of curvature of about 2 mm. The results did not show any significant change in the superconducting properties due to the bends, except, perhaps, for some minor filament inhomogeneities and breakage. Measurements were made with the magnetic field in the plane of the coil, pointed down in the figure. The critical current at 1 μV/cm was measured for the seven pairs of adjacent voltage taps in perpendicular field-sections, and the resulting critical current data had a range of only 2% indicating a relatively uniform sample. This configuration has a number of sections that are essentially (within 10°) parallel or perpendicular to the magnetic field. The ends of the sample are in parallel field. These sections are sequentially numbered for reference on Fig. 3 so that all of the odd-numbered sections are in parallel field and the even-numbered in perpendicular field. The current contacts at each end of the wire were 0.5 cm long. The first and the last sections, 1 and 11, were 6.6 cm and 6.3 cm long respectively. As mentioned above, with a parallel field section this long, the current transfer due to the parallel field critical current density is essentially complete before the first perpendicular field section. Notice also the fact that the magnetic field at the ends of the sample is not exactly parallel with the sample (because of alignment and field profile) would only cause the effect in the first perpendicular field section to be smaller than if the ends were in a perfectly parallel field.

The data were taken by recording the voltage as a function of current as the current was ramped up and then down. The voltage was measured to an accuracy of 2% ±2 nV and the current to an accuracy of 0.5% ±0.2 A. The current ramp rate was relatively slow (a few minutes from zero to I_c), but there still were significant voltages induced in the voltage leads to the sample because of this ramp. These induced voltages were accounted for by using the recorded voltages, up and down, and the known current ramp rate. The resulting voltage-current curves were consistent with voltage-current points obtained by holding the current fixed (actually the current was still drifting, but at a rate at least 20 times less). Thus the final voltage-current curves were independent of ramp rate in the range tested and the observations are not the result of any inductive effect.

Evidence of the response of the current distribution to multiple parallel and perpendicular field sections is also given on Fig. 3. The measured voltage and tap separation of each adjacent pair of taps is indicated for a current of 75 A in a field of 8 T. The critical current (75 A) at 1 nV/cm was determined from a measurement of another specimen, so the small additional voltage on the inner configuration taps could be due to a difference in the critical current, the continuing transfer, or filament inhomogeneities. All of the voltages are positive. They changed sign and had the same magnitude (within the accuracy of the measurement) when the current direction was reversed. This indicates a symmetry of current transfer (in and out) with the direction of current flow. Furthermore there is a symmetry of current transfer voltage about the center of the configuration, section 6. Notice the similarity of the voltages seen on the following pairs of sections: 1 and 11; 2 and 10; 3 and 9; 4 and 8; 5 and 7.

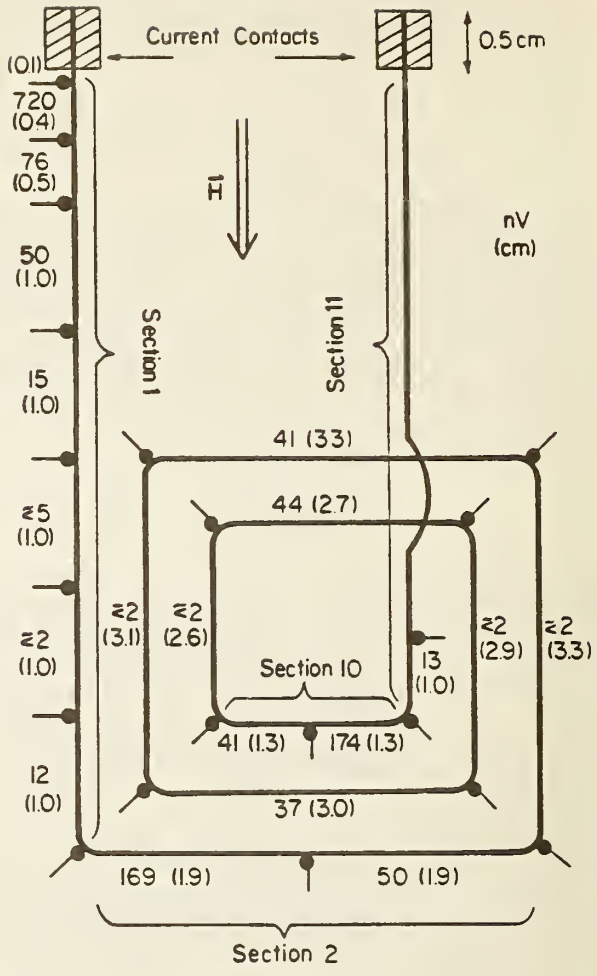

Figure 3. Rectangular pancake coil sample with voltage in nV (tap separation in cm) for each adjacent pair of taps at a current of 75 A with a field of 8 T in the plane of the coil.

Discussion

The above symmetry of current transfer voltage is somewhat surprising on first consideration. Notice that when the current reaches the first (for now assume electron current flow and section 1 is connected to the negative contact) perpendicular field section, 2, the current then will have to transfer into the inner filaments, since the reduced critical current density forces the current distribution among the filaments to be more uniform than that in the parallel field region, 1. The expected voltage profile due to this current transfer is observed along this perpendicular section, 2. Now consider the symmetric section, 10, here the voltage profile indicates that the current starts to transfer to the outer filaments in the same way that the current transferred to the inner ones in section 2. In fact, almost all of this transfer takes place in section 10, relatively little takes place around the corner in section 11, just as happened in section 1. Why does the current start to transfer out in section 10? If the current wants to transfer out before it reaches a parallel field section, why doesn't it transfer out at the end of sections 2, 4, 6, or 8? These results suggest that the presence of the current contact must be affecting the current distribution for a long length.

The effect of the current contact can be illustrated with equipotential lines as indicated by the

data. A schematic diagram of the equipotential lines is given on Fig. 4. Using a time-reversal argument, these lines will be the same for current entering and leaving the superconductor. The outer copper jacket is not shown on this figure. The equipotential surfaces in the copper jacket should extend radially outward from the surface of the core, except near the current contact. The parallel and perpendicular field regions are treated here separately. The effect that the presence of the perpendicular region has on the parallel region is discussed in the appendix. The appendix also has a list of rules for qualitative construction of equipotential lines in superconductors and another example. The equipotential lines in Fig. 4 do take into account the interaction of these two regions; however, in the following discussion this interaction was omitted for clarity.

Consider first the easier case to imagine, that of the current entering the superconductor. The copper jacket on the superconductor will ensure that the current entering the core of the conductor at the current contact will be essentially radially symmetric.[2] The current is injected into the outer superconducting filaments at the joint and it starts to flow along these filaments. However, the current density is above the critical current density (except at the very low currents), and thus, a flux-flow voltage drop will occur along these filaments which will cause some of the current to transfer through the resistive interfilament material (bronze) into the next inner layer of superconducting filaments. This process continues until the current density in the outer filaments is essentially J_c^*, where J_c^* is the current density below which the superconducting filament resistivity is zero. I_c in parallel field is about four times I_c in perpendicular field, so it is expected that J will not be uniform throughout the conductor in parallel field, no matter the length, for any current less than the I_c measured in perpendicular field. There will be a low J in the inner filaments, thus all the inner filaments will be at about the same potential and there will be very little voltage drop along them. As the current enters the perpendicular field region, J_c drops and the outer filaments will again have a flux-flow voltage drop which causes more transfer. If the current is close to I_c, then the equipotential surface will eventually become flat and perpendicular to the axis of the conductor. Some transfer may occur due to inhomogeneities in the superconducting properties, but other than this, the equipotential surface will stay flat through the parallel and perpendicular regions until the last perpendicular region. The current will start to transfer out in the last perpendicular field region. This transfer out is a little harder to imagine because the presence of the current contact effects the equipotential surfaces in the multifilamentary superconductor a relatively long distance away, more than 6 cm or 150 times the diameter of the core. The extent of this long range effect has been observed before in this sample and in Cu-NbTi samples where anomalous voltages were reported.[2] The current starts to transfer out of the center filaments because these filaments are at a higher potential than the adjacent filaments. This transfer out will cause the outer filaments to have a flux-flow voltage drop, the inner filaments will be at about the same potential and there will be very little voltage drop along the inner filaments. Once the current has entered the parallel field region the flux-flow voltage drop along the outer filaments will become very low and very little transfer out will occur. As the current gets closer to the contact, the transfer out will increase and more and more flux-flow voltage will appear along the wire and ultimately the current will leave the conductor at the current contact.

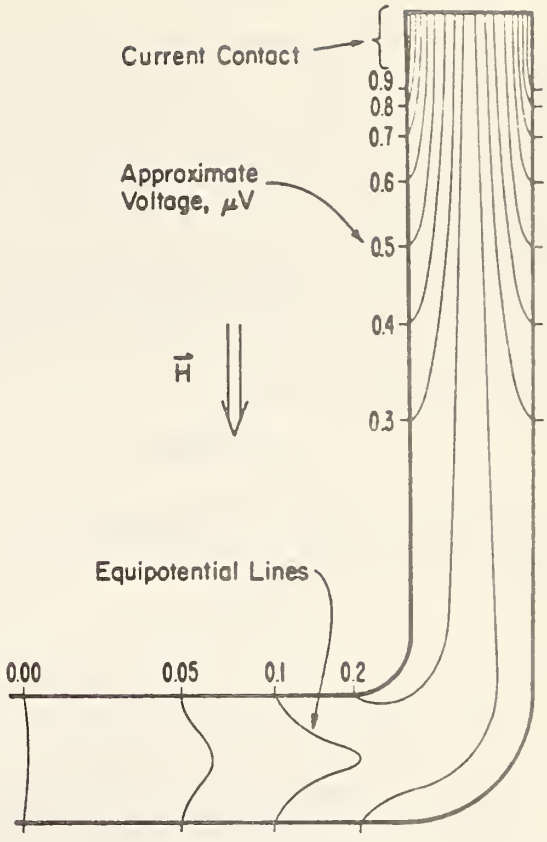

Figure 4. Schematic diagram of the equipotential lines in the core of the superconductor with the magnetic field pointing down the figure.

These data also indicate that the ultimate current distribution of a multifilamentary superconductor is not uniquely defined by the local conditions. Where the electric field is zero, the current density in a superconducting filament can be any value below J_c^*.[3] The value that it will have is determined by the boundary conditions (current contact) and the external magnetic field in regions where the electric field is non-zero. The voltage drops along the configuration's inner parallel field sections (3, 5, 7, and 9) indicate there is very little transfer occurring. The voltage drops along the configuration's inner perpendicular field sections (4, 6, and 8) could result in part from slight inhomogeneities and filament breakage at the bends. So the transfer that occurs here because of the field orientation change is at least eight times smaller than that of the first and last perpendicular field sections (2 and 10), if this transfer occurs at all. This suggests that the interfilament material, the bronze, is effectively isolating the superconducting filaments from each other.† This does not rule out the possibility that a transfer out would occur if the low or parallel field section were much longer. Conceivably, this could occur by means of selective transfer (toward the lower free energy state of the superconductor) at filament inhomogeneities and discontinuities. If this were to occur, the transfer back in would take place at the next perpendicular field section.

† If the conductor were a monofilament, then the current distribution in the configuration's inner parallel field sections would not be as uniform as that for the configuration's inner perpendicular field sections because the free energy of the superconductor is lower for the current flowing in the outer area.

Conclusion

The current will complete the tranafer to a more uniform distribution in the first perpendicular magnetic field section. After the current has a uniform distribution, it will not transfer among the filaments everywhere the magnetic field changes. The current will start the transfer to the outer filaments during the last perpendicular magnetic field section. The implication of this for superconducting magnet design is that once the current has transferred to a uniform distribution among the filaments, it may stay in this distribution through low or parallel field sections until the last perpendicular field section. Thus, putting each end of the magnet wire through an external, high-field region would force the current into a uniform distribution that would remain for the whole length within the magnet.

Acknowledgments

The author wishes to thank F. R. Fickett and A. F. Clark for our numerous discussions; J. W. Ekin and J. R. Clem for their review; and V. L. Grove for preparing this manuscript.

References

1. L. F. Goodrich and F. R. Fickett, "Critical current measurements: a compendium of experimental results," Cryogenics 22, 225-241, 1982.

2. L. F. Goodrich, J. W. Ekin, and F. R. Fickett, "Effect of twist pitch on short-sample V-I characteristics of multifilamentary superconductors," Adv. Cryo. Eng. 28, 571-580, 1982.

3. J. R. Clem, private communication.

Appendix

The presence of the perpendicular region has an effect on the equipotential lines in the parallel field region. First consider some rules for qualitative construction of equipotential lines in superconductors:

1) Equipotential lines can not cross a superconducting filament where J in that filament is less than J_c^*.

2) The potential of a superconducting filament where J in that filament is less than J_c^*, is determined at the first or last place where $J = J_c^*$.

3) If J in a superconducting filament is everywhere less than J_c^*, then the potential of that filament is determined by the potential of the adjacent material.

4) The current will flow toward a lower potential even if it is in a superconducting filament that is below its J_c^*.

5) The electric field in the superconducting filaments at any point along the wire will be larger for the outer filaments than for the inner filaments (except when zero or near inhomogeneities).

First consider the case where the whole superconductor is in a uniform magnetic field, either zero, parallel, or perpendicular, and the current is below I_c^* (the critical current equivalent to J_c^* in all of the filaments). A schematic diagram of the equipotential lines for this case is given on Fig. A1. The equipotential surfaces, shown in cross section as lines, are rotationally symmetric about the wire axis. The

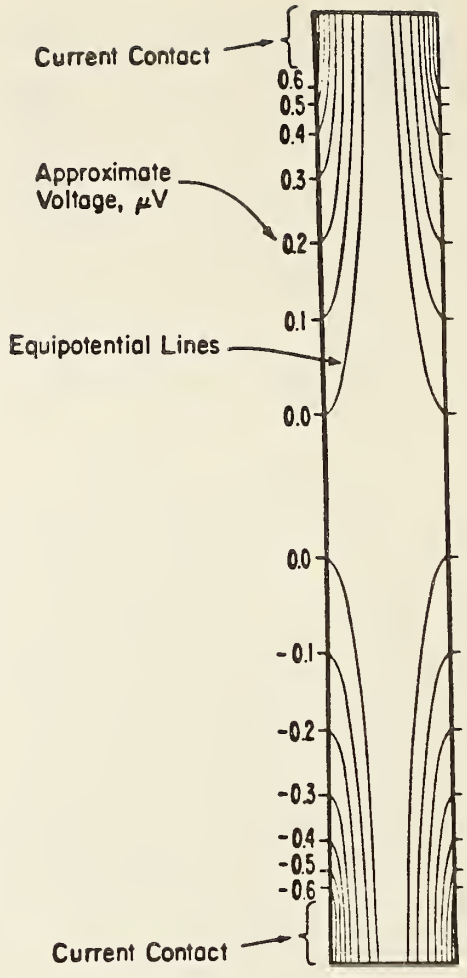

Figure A1. Schematic diagram of the equipotential lines in the core of the superconductor with a uniform external magnetic field.

voltage for each equipotential surface will scale approximately with the current. The equipotential lines on each end will look like those on Fig. 4 from the current contact to the 0.3 line (the lines on Fig. 4 marked 0.00 to 0.2 will not be there). Notice that if the current is below I_c^* and the distance between the current contacts is long enough, then a region such as that between the two 0.0 potential lines will exist and the potential everywhere in this region will be the same. As the current approaches I_c^*, the space between the 0.0 lines (on Fig. A1) gets smaller (both along and across the wire) and ultimately meet at I_c^*.

Now consider the case represented on Fig. 4, where there are two regions of different I_c^*'s (parallel and perpendicular field regions in this specific case) with the second region having a lower I_c^*. The other end of the configuration will be an image of this end. The presence of the perpendicular field region will cause equipotential lines such as the 0.1 and 0.2 lines (in Fig. 4) when the current is above the I_c^* of the perpendicular field. When the current is below the I_c^* of the perpendicular field, a line such as the 0.2 line will be the last line before the image lines at the other end of the configuration. Notice that the center filaments in the parallel field region have a different potential because of the presence of the perpendicular field. This results in a radial electric field and, thus, some current transfer even though the filaments in this region are below their J_c^*.

APPENDIX D

CRITICAL CURRENT MEASUREMENTS ON A NbTi SUPERCONDUCTING WIRE STANDARD REFERENCE MATERIAL*

L. F. Goodrich, D. F. Vecchia, E. S. Pittman, and A. F. Clark

Electromagnetic Technology and Statistical Engineering Divisions
National Bureau of Standards
Boulder, Colorado

INTRODUCTION

The National Bureau of Standards is producing a standard reference material (SRM) for the measurement of the superconducting critical current (I_c). This SRM and the recently adopted American Society for Testing and Materials (ASTM) standard test method (B714-82) will aid both the commerce and technology of superconductors through the promotion of more uniform measurements. The SRM will serve as an artifact for interlaboratory comparison to further advance the consensus and evolution of the new test method. The general use and philosophy of an SRM are given in Ref. 1.

To perform well as an SRM, the conductor chosen should be as homogeneous as possible. Conductors were purchased from the inventories of each of the United States wire manufacturers. Each conductor was selected by the manufacturer as a good candidate for an SRM. Preliminary screening measurements were performed on each conductor to determine the short- and long-range spatial variations in the critical current. The choice of the SRM was based primarily on these data.

The conductor selected for the critical current SRM was despooled onto 500 distribution spools, each with ~2.2 m of wire.

*Work supported in part by the NBS Office of Standard Reference Materials and the Department of Energy.

953

Adv. Cryog. Eng. - Materials, Vol. 30,

Plenum Press, New York (1984), 953-960.

Measurements on a sample of the spools were used to determine the likely outcomes if the spools for distribution were measured. The statistical analysis presented is for data taken at 4.07 K. A complete description of the measurement procedure, temperature dependence, and statistical analysis will be reported elsewhere.[2] This analysis will be based on the user making one measurement, on one spool, at one of the given magnetic fields (2, 4, 6, and 8 T) and at any temperature from 3.90 to 4.24 K.

EXPERIMENT

The only significant change from the common instrumentation[3] used to measure I_c, was the addition of a digital processing oscilloscope. This allowed the automation of the data analysis and higher precision in the processing of the voltage-current (V-I) curves than using an analog X-Y recorder alone. A number of acquisition and analysis variables were identified and their effect on the precision and accuracy of the critical current measurement determined. The acquisition variables considered were: current ramp rate, digital sampling rate, and voltage filtering and amplification. The analysis variables and corrections considered were: corrections for the inductive voltage and changes in thermoelectric voltage, and the number of points in the curve fitting. A correction for the magnetic field profile was made to I_c measured on adjacent voltage taps. The hydrostatic head and stratification of the liquid helium bath were also measured and the correct liquid helium vapor pressure used for the temperature determination.

The principal sample geometry used was a helical coil. There are many tradeoffs for each geometry (e.g., long straight, short straight, hairpin, etc.), but the coil seemed the best for this type of testing. With the coil, a number of segments of a given specimen could be measured to test the short range variations. Also the problems of negative voltage,[4] magnetic field angle and field uniformity are less in this geometry. The only major problem is the effect of bending strain which is not well known and is hard to measure[2] for NbTi superconductors; however, an upper limit can be put on the effect using uniaxial strain data.[5] The plastic flow of the copper matrix,[6] which would reduce the bending strain on the NbTi filaments, would make the estimated correction based on uniaxial strain data an upper limit. With a coil diameter of 3.2 cm and a sample of 0.05 cm diameter, the peak bending strain would be approximately 1.6%, assuming the neutral axis does not shift. A uniaxial strain of 1.6% would decrease I_c by about 8% at a magnetic field of 8 T. The integral of this effect over the cross section results in a 2% decrease in the overall value of I_c of the wire assuming the twist pitch is longer than the current transfer length,[6] which is a reasonable assumption for these NbTi superconductors. Because the bending strain correction is not

exactly known, the correction of the I_c data to the unbent state was not made, but it should be less than 2% at 8 T and even less at the lower magnetic fields.

The calibration of the instruments used to measure voltage, current, magnetic field, pressure, and length was performed.[2] The estimated systematic errors (inaccuracies) and random errors (precision limits) are given in Table 1. The random errors are included in the observed variation in the critical current and for this reason were separated from the systematic errors. The error in each of the critical current variables is expressed in terms of the resultant percentage error in the critical current at each of the magnetic fields. These errors were estimated using the known dependence of the critical current on each of the variables. The periodic and random deviation (PARD) of the current and magnetic field are not included because the sample current source was a battery power supply and the magnet was used in persistent mode. The sum and the root-mean-square of the estimated errors are given at the bottom of the table for each magnetic field.

PRELIMINARY SCREENING

The selection, from the five candidate conductors for the SRM, was based on the best balance of properties for use as an SRM. The chosen conductor may not be the best for any other

Table 1. Systematic and Random Errors Expressed in Percent Error in I_c at Magnetic Fields of 2, 4, 6, and 8 T.

	Systematic error (%)				Random error (%)			
Variable	2 T	4 T	6 T	8 T	2 T	4 T	6 T	8 T
Current	.25	.25	.25	.25	.05	.05	.05	.05
Electric field	.05	.05	.05	.07	.05	.05	.05	.07
Magnetic field	.10	.12	.21	.45	.04	.05	.05	.09
Temperature	.02	.02	.03	.04	.06	.08	.10	.17
Magnetic field profile	.02	.03	.05	.10				
Magnetic field angle	.10	.10	.10	.10				
Tensile strain	.15	.15	.15	.15	.07	.07	.07	.07
$\Sigma\Delta$	.69	.72	.84	1.16	.27	.30	.32	.45
$\sqrt{\Sigma(\Delta^2)}$	.33	.34	.38	.56	.12	.14	.15	.22

application. A brief preliminary screening was designed to test two properties, the long-range (spool-to-spool) and the short-range (tap-to-tap) homogeneity of I_c. Two other key properties were an adequate length and a usable copper-to-superconductor ratio. These four properties were sufficient to pick the conductor to be the SRM.

The homogeneity of I_c for each candidate was determined by measuring two specimens, one 5 and one 50 meters from the end of the shipping spool of each. Five pairs of voltage taps were placed on each specimen. The length of the specimen measured by each pair of voltage taps was about 2 cm and the centers of the adjacent pairs were separated by about 10 cm. The results of this limited preliminary screening pointed out problems with two of the candidates. Although the problem might not be present throughout, both candidates with a possible problem were eliminated.

In no case were the above mentioned problems identifiable with the choice of a given or measured physical parameter or combination of parameters. So the particular parameters for each sample will not be identified. Only the values will be listed here, nonrespectively, for completeness. The wire diameters were: 0.40, 0.51, 0.51, 0.51, and 0.64 mm. The number of superconducting filaments were: 54, 54, 60, 126, and 180. The approximate superconducting filament diameters were: 23, 26, 34, 42, and 50 μm. The copper-to-superconductor ratios were: 1.4, 1.6, 1.8, 1.9, and 2.0 to 1.

The results of the tests on short and long range homogeneity for all five conductors are summarized in Figs. 1 and 2. Figure 1 is a plot of the percentage difference between I_c of the two specimens for each sample at various magnetic fields. Notice that the differences for each sample are about the same at all magnetic fields measured. Sample 4 had a large shift in I_c. Another specimen of this sample, 150 m into the spool, was then measured. The I_c of this specimen had decreased another 1.1% from the value of the 50 m specimen. This may have been due only to an end effect, but this trend did not look good, so sample 4 was eliminated. Figure 2 is a plot of the percentage difference between the measured I_c on the center voltage tap and that of the other four taps for both the 5 and 50 m specimen of each sample. The expected tap profile due to the magnetic field profile has been corrected. Notice that sample 5 seems to have substantially larger variations and, for this reason, was eliminated.

The other two key properties were then used to select the one conductor to be the SRM. One of the remaining candidates was eliminated because the length delivered was considered to be too short (less than 400 m) and an adjacent spool could not be obtained. One of the two candidates left had the lowest copper-to-superconductor ratio (1.4:1). It was eliminated even though the low ratio did not seem to adversely affect the I_c determination, but it

could affect the usage of the SRM throughout the many kinds of testing anticipated for an SRM. This left one conductor for further testing.

PROVISIONAL DATA AND STATISTICAL ANALYSIS

Critical current measurements were performed on the chosen SRM. Specimen spools were selected by a systematic sampling procedure to assure that spools were selected along the whole length of wire. No trend or cycle related to distance along the wire was found.

The critical current data were obtained by placing three pairs of voltage taps on each specimen. The length of wire measured by each tap was about 2 cm and the centers of adjacent pairs were separated by about 20 cm. At magnetic fields of 2, 4, 6, and 8 T, two repeat determinations of I_c on each tap were recorded, producing a total of six measurements on each specimen at given (controlled) temperature. Data have been collected from nine spools equally spaced along the length of wire. The physical theory on the shape of the V-I curve and dependence on the weak

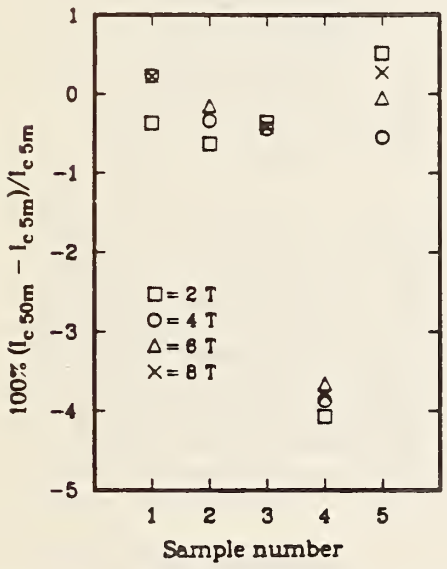

Fig. 1. The percentage change in I_c between the 5 and 50 m specimens of each sample, long range homogeneity.

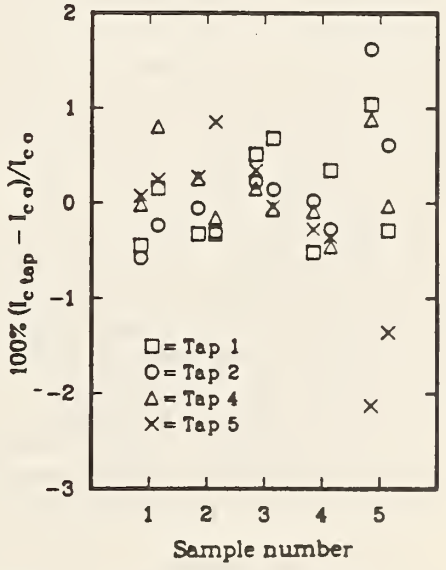

Fig. 2. Short range homogeneity of the 5 and 50 m specimens of each sample (percentage differences relative to center tap).

link suggests that critical current measurements may be nearly summable on a logarithmic scale. Therefore, the data were first transformed to estimate the quantities of interest, and then results on the adjusted scale were converted to the original units of measurement. In the discussion to follow, the estimates of critical current are, in fact, geometric means of the original data because they are derived from simple averages of data on the logarithmic scale.

Critical current measurements at a given field strength can be represented by the statistical model given by,

$$Y_{ijk} = \mu + D_i + T_{ij} + e_{ijk} \qquad \begin{cases} i = 1,\ldots,9; \\ j = 1, 2, 3; \\ k = 1, 2, \end{cases}$$

where Y_{ijk} is the logarithm of the measured critical current for the k-th repeat determination at the j-th tap on the i-th sample spool. Each measurement is thought of as the sum of four components: the mean critical current, μ; a long-range inhomogeneity, D_i, corresponding to distance along the wire; short-range inhomogeneity, T_{ij}, corresponding to the particular tap location on a given spool; and a random measurement error, e_{ijk}. The long- and short-range inhomogeneity terms are considered to be random deviations from the mean critical current for any given spool and tap location. Both the D_i's and T_{ij}'s are assumed to follow Gaussian probability distributions with mean zero and variances σ_D^2 and σ_T^2, respectively. The measurement errors, e_{ijk}, are assumed to have variance σ^2.

An important question for certification is whether all the available spools for this SRM can be treated as identical. The components of variance associated with the long- and short-range material variability of the wire provide a quantitative measure of inhomogeneity in the critical current SRM, so estimates of each type of variation were obtained. The estimated standard deviations, expressed as a percentage error in the critical current at each of the magnetic fields, are given in Table 2. The table illustrates that long-range inhomogeneity is more evident at 2 T and decreases with increasing magnetic field.

Because the critical current measurements revealed substantial long- and short-range variation, the uncertainty statement for the reported critical current at each magnetic field is a statistical tolerance interval. This statistical procedure allows for the observed variation in critical current by estimating limits for the critical current of individual spools, rather than limits on the overall average critical current of all spools.

Table 2. Estimated Long- and Short-Range Inhomogeneity Expressed in Percent Error in I_c at 4.07 K and 0.2 μV/cm.

Magnetic Field	Spool-to-Spool Standard Dev. ($\hat{\sigma}_D$)	Taps within Spool Standard Dev. ($\hat{\sigma}_T$)	Total $(\hat{\sigma}_D^2 + \hat{\sigma}_T^2)^{\frac{1}{2}}$
2	0.41	0.33	0.53
4	0.29	0.26	0.39
6	0.19	0.25	0.31
8	0.18	0.25	0.30

A tolerance interval for the distribution of critical currents for a length of wire of about 2 cm has the form, $\exp [\bar{Y} \pm K S_Y]$, where $\bar{Y}$ is the sample mean of all measurements on the logarithmic scale, S_Y is the estimated standard deviation of a single measurement, and K is usually taken from tables such as in Weissberg and Beatty.[7] The value of $K = K(N, f, P, \gamma)$ depends on:

(1) N: the effective number of observations for $\bar{Y}$;
(2) f: the degrees of freedom associated with S_Y;
(3) P: the proportion of critical current measurements to be covered; and
(4) γ: the probability level associated with the tolerance interval.

The estimated superconducting critical currents for an electric field criterion 0.2 μV/cm for a wire length of 2 cm are given in Table 3. The uncertainty of the reported value, ignoring systematic errors, is the statistical tolerance interval constructed such that it should cover 99% of critical current determinations with probability 0.95. The tolerance limits in Table 3 are expressed in terms of the resultant percentage error at each magnetic field and apply to a single measurement on any given spool for a length of wire of about 2 cm. Uncertainties for wire lengths greater than 2 cm are expected to be less than those in Table 3. The experimental systematic error and the tolerance limit are summed to give the total uncertainty and are all expressed as percent error in I_c.

CONCLUSIONS

A carefully controlled acquisition and analysis system was developed to measure I_c. Two of the five candidate conductors displayed short- or long-range inhomogeneity that made them seem unfit for use as an SRM. The conductor chosen for the SRM had substantial long- and short-range variation in I_c; therefore the uncertainty

Table 3. Provisional Results at 4.07 K and 0.2 μV/cm.

Magnetic Field (T)	Critical Current (A)	Total Uncertainty (%)	Tolerance Limits (%)	Systematic Error (%)
2	301.34	2.40	2.07	0.33
4	193.87	1.86	1.52	0.34
6	130.65	1.53	1.15	0.38
8	75.58	1.68	1.12	0.56

statement was calculated using statistical tolerance limits. The resulting total uncertainty was within the objective of the study.

ACKNOWLEDGMENTS

The help and support of the Superconductors and Magnetic Materials Group, especially F. R. Fickett and J. W. Ekin, are gratefully acknowledged. Suggestions on the content and presentation of this paper from W. S. Liggett, Jr. of the Statistical Engineering Division are appreciated.

REFERENCES

1. J. D. Cali, T. W. Mears, R. E. Michaelis, W. P. Reed, R. W. Seward, C. L. Stanley, H. T. Yolken, and H. H. Ku, "The Role of Standard Reference Materials in Measurement Systems," NBS Monograph 148, National Bureau of Standards, Washington, D.C. (1975) 54 pp.
2. L. F. Goodrich, D. F. Vecchia, E. S. Pittman, A. F. Clark, and J. W. Ekin, to be published.
3. L. F. Goodrich and F. R. Fickett, Critical current measurements: A compendium of experimental results, Cryogenics 22:225-41 (1982).
4. L. F. Goodrich, J. W. Ekin, and F. R. Fickett, Effect of twist pitch on short-sample V-I characteristics of multifilamentary superconductors, Adv. Cryog. Eng. 28:571-80 (1982).
5. J. W. Ekin, Mechanical and properties and strain effects in superconductors, in: "Superconductor Materials Science: Metallurgy, Fabrication, and Applications," S. Foner and B. B. Schwartz, eds. (Plenum Press, New York, 1981) p. 455.
6. J. W. Ekin, private communication.
7. A. Weissberg and G. H. Beatty, Tables of tolerance - Limit factors for normal distributions, Technometrics 2:483-500 (1960).

U.S. DEPARTMENT OF COMMERCE
National Bureau of Standards

APPENDIX E

Standard Reference Material 1457

Superconducting Critical Current

NbTi Wire

Winter 1984

The NBS Office of Standard Reference Materials announces the availability of the first superconducting wire for critical current measurements as a Standard Reference Material (SRM). It is intended to provide a means for testing the performance of measurement systems used in the development of superconductors. This SRM consists of approximately 2.2 m of a multifilamentary niobium-titanium, copper stabilized, superconducting wire wound in a single layer onto a spool with a core diameter of 8.7 cm.

SRM 1457 should prove valuable in determining the overall accuracy of a critical current measurement system that is dependent on numerous variables and effects that can make this seemingly easy measurement very difficult.

The critical current for SRM 1457 has been certified at magnetic fields of 2, 4, 6, and 8 T, for temperatures from 3.90 to 4.24 K, and electric field criteria from 0.05 to 0.2 μV/cm.

An effort was made to keep the use of this SRM as unrestricted as possible. The precautions listed on the certificate, together with the American Society for Testing and Materials (ASTM) Standard Test Method (B714-82), are sufficient for a valid user measurement technique. Some deviations in testing technique, from the method on which the certification was based, were accommodated by increasing the total uncertainty of the certified critical current. The deviations that are allowed, and the ones that are not allowed, are identified in the precautions sections of the certificate.

SRM 1457 may be purchased from the Office of Standard Reference Materials, Room B311, Chemistry Building, National Bureau of Standards, Washington, DC 20234, at a price of $219.

0384

U. S. Department of Commerce
Malcolm Baldrige
Secretary
National Bureau of Standards
Ernest Ambler, Director

National Bureau of Standards

Certificate

Standard Reference Material 1457

Superconducting Critical Current – NbTi Wire

This Standard Reference Material (SRM) is intended for use in checking the performance of measurement systems used in superconductor technology. This SRM consists of 2.2 m of a multifilamentary niobium titanium, copper stabilized superconducting wire wound in a single layer onto a spool with a core diameter of 8.7 cm. Critical current (I_c) for the SRM is certified over a range of magnetic fields, temperatures, and electric field criteria.

Measurement Technique: Adherence to the precautions given in this certificate (see section Precautions), together with the American Society for Testing and Materials (ASTM) Standard Test Method B714-82[1], is necessary and sufficient for a valid certification. Measurements for certifying SRM 1457 were obtained on a coil of diameter 3.18 cm with a voltage tap separation of 2 cm. The critical current is defined as the average of the values measured with increasing and decreasing current.

Certified Critical Currents: The certified critical currents in amperes at 4.2 K for an electric field criterion of 0.2 μV/cm are given in the table below. At respective magnetic fields, critical currents of this SRM can be calculated for temperatures from 3.90 to 4.24 K and electric field criteria from 0.05 to 0.2 μV/cm using:

$$I_c(T, E) = I_c(4.2, 0.2) \cdot \left\{\exp[A(4.2 - T) + B(4.2 - T)^2]\right\} \cdot [E/0.2]^C$$

where I_c (4.2, 0.2) and the coefficients A, B, and C are given in the table. Critical currents for SRM 1457 were derived from an empirical equation for the dependence of critical current on temperature (T) and electric field criterion (E):

$$\ell n(I_c) = \ell n(I_r) + A(T_r - T) + B(T_r - T)^2 + C\ \ell n(E/E_r).$$

In this equation, $\ell n(I_c)$ is the natural logarithm of the critical current and I_r is the critical current at the reference temperature, T_r, and reference electric field criterion, E_r. The experimental data at each magnetic field were fitted by a maximum likelihood procedure using a statistical model [2] that combines the empirical expression above with terms that allow for material variability (inhomogeneity) among the spools of wire.

Certified Value of Critical Current (I_c) at 4.2 K and 0.2 μV/cm and Coefficients for Temperature and Electric Field Extrapolation.

Magnetic Field (T)	Critical Current (A)	Total Uncertainty (%)	Coefficients for Extrapolation A	B	C
2.000	293.30*	±2.57	0.218625	−0.04755	0.0172089
4.000	187.38	±2.01	0.266361	−0.04682	0.0176600
6.000	124.72	±1.71	0.369479	−0.10488	0.0194218
8.000	69.72	±1.97	0.649242	−0.27906	0.0248311

*Extra digits are provided for accurate extrapolation.

Statistical design and data analysis were provided by D.F. Vecchia of the Statistical Engineering Division. Measurements for certification of SRM 1457 were coordinated by L.F. Goodrich. The measurements leading to the development and certification of SRM 1457 were performed by L.F. Goodrich, E.S. Pittman, and A.F. Clark of the Electromagnetic Technology Division.

The technical support aspects involved in the preparation, certification, and issuance of this Standard Reference Material were coordinated through the Office of Standard Reference Materials by R.K. Kirby.

Gaithersburg, MD 20899
June 19, 1984

Stanley D. Rasberry, Chief
Office of Standard Reference Materials

Interpretation of Uncertainty: The uncertainty of a certified critical current at each magnetic field is the sum of an estimated systematic error and statistical tolerance limits computed from the experimental data. The total uncertainty is expressed as percent error in I_c and does not change for extrapolated critical currents over the allowable range of temperatures and electric field criteria.

The statistical tolerance limits were constructed so that they should include 99 percent of the critical current measurements with probability 0.95. The resulting tolerance interval (and total uncertainty) is valid for a single measurement on any given spool that is made as directed on a coil of diameter 3.18 cm with a voltage tap separation of 2 cm.

Precautions:

1) This SRM should be carefully handled and stored to protect it against physical damage such as: excessive bending, scraping, and other deformation. Any excessive physical damage will invalidate the certification.
2) On each spool, the twisted wire ends and an additional 2 cm on each end of the spool core should be discarded. These sections of the wire are not certified.
3) This certification is invalidated if this SRM is mechanically cycled by demounting and remounting on a specimen holder. Mechanical cycling can concentrate handling stress, which would lower I_c in the stressed regions of the conductor.
4) This certificate is based on a slow cooling of the specimen mounted on a G-11 tube (circumferential fiber direction) by gas heat exchange with a liquid nitrogen precooled Dewar [2]. For a valid certification, the specimen must be measured on a suitable specimen holder [1]. The effect of a rapid cooling by immersion into liquid nitrogen or liquid helium can change I_c owing to dynamic differential thermal contraction. For rapid (immersive) cooling, 0.25% must be added to the total uncertainty even if a suitable specimen holder is used. It is conceivable that a user could demonstrate that the particular system and technique employed does not have a cumulative thermal or mechanical cycling effect. In this case, the specimen still has utility, but this SRM cannot be certified beyond one thermal cycle.
5) This certification is only valid for a zero-to-I_c ramp time in the range of 30 to 300 seconds for all magnetic fields [2]. Also, the certification was based on the assumption that voltage filtering and instrumentation response times contribute negligible error to the measured value of I_c. A nonnegligible effect can be removed by averaging the I_c values measured with increasing and decreasing current at a constant ramp rate. A nonnegligible effect must be removed for a valid certification.
6) A chemical wire stripping compound should be used to remove the insulation from this SRM. A phenol/methylene chloride wire stripping compound was found to adequately remove this insulation.
7) If the specimen temperature exceeds 250 °C, the certification is invalidated. The current and voltage contacts should be soldered carefully to avoid overheating and physical damage. If a specimen enters the normal state (quenches) while carrying a high current density, it could melt within a few seconds. An adequate quench protection circuit may be necessary [1]. A typical current shutdown time of 10 ms is adequate.
8) For a voltage tap separation of more than 2 cm, the uncertainty in I_c should be less. For a voltage tap separation of less than 2 cm, the uncertainty in I_c may be more. This certification is only valid for a voltage tap separation greater than or equal to 2 cm.
9) If this SRM is measured with a bend diameter other than 3.23 cm (coil of diameter 3.18 cm), the results may be different. Uniaxial strain data was used to determined the expected upper limits to the bending strain effect. For bending diameters from infinity (straight) to 1.6 cm, the certified critical current values can be used only if the following amount is added to the total uncertainty:

$$G \cdot \left| 1 - (3.23/d)^2 \right|,$$

where d is the bend diameter in centimeters and G=1.10, 1.20, 1.36, and 1.70% at 2, 4, 6, and 8 T, respectively.

Noncertified Values at Other Criteria: Critical current measurements were made on the sample spools at electric field criteria 0.02 and 0.5 μV/cm. However, SRM 1457 is not certified to the extended range of electric field because measurements at the additional criteria did not conform to the required measurement procedure. A comparison of observed critical currents to values extrapolated from the certifying equation is given in reference 2 for information only. Most of the measurements were within the range computed using tolerance limits that are only valid between 0.05 and 0.2 μV/cm.

References:

1. Standard Test Method for D-C Critical Current of Composite Superconductors, Annual Book of ASTM Standards, ASTM B714-82, Part 2.03, pp. 595-98, American Society for Testing and Materials, Philadelphia, Pa. (1983)
2. Goodrich, L.F., Vecchia, D.F., Pittman, E.S., Ekin, J.W., and Clark, A.F., Critical Current Measurements on an NbTi Superconducting Wire Standard Reference Material, NBS Special Publication 260-91 (1984)

NBS-114A (REV. 2-8C)

U.S. DEPT. OF COMM. BIBLIOGRAPHIC DATA SHEET (See instructions)	1. PUBLICATION OR REPORT NO. NBSIR 85-3027	2. Performing Organ. Report No.	3. Publication Date January 1985

4. TITLE AND SUBTITLE

DEVELOPMENT OF STANDARDS FOR SUPERCONDUCTORS
Interim Report
January 1982--December 1983

5. AUTHOR(S) L. F. Goodrich, J. V. Minervini, A. F. Clark, F. R. Fickett, J. W. Ekin, E. S. Pittman

6. PERFORMING ORGANIZATION (If joint or other than NBS, see instructions)

NATIONAL BUREAU OF STANDARDS
DEPARTMENT OF COMMERCE
WASHINGTON, D.C. 20234

7. Contract/Grant No.

8. Type of Report & Period Covered

9. SPONSORING ORGANIZATION NAME AND COMPLETE ADDRESS (Street, City, State, ZIP)

Department of Energy
Washington, D.C. 20545

10. SUPPLEMENTARY NOTES

☐ Document describes a computer program; SF-185, FIPS Software Summary, is attached.

11. ABSTRACT (A 200-word or less factual summary of most significant information. If document includes a significant bibliography or literature survey, mention it here)

A cooperative program with the Department of Energy, the National Bureau of Standards, and private industry is in progress to develop standard measurement practices for use in large scale applications of superconductivity. The goal is the adoption of voluntary standards for the critical parameters and other characterizations of practical superconductors. Progress for the period January 1982 through December 1983 is reported. The major effort was the procurement, selection, and certification of the first superconducting wire for critical current measurements as a Standard Reference Material (SRM 1457). Other work reported here includes: effect of geometry on current transfer; lap-joint resistance; and ac losses.

12. KEY WORDS (Six to twelve entries; alphabetical order; capitalize only proper names; and separate key words by semicolons)

critical current; critical parameters; losses; measurement methods; standards; superconductor

13. AVAILABILITY

☒ Unlimited
☐ For Official Distribution. Do Not Release to NTIS
☐ Order From Superintendent of Documents, U.S. Government Printing Office, Washington, D.C. 20402.
☒ Order From National Technical Information Service (NTIS), Springfield, VA. 22161

14. NO. OF PRINTED PAGES 168

15. Price

USCOMM-DC 6043-P80

☆ U.S. GOVERNMENT PRINTING OFFICE:1985—579-977 / 25313